

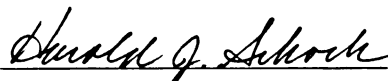


3 1293 00882 4199

This is to certify that the
thesis entitled
EFFECTS OF POCKET CONFIGURATION AND APEX
SEAL LEAKAGE ON THE FLOW FIELD IN A
ROTARY ENGINE ASSEMBLY

presented by
Michael Scott DeFilippis

has been accepted towards fulfillment
of the requirements for
Master of Science—degree in Mechanical Engineering


Major professor

Date 3/6/92

LIBRARY
Michigan State
University

PLACE IN RETURN BOX to remove this checkout from your record.
TO AVOID FINES return on or before date due.

DATE DUE	DATE DUE	DATE DUE
_____	_____	_____
_____	_____	_____
_____	_____	_____
_____	_____	_____
_____	_____	_____
_____	_____	_____
_____	_____	_____

MSU Is An Affirmative Action/Equal Opportunity Institution

c:\circ\datedue.pm3-p.1

**EFFECTS OF POCKET CONFIGURATION AND APEX
SEAL LEAKAGE ON THE FLOW FIELD IN A
ROTARY ENGINE ASSEMBLY**

by

Michael Scott DeFilippis

A THESIS

Submitted to
Michigan State University
in partial fulfillment of the requirements
for the degree of

MASTER OF SCIENCE

Department of Mechanical Engineering

1992

701-3267

ABSTRACT

Effects of Pocket Configuration and Apex Seal Leakage on the Flow Field in a Rotary Engine Assembly

by

Michael Scott DeFilippis

Abstract

The purpose of this study was to examine the change in the intake and early compression region flow field for two different rotor pocket geometries and to examine the impact of apex seal leakage on the flow field within a motored rotary engine assembly experimentally. Two-dimensional Laser Doppler Anemometry (LDA) measurements were taken over a central plane grid during intake and early compression under motored conditions of 2000 rpm and wide open throttle (WOT). A comparison of the flow fields for the two different rotor pocket geometries showed little difference in the regions studied under the stated conditions. The intake flow field for both rotors was dominated by a large scale circulation in the opposite direction of the shaft rotation. Small changes in the flow field were seen with the change in pocket configuration and apex seal leakage. The results of this study seem to indicate the intake port configuration is the dominant controlling parameter in the establishment of the flow field in a rotary engine.

**Copyright by
Michael Scott DeFilippis
1992**

**This thesis is dedicated to my fiancée Sheila, and
my parents Carmine and Jeanette DeFilippis**

Acknowledgments

I would like to express my appreciation for the financial assistance of NASA Lewis Research Center, and for Dr. Harold Schock hiring me as a research assistant. With out the financial support they provided I would not have completed my masters degree.

Craig Olbrich, who provided more help and support than I really deserved, and was partially responsible for me being hired at the engine lab in the first place, (I am not sure if I should thank him for that or not). Dr. Craig Somerton, whose genuine interest in teaching and consistently good advice are very much appreciated. Colin MacKinnon and Dr. M. Koochesfahani, who very graciously helped with the development of the video animation of the results. Mark Novak, who did the bulk of the PV-WAVE programing.

Everyone who was part of the MSU student chapter of the Society of Automotive Engineers. They provided me with the overwhelming majority of enjoyable and educational experiences I have had over the past two years.

TABLE OF CONTENTS

LIST OF TABLES	xiii
LIST OF FIGURES	x
CHAPTER 1 - INTRODUCTION	1
1.1 Problem Statement	1
1.2 Literature Review	2
CHAPTER 2 - EXPERIMENTAL EQUIPMENT	7
2.1 Rotary Engine Assembly	7
2.2 Laser Doppler Anemometry System	8
2.3 Data Reduction and Display Software	9
CHAPTER 3 - EXPERIMENTAL PROCEDURE	13
CHAPTER 4 - RESULTS	15
4.1 Effects of Pocket Configuration on the Flow Field	15
4.2 Effects of Apex Seal Leakage on the Flow Field	18
4.3 Assessment of Uncertainty in the Measurements	20
CHAPTER 5 - CONCLUSIONS	21
CHAPTER 6 - RECOMMENDATIONS	24

TABLE OF CONTENTS, Cont.

APPENDIX A - RTOVEL PROGRAM	62
APPENDIX B - ROTOR_DOUBLE PROGRAM	74
REFERENCES	81

LIST OF TABLES

TABLE 1 - ROTARY ENGINE SPECIFICATIONS	8
-----------------------------------------------	----------

LIST OF FIGURES

Figure 1.	Mazda Leading Deep Recess and Symmetric Recess Rotors	27
Figure 2.	Stock and Modified Mazda 12A Central Housings	27
Figure 3.	Rotary Engine Assembly	28
Figure 4.	Laser Doppler Anemometry System	28
Figure 5.	Displayed Results from Hamady [29]	29
Figure 6.	Measurement Locations	29
Figure 7.	U Component of Velocity versus Crank Angle for 5 and 10 MHz	30
Figure 8.	Comparison of the Flow Fields for the LDR and SMR Rotors with Compression	31
Figure 9.	Comparison of 30 and 50 Count Minimums	43
Figure 10.	Velocities of the Leading and Trailing Apex Seals	45
Figure 11.	Volume of Working Chamber versus Crank Angle	46
Figure 12.	Comparison of the Flow Fields for the SMR Rotor with and without Compression	46
Figure 13.	Locations and Crank Angles used for Figures 14 and 15	57
Figure 14	Data Distributions for Location A	58
Figure 15	Data Distributions for Location B	59

Chapter 1

INTRODUCTION

1.1 Problem Statement

The purpose of this study was to examine the change in the intake region flow field for two different rotor pocket geometries and to examine the impact of apex seal leakage on the flow field experimentally under the same motored conditions of 2000 rpm and wide open throttle (WOT). This data can also be used to provide a quantitative comparison with the results of numerical simulations. Developing an understanding of the characteristics of the flow field within the rotary engine and how these characteristics influence the combustion process is one of the most important steps in optimizing the engine's performance. Ideally, analytical models will be developed to the point where design changes, such as pocket geometries and compression ratios, can be tested analytically without the time and expense of making a full prototype and testing it on a dynamometer. An important step towards this goal is the acquisition of experimental data with which to verify these models. Analytical models which attempt to predict the flow field within the rotary engine have had little experimental data to use for comparison [1-9]. Computational models of rotary engines, which are aimed at calculating quantities such as the indicated mean effective pressure (IMEP) or rate of combustion [10-14], have had a larger base of experimental results with which to compare [12-21].

1.2 Literature Review

Hamady et al. [22] presented high speed films of the flow field during the intake and early compression strokes in a motored rotary engine at both 675 rpm and 1170 rpm. In a corresponding study by Chouinard et al. [23], selected laser Doppler anemometry (LDA) measurements were made in the same engine assembly, under the same conditions, in an attempt to quantify some of the major flow field characteristics. These two studies reported a significant amount of blowby, gases leaking past the apex seals from the compression region into either the exhaust or intake regions. These studies stated that the blowby created a large circulating flow field in the intake region when it interacted with the entrained intake charge. This circulating flow was aided by the fact that the test rig used for those studies, and for this study, was peripherally ported, not side ported or a combination of side and peripheral. The studies done by Hamady [22] and Chouinard [23] were done at low shaft speeds, roughly equivalent to idle for an actual engine, with light weight graphite apex seals under motored conditions. Other studies [24-28] have shown the apex seals may lose contact with the surface of the rotor housing at higher shaft speeds under both motored and firing conditions. The combination of low shaft speed and graphite apex seals significantly reduces the centrifugal force on the seal when compared to higher speeds and steel apex seals. A later study by Hamady et al. [29] showed the intake region flow field for a Mazda 12A assembly with steel apex seals at 2000 rpm. Selected LDA

measurements were made to quantify some of the flow features, and again the flow field was reported to circulate in the opposite direction of the rotor.

Experimental and computational studies have been done in an attempt to determine the movement of the apex seal as it goes through a cycle under motored and firing conditions. Matsuura [24] reported experimental data on the lateral movement of the apex seal to the apex seal slot. Matsuura [25] also examined the behavior of the apex seal against the trochoidal surface, in a firing rotary engine using several different apex seals. The results of the later study [25] showed the apex seals lose contact with the trochoidal surface for various engine shaft speeds, up to 6000 rpm, and under various operating loads. A study by Knoll et al. [26] again examines the issue of rotary engine seal dynamics but by means of a computational analysis in which real time pressure data is input into the governing equations. The results of Knoll compare reasonably well with Matsuura, with the exception that the Matsuura results showed an increasing gap between the apex seal and the trochoidal surface with increasing engine speed above 2000 rpm and Knoll's results showed the opposite, a decreasing gap with increasing shaft speed. In order to develop more accurate computational models of the flows within the rotary engine, the motion of the apex seal under various conditions and the impact of that motion on the flow field must be better understood. It is interesting to note that Knoll's study reported calculated results for 2053 rpm, under motored conditions at WOT,

among other conditions, for the Mazda 12A engine configuration. These conditions correspond to those used in Hamady et al. [29] and in this study. Knoll's results showed the apex seal shifting from the leading to trailing edge of the apex slot at 460 crank angle degrees (cad) with no separation of the apex seals from the surface of the rotor housing. Hamady's results claimed the blowby event, indicating loss of contact between the apex seal and the trochoidal surface, occurred at between 470 and 480 cad (after adjusting Hamady's definition of 0 cad to match Knoll's definition). A numerical study by Rachel et al. [28] examined frictional power losses associated with the apex and side seals in a rotary engine. Their results showed the radial acceleration force becoming negative, indicating apex seal lift-off, from 3000 to 7000 rpm with a IMEP of 412.5 kPa. This loss of contact occurred between 134 and 216 cad, after adjusting Rachel's definition of zero cad to match the one used in this study, for 3000 rpm and increased to 123 and 237 cad for 7000 rpm.

The effects of the apex seal leakage in computer models of rotary engine flows and performance have been handled differently by different investigators depending on the goal of the study. References [1-8] are computational studies of either the flow fields in the rotary engine, fuel-air mixing in the rotary engine or both. These predictions do not include the effects of apex seal leakage. The importance of this omission depends on the desired results and the impact the leakage may have on these results. An important initial attempt at estimating the effects of apex seal leakage was done by Eberle and Klomp [10]. Their model assumed a constant

apex seal leakage area throughout an entire cycle (1080 cad) for lack of better information at the time. A later study by Ferguson [12], which also included the effects of apex seal leakage, examined the exhaust composition and flow rate both experimentally and numerically. Ferguson [12] suggested a possible large scale recirculating flow established by the leakage of the apex seal as a source for the discrepancy between experimental and calculated results. This type of recirculating flow was seen in the intake region by Hamady [22,29]. Computational studies of the apex seal motion [26] indicate the corresponding leakage past the apex seal into the exhaust region should be greater in magnitude than that into the intake region.

Li et al. [9] used a computational model to examine the effect of apex seal leakage on flow fields within the rotary engine. This study examined the effects of engine speed, leakage area, and compression ratio on the velocity field, distribution of turbulent kinetic energy and volume-averaged pressure in a two-dimensional model. Previous numerical studies of flows in the Wankel engine [1-8] have assumed apex seal leakage to be negligible. Li et al. [9] examined engine speeds of 5,000 and 10,000 rpm, compression ratios of 4.93 and 6.86, open and closed intake and exhaust ports for three different leakage models. The leakage models used assumed the leading apex seals lost contact with the trochoidal bore at 2.5π radians before TDC and the trailing apex seals lost contact at 0.5π radians before TDC. The leading and trailing apex seals were assumed to remain at a constant distance from the trochoidal

bore until TDC. Three different separation distances were examined in the study. The leakage model was based on the observed flow fields in Hamady [22] and Chouinard [23], which were conducted at 675 and 1170 rpm with graphite apex seals. The results of Li's numerical study [9] showed a recirculation region from the leading edge of the rotor pocket to the leading apex seal. This recirculation was a result of the leakage model used and was seen to increase with increasing apex seal leakage. The results of Li [9] did not show the large scale recirculation seen in this study.

This study examines the two-dimensional, central plane flow field for a peripherally ported rotary engine assembly being motored at 2000 rpm. The results of this study offer quantitative, experimental data which was previously unavailable. Comparing the results from this study to results which could be obtained from numerical studies done with the same parameter is a critical step in developing accurate numerical models. Even though numerical models for the flows in a rotary engine have been under development for some time their accuracy has not been established since there have been no experimental results for comparison.

Chapter 2

EXPERIMENTAL EQUIPMENT

2.1 Rotary Engine Assembly

The rotary engine assembly used for this study is a single rotor peripherally ported assembly. This single rotor device is derived from Mazda 12A components. A leading deep recess rotor [LDR] and a symmetric recess rotor [SMR] were studied, as shown in Figure 1. The SMR was run in both a stock Mazda 12A central housing and a modified non-compression version. The non-compression version had a rectangular port equal in area to the intake port machined into it at the location of the upper spark plug, Figure 2. The pocket volumes were 20.1 and 23.37 cc for the SMR and LDR respectively. These pocket volumes resulted in a compression ratio of 9.51 for the SMR and 9.05 for the LDR. Figure 2 shows the rotary engine assembly. Optical access for the LDA measurements is provided by sapphire windows mounted in the end housings. The windows constitute approximately one third of the total area of the trochoidal profile, Figure 3. Production Mazda 12A side, oil and two-piece steel apex seals were used throughout the study. The same seals were used in both rotors. The engine assembly was lubricated in the same manner as the actual engine, SAE 20w-50 motor oil was supplied at 175-280 kPa [25-40 psi] to the main bearing carrier. The oil is returned to a reservoir by means of a vacuum pump which is regulated by a flow control valve operated at 41 kPa (12" Hg). This is a closed system that originates and terminates at the reservoir. The main

reason for using the vacuum oil return is to reduce window fouling. Selected specifications of the RCE engine are given in Table 1.

Table 1. Rotary engine specifications

Major axis (y)	120 mm
Minor axis (x)	90 mm
Generating radius (R)	105 mm
Eccentricity (e)	15 mm
Intake port opening (IPO)	987°
Intake port closing (IPC)	1070°
Exhaust port opening (EPO)	732°
Exhaust port closing (EPC)	786°

2.2 Laser Doppler Anemometry System

The laser Doppler anemometry system shown in Figure 4 consists of a 4 watt argon-ion laser manufactured by Coherent, optical and signal processing equipment designed and built by TSI, Inc., and an IBM PS/2 80 computer for data acquisition [29]. The system is currently operating in a single-line mode, permitting the measurement of one velocity component at a time. A Model 9180 frequency shift system consisting of a Bragg cell and frequency shifter is being used to allow directional velocity measurements and detection of flow reversals. The laser, the transmitting optics and the receiving optics are mounted on a rigid traverse table, Model 9900-1, specifically designed for traversing a LDA optical system. This method of traversing provides flexibility in relocating the probe volume within the cylinder, as the distance from the focusing lens to control volume remains fixed. Translations in the x, y and z direction are achieved via a keypad style controller with an accuracy

of 25 μm . The data processing equipment consists of a Rotating Machinery Resolver (Model 1998), a counter type processor (Model 1990) and a master interface (Model MI990), all manufactured by TSI, Inc. This equipment collects and processes the data coming from the photomultiplier and sends the data to an IBM PS/2 80, where it is manipulated and displayed in graphical form.

The seed delivering system is a Model 9306 six-jet atomizer manufactured by TSI, Inc. In this study propylene glycol dissolved in 5 parts of water is used to form the seed particles. The particle size distribution reported by TSI is between 0.5-0.8 μm in mean diameter. The propylene glycol provided excellent data rates without the problem of contaminating the transparent windows, so often encountered in LDA measurements.

2.3 Data Reduction and Display Software

An important development over previous studies [23,27,29] was the data reduction and graphical display software created for this work. Figure 5, from Hamady [29], is representative of the displayed results for experimental flow field data taken in a rotary engine. The blank region from 30 to 110 cad is a result of the rotor blocking the measurement volume. The results are accurately displayed but do not help the reader visualize the entire intake process and require a separate graph for each measurement location. The programs developed for this work, RTOVEL and ROTOR_DOUBLE [30], allow the reader to interpret the results

from fifty measurement locations simultaneously.

The data reduction program, RTOVEL, is included in Appendix A. This program reads in velocity data files created by the PHASE software package and reduces the data to produce the velocity mean versus crank angle for the selected input files. Both the RTOVEL and PHASE programs are designed to be run on IBM compatible personal computers using DOS 3.3 or higher. The PHASE (Phase Resolved) software was developed by TSI Inc. to collect and display data from the LDA and signal processor system. There are two velocity files associated with each measurement location, a U component and a V component velocity file. This study examined 50 measurement locations for three different cases, creating a total of 300 velocity files each containing 20,000 individual measurements. Figure 6 shows the measurement locations within the central housing. The origin of the coordinate system is at the center of the crank shaft.

The first 253 lines of the velocity files, the file header, contain all of the relevant parameters associated with the file. Information such as the number of data points, creation date, component, measurement location, and frequency shift used are all included in the header. The remainder of the velocity file contains each velocity measurement. The RTOVEL program reads the header information to get the number of data points, the velocity component and the measurement location. The number of data points is used as the loop counter for reading the data and the velocity component is used to confirm there is only one u and one v

component data file for each measurement location. The measurement locations are based on the coordinate system seen in Figure 6. The coordinate pair is converted from millimeters to the non-dimensionalized coordinates used by the ROTOR_DOUBLE program for the final display. The resulting output file is an 18,050 X 5 array with the columns being x and y position, u and v velocity component (mean velocity) and crank angle.

The ROTOR_DOUBLE program is actually a command file for use within PV-WAVE. PV-WAVE is a workstation analysis and visualization environment developed by Precision Visuals Inc. The version of PV-WAVE used in this study, version 3.0, is designed for use in a UNIX operating system. All of the work done with PV-WAVE was performed on a Sun 4/260 workstation. The ROTOR_DOUBLE program reads in the reduced data and displays the resulting vector field within the representation of the rotor and central housing. The output of the program could either be displayed on the computer screen, sent to a printer in the form of a postscript file, sent to an encapsulated postscript file or sent to a TIF format graphics file. There are other output devices available with PV-WAVE but only the above mentioned devices were utilized in this study. The screen and postscript displays allowed immediate examination of the resulting graphical output. The encapsulated postscript output creates a file which is intended for use with a word processor type of application, such as this text. The vector fields in figures 8 and 12 are encapsulated postscript files which were

generated with the ROTOR_DOUBLE program. The final output device, the TIF graphics image, was used to create a computer animation of the flow field. The ROTOR_DOUBLE program generated a TIF file for every crank angle. These files were then loaded onto a Recognition Concepts Inc. Trapix 5500 Image Processor. The image processor cycled through the TIF files and the resulting screen images were recorded onto a VHS format tape with a conventional video cassette recorder.

Chapter 3

EXPERIMENTAL PROCEDURE

All of the data was collected at a shaft speed of 2000 rpm, WOT and under naturally aspirated conditions. The data was collected in forward scatter, made possible by having sapphire windows in both end housings, with 10 MHz frequency shift. The criteria for acceptance of the velocity data were as follows: The mean velocity has been measured for two different frequency shifts, 5 and 10 MHz, at the same position and operating conditions to verify that the shifting did not have a significant effect on the measurements. Figure 7 demonstrates the results of mean velocity, u component only, versus crank angle at one location with both 10 MHz and 5 MHz frequency shift and is typical of the results for all of the measurement locations. The 10 MHz frequency shift was used because it provided the widest measurement range. The signal filter settings used throughout the study were 30 kHz and 50 MHz for the low and high filters respectively. This results in a working measurement range of -25.8 m/s to 103.4 m/s for the 10 MHz frequency shift and 2.5853 micron fringe spacing used. The 50 measurement locations, as seen in Figure 6, are all in the rotor housing central plane, equidistant from both end housings. The locations are on a 12 mm grid with the exception of six points around the major axis which were needed for a more complete picture of the flow field. The origin of the coordinate system is the center of the crank shaft. Forty thousand data points were collected at each location, 20,000 for the u component and 20,000 for the

v component. The 40,000 data points per location is the practical limit for the current system given the available disk space for storage of the data and the counter/processor in use.

The data collection window started at 0 cad and closed at 360 cad. The position encoder used returned to 0 after reaching 360 cad. The data collection window was subsequently reopened at this point. This resulted in the data from each of the three rotor faces being superimposed upon each other. Previous studies [22,23,29] have shown no appreciable difference in the intake flow field between the different rotor faces under motored conditions. This would not necessarily be true for a study done under firing conditions. Local fuel/air ratio fluctuations can cause significant cycle-to-cycle variability in the IMEP [17], which could affect the apex seal leakage and the intake flow field.

Chapter 4

RESULTS

4.1 Effects of Pocket Configuration on the Flow Field

Figure 8 shows the measured mean velocity fields for both the LDR and SMR rotors with compression. The magnitudes of the velocities are proportional to the length of the vectors. The key vector in the upper left hand corner of the plots represents 10 m/s and the black mark on the housing represents the upper spark plug hole. Fluctuations in the seeding resulted in some of the measurement locations having insufficient individual measurements to qualify as a valid measurement point. If less than fifteen velocity measurements were available for either the u or v component the velocity at that location was given a magnitude of zero for that crank angle. The minimum value of fifteen measurements for each component was arrived at after examining the results for minimums of 50 and 30 measurements per component. Figure 9 shows examples of the results for the 30 and 50 count minimums for 190 and 250 degrees. The 15 count minimum displayed a greater number of vectors while being consistent with the results for 30 and 50 count minimums.

The early stages of intake, Figure 8, crank angles 130 and 160, show relatively high fluid velocities when compared to the leading and trailing apex seal velocities. The velocities for the leading and trailing apex seals versus crank angle were calculated using equations from

Ansdales [31] and are shown in Figure 10 for 0 to 360 cad. The maximum measured fluid velocities near the intake port during intake are approximately twice the maximum apex seal velocity, approximately 21 m/s for the fluid versus 10.5 m/s for the apex seal. The fluid velocities near the intake port can be estimated by calculating the average velocity through the intake that would be required to fill the increase in volume of the working chamber over a small change in crank angle, assuming the fluid to be incompressible. Figure 11 shows the calculated volume of the working chamber versus crank angle, using equations from Yamamoto [32], for 0 to 360 cad. The calculated change in volume, for the LDR rotor, from 180 to 195 cad is 42.97 cc, the cross sectional area of the intake port is 14.52 cm² and the elapsed time for the crank to rotate 15 degrees at 2000 rpm is 1.25 ms. The estimated intake velocity is calculated as follows:

$$\text{Average velocity} = \Delta V / (\Delta T \times A_c) \quad (1)$$

Where, ΔV is the change in volume of the working chamber, ΔT is the elapsed time and A_c is the cross-sectional area of the intake port. The estimated average velocity throughout the intake at 2000 rpm for both the LDR and SMR rotor was 23.68 m/s. The average magnitude of the three measurement locations closest to the intake port over the same 15 degree span was 18.61 m/s and 18.86 m/s for the LDR and SMR rotors respectively. Some of the difference is a result of the measurements being within the central housing where the fluid can diverge.

Circulation of the intake flow field is apparent for both rotors at 160 cad, Figure 8. The fluid velocities relative to the rotor surface range from 0 near the leading apex to 16 m/s near the intake port moving from the trailing apex towards the leading apex. The intake charge moves along the rotor face until it approaches the leading apex seal. At this point the fluid still has considerable momentum and begins to recirculate along the surface of the central housing.

At 190 cad, Figure 8, the effects of the rotor configuration on the flow field begin to become apparent. The similar characteristics of the flow fields for both the LDR and SMR rotors are a large scale circulation, a region of entrained fluid next to the rotor face extending from the leading edge of the rotor pocket to the leading apex seal and a small separation region just above the intake port. The difference between the flow fields at 190 cad is that the center of the circulation is closer to the leading apex seal for the LDR rotor than that for the SMR rotor. This difference is a result of the leading deep pocket allowing the intake flow to penetrate further into the working chamber before exiting the pocket and beginning to recirculate. This pattern continues to develop throughout 220 and 250 cad. By 280 cad the intake stroke is ending and the velocities, for both rotor configurations, near the intake are below 5 m/s. The separation region at the upper edge of the intake port decreases with the decreasing intake velocities.

The back flow, the flow exiting the intake, seen at 310 cad for both rotors was observed from 297 to 314 cad for the SMR rotor and from

295 to 314 cad for the LDR rotor. Once the intake port is closed, at approximately 340 cad, the velocity field is driven by the rotor motion and the remaining fluid inertia. By 10 cad, (370 cad by notation), the recirculation initiated during intake is almost indistinguishable and the rotor motion seems to be the sole driving force behind the fluid motion. This trend continues for 40 cad (400 cad) and 70 cad (430 cad). The final two vector fields, 70 and 100 cad, are included for completeness. The interference of the rotor and very low data rates in late compression resulted in relatively few valid measurement locations for crank angles 70 through 130.

There is no conclusive evidence of apex seal leakage for either the LDR or the SMR rotors at any point during the cycle, 0 to 360 cad. The measurement locations close to the inner surface of the central housing did not have valid measurements immediately following the passing of the rotor. Valid results at these measurement locations did not begin until 15 to 25 cad after the rotor had passed through the location. Likewise, valid results continued at these measurement locations until approximately 15 to 25 cad before the rotor passed through that point. The flow fields for both rotors, Figure 8, do not exhibit a strong jet-like flow along the inner surface of the central housing which can be directly attributed to apex seal leakage.

4.2 Effects of Apex Seal Leakage on the Flow Field

In order to observe the impact apex seal leakage has on the flow field, the study previously discussed was repeated for the SMR rotor with

a modified central housing. This central housing had a rectangular port machined into the housing equal in area to the intake port and centered on the upper spark plug hole, Figure 2. This was done so that there would be no significant pressure differential across the apex seal. The new port does not permit the working chamber to undergo compression at any point in the cycle. It is assumed there is no apex seal leakage since there is a negligible pressure differential .

Figure 12 shows the vector fields for the SMR with and without compression. The early stages of intake, 130 and 160 cad, show very little difference between one another as was the case in Figure 8. At 190 cad, Figure 12, the flow fields for both configurations have developed recirculation. At this point there does not appear to be an appreciable difference in the flow fields.

Repeating the comparison of the average measured velocity at the three locations nearest the intake from 180 to 195 cad results in an average velocity of 20.27 m/s. The estimated average velocity, as stated earlier, is 23.68 m/s. The average measured velocities for the LDR and SMR with compression were 18.61 m/s and 18.86 m/s respectively. The difference in the measured velocities could be a result of apex seal leakage occurring during compression. If the fluid is again viewed as incompressible, any fluid entering the working chamber via apex seal leakage would decrease the total mass of air entering through the intake port over the same time differential.

The flow fields for both cases demonstrate the same general

features for both 220 and 250 cad, Figure 12. These features are the same as those seen in Figure 8, a large circulation region in the center of the field and separation regions near the leading apex and the upper edge of the intake. The center of the circulation is slightly closer to the leading apex seal for the rotor undergoing compression. The flow field appears to be more uniform for the rotor which is not undergoing compression. This suggests that apex seal leakage may have a slight influence on the flow field.

Even though the anti-compression port opens at 260 cad, the flow fields for 280 cad are very comparable to one another. At 310 cad, Figure 12, the fluid can be seen exiting the housing through the new port. The remaining crank angles are included for completeness.

4.3 Assessment of Uncertainty in the Measurements

The two primary sources of fluctuation in the velocity measurements are the inability of the measurement technique to precisely measure the velocity and the cycle to cycle variability of the flow through a point. The fidelity with which the seed particles follow the flow is the primary source of measurement imprecision in the LDA system. A previous study by Chouinard [33] showed that the 0.5-0.8 μm diameter seed particles used in this study faithfully follow the flows in the rotary engine assembly under the conditions tested. In this study the measurements for each of the three rotor faces were superimposed on each other since the PHASE software used for data collection did not

permit data collection on a 1080 degree cycle. It is not possible to separate the fluctuations which result from measurement imprecision, rotor-face to rotor-face variability and the cycle to cycle variability on a single rotor face in the existing data. Figures 14 and 15 show the data distributions for two locations, two crank angles and both velocity components for the SMR rotor which is not undergoing compression. The locations and crank angles are shown in Figure 13. These distributions are representative of the data distributions found throughout the study. The bin size used for the experimental data curves was 0.25 m/s. Equation 2 [34] was used to produce the normal distribution curves.

$$F(x) = (y_{\max})e^{-0.5((x-\mu)/\sigma)} \quad (2)$$

Where y_{\max} is the maximum number of occurrences in a bin, μ is the mean value for the sample and σ is the standard deviation.

The range of total data points per sample, for Figures 14 and 15, is a maximum of 308 data points at location A for 190 cad, v component, and a minimum of 24 data points at location B for 190 cad, u component. It is not immediately clear how many data points are needed to fully characterize the flow at any one location and crank angle for a given velocity component. The data distribution for location A, 190 cad, u component closely approximates a normal distribution with a total of 139 data points. The data distribution for the same location and crank angle, v component is not as close an approximation to the normal distribution with 308 total data points. In order to obtain sufficient data to examine

the fluctuations in the flow field improvements need to be made in the data processing equipment and the data storage and reduction equipment. Practical system limitations, such as the amount of disk space available to store the data and relatively low data rates, prevented the collection of additional data for this study.

CHAPTER 5

CONCLUSIONS

This study has presented a quantitative experimental study of the flow field for two different rotor pocket geometries in a motored rotary engine assembly at 2000 rpm and WOT with and without compression occurring. The fluid flow through the intake port was seen to create a recirculation which dominated the intake flow field for both rotor pocket geometries, with and without compression. Based on the material presented the following concluding remarks can be made:

1. For the 2000 rpm shaft speed tested, the intake fluid velocities near the intake were found to be nearly twice the maximum apex seal velocity. This created a recirculating flow field during the intake stroke.
2. The center of the recirculation was closer to the leading apex seal for the LDR rotor than for the SMR rotor with both rotors undergoing compression. The center of the recirculation for the SMR was seen to move slightly towards the trailing apex for the case where the rotor does not undergo compression.
3. Once the intake port is closed for the rotors undergoing compression, the flow field quickly loses the recirculation exhibited during intake and the flow field is driven by the rotor motion.

4. A small difference in the intake velocities for the SMR rotor with and without compression was measured. Slight differences in the flow fields were also noted when these two configurations were compared. This seems to indicate that apex seal leakage is occurring for the rotor undergoing compression.
5. Under the conditions tested, 2000 rpm, WOT and normally aspirated, apex seal leakage does not contribute significantly to the circulating flow field seen during the intake process in the peripherally ported rotary engine assembly.

CHAPTER 6

RECOMMENDATIONS

The following is a list of recommendations for both future work and improvements in the system used in the experiments.

- 1) Develop a technique for determining if and when the apex seals are losing contact with the trochoidal housing. The technique described in Matsuura [25] can be used but may prove to be too labor and cost intensive to be practical. Comparing measured pressure traces to calculated isentropic pressure curves can be used to determine leakage from the working chamber but determining whether the leakage is occurring at the side, apex or button seals may prove difficult.
- 2) Develop a version of the TSI PHASE software which will permit data collection over an 1080 degree cycle. Currently either 360 or 720 degree cycles are available. The 1080 degree cycle could be used to confirm the lack of variability in the flow field from rotor face to rotor face.

Figures

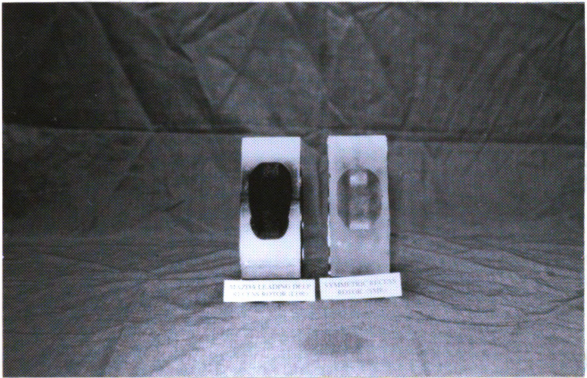


Figure 1 Mazda Leading Deep Recess and Symmetric Recess Rotors

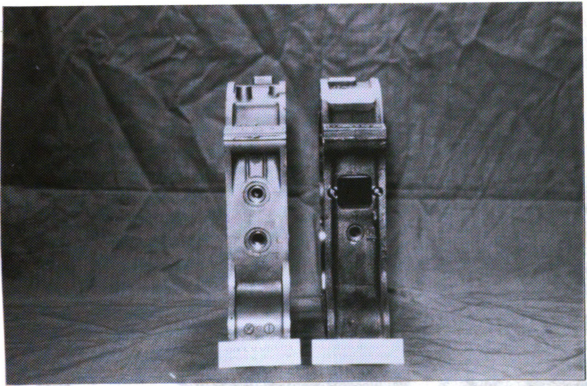


Figure 2 Stock and Modified Central Housings

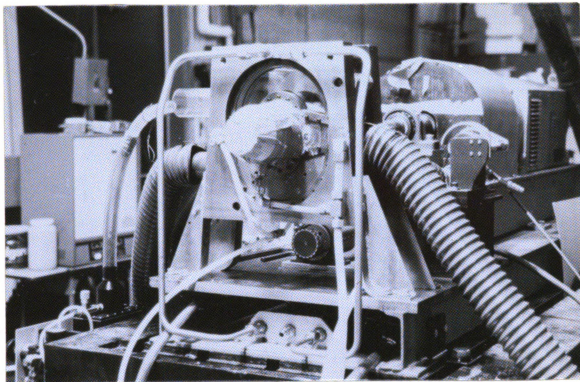


Figure 3 Rotary Engine Assembly



Figure 4 Laser Doppler Anemometry System

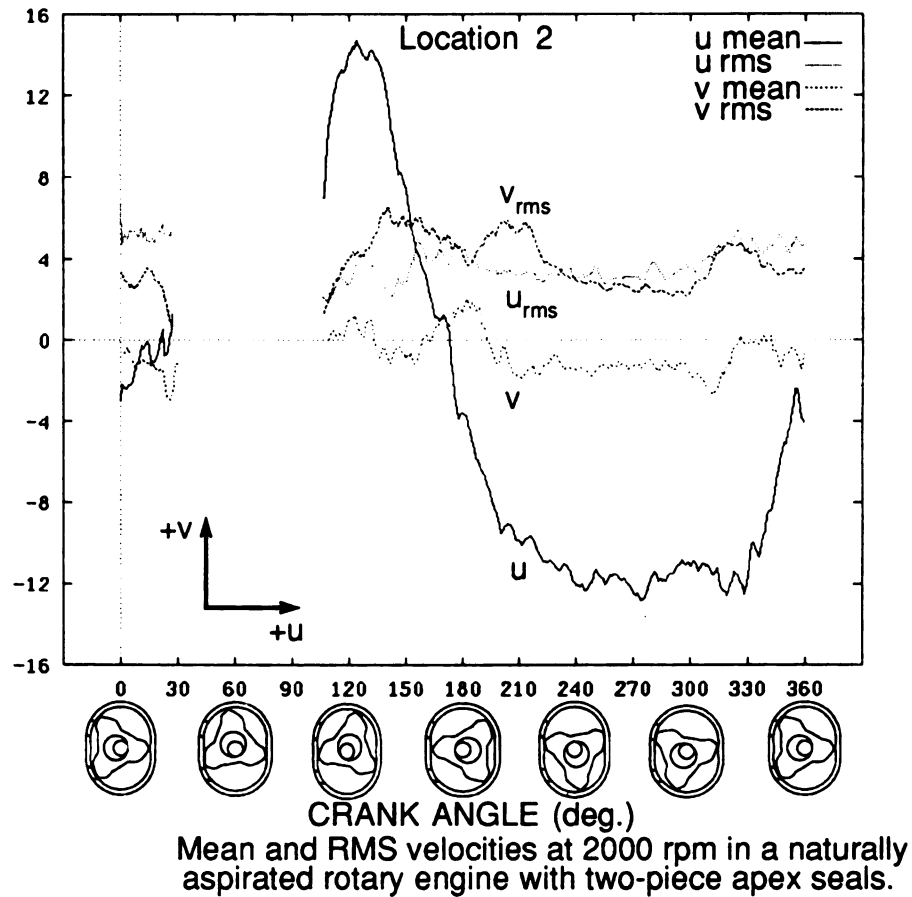


Figure 5 Displayed Results from Hamady [29]

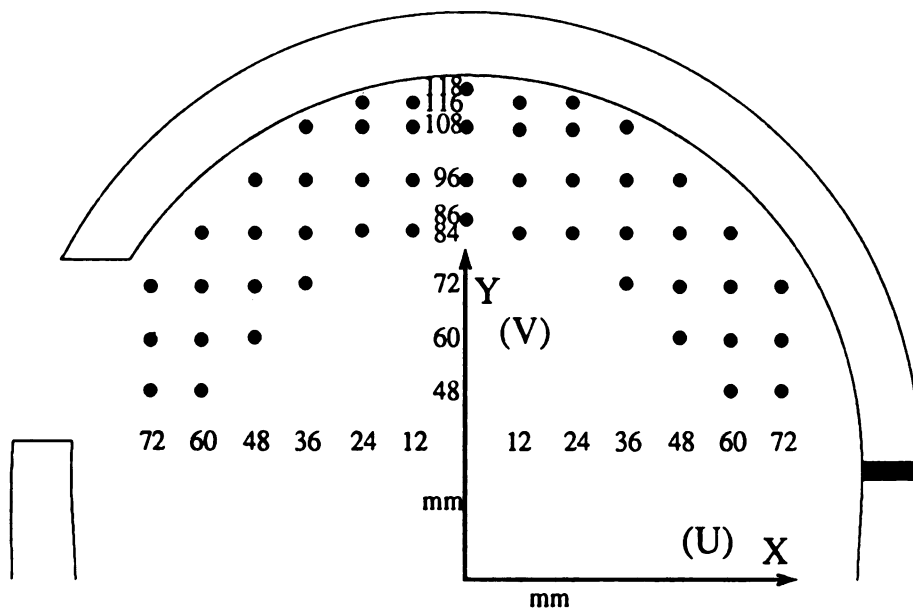


Figure 6 Measurement Locations

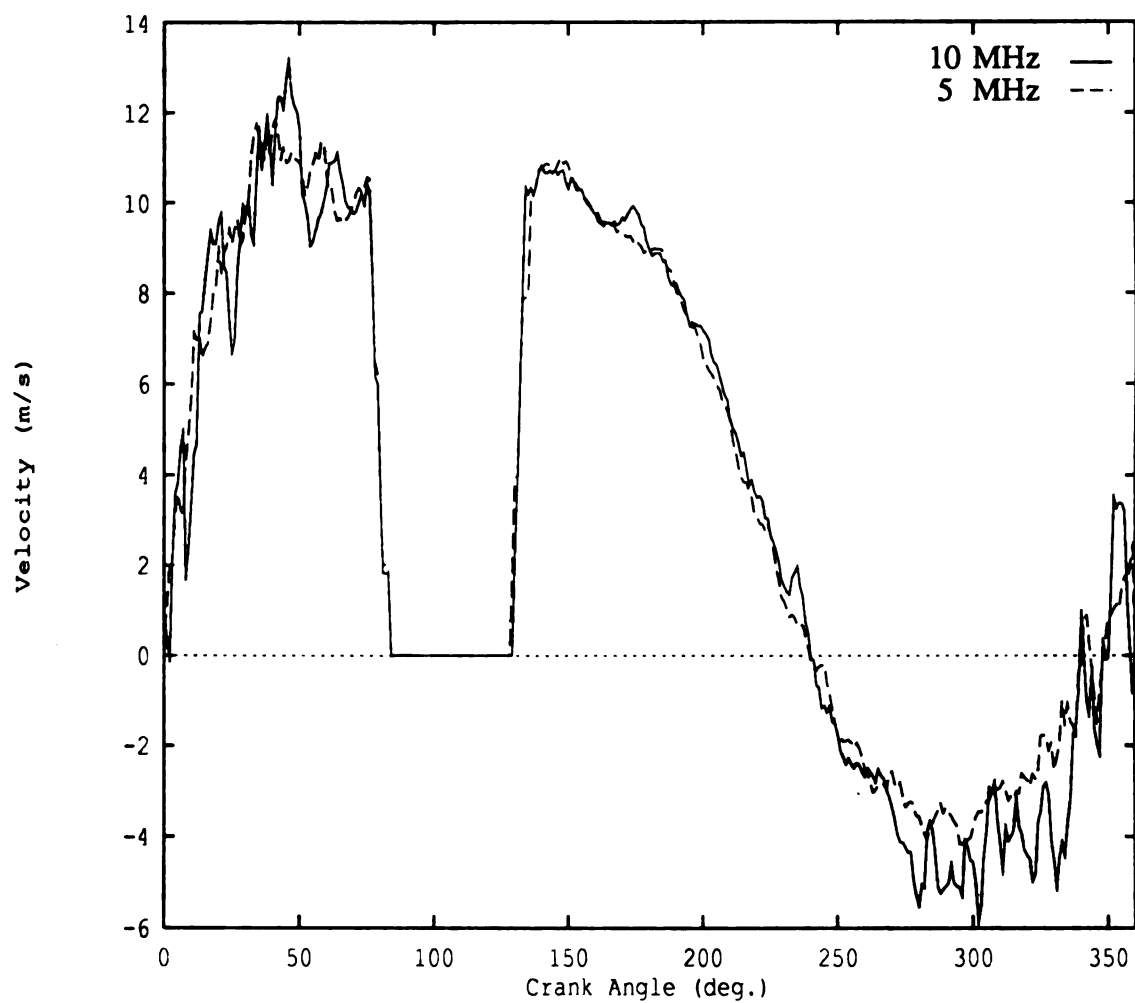
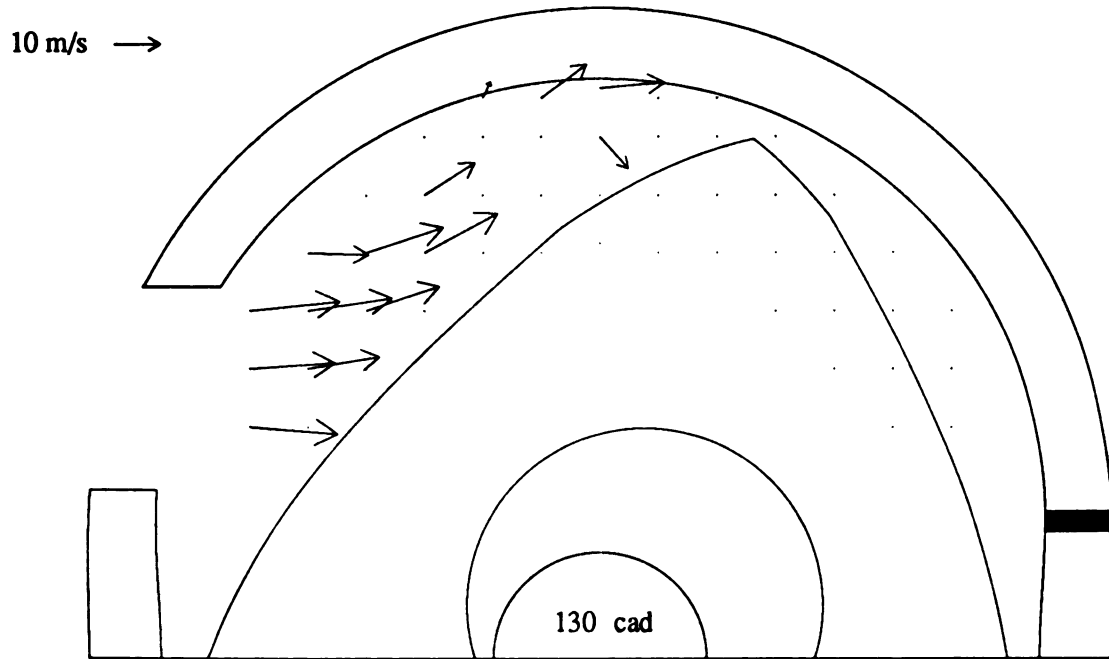
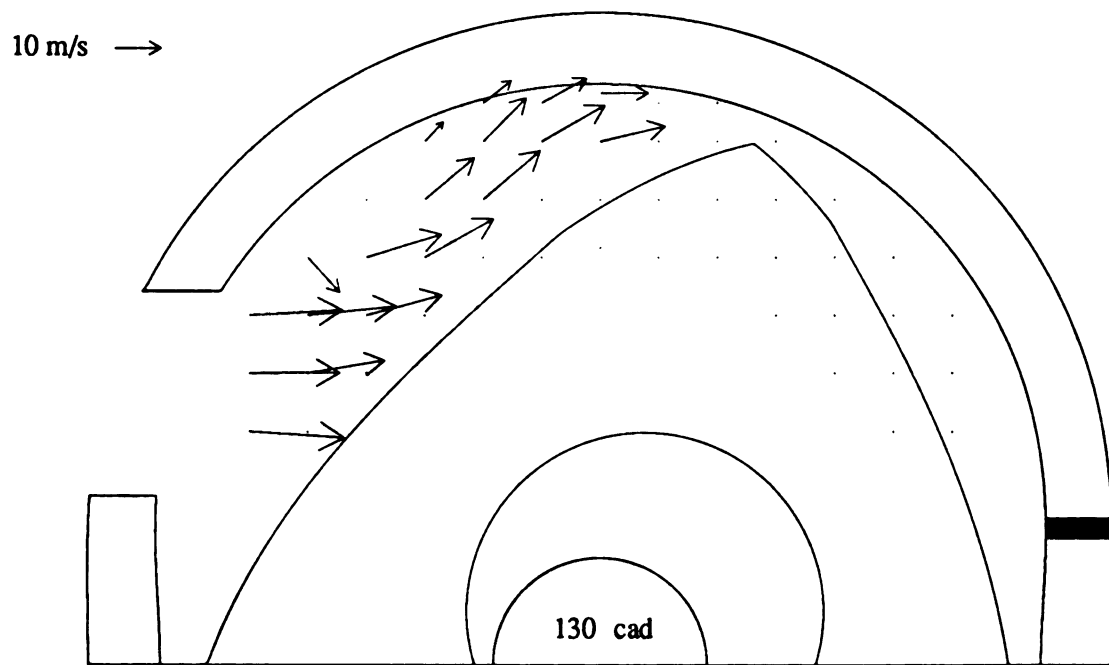


Figure 7 U Component of Velocity versus Crank Angle for
5 and 10 MHz Frequency Shift



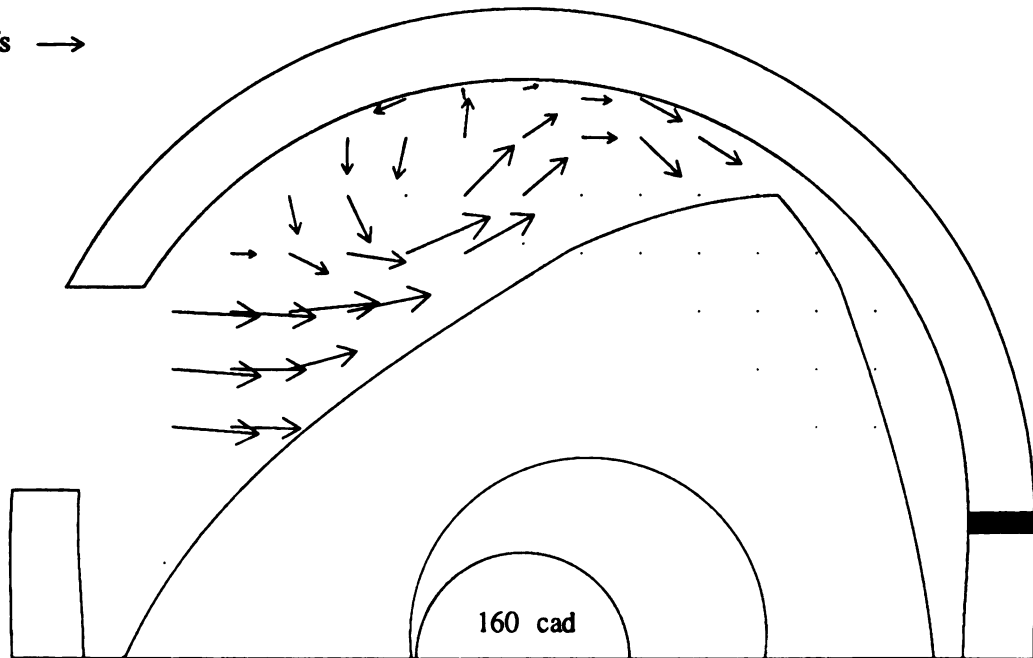
Mazda Leading Deep Recess - Mean Velocity



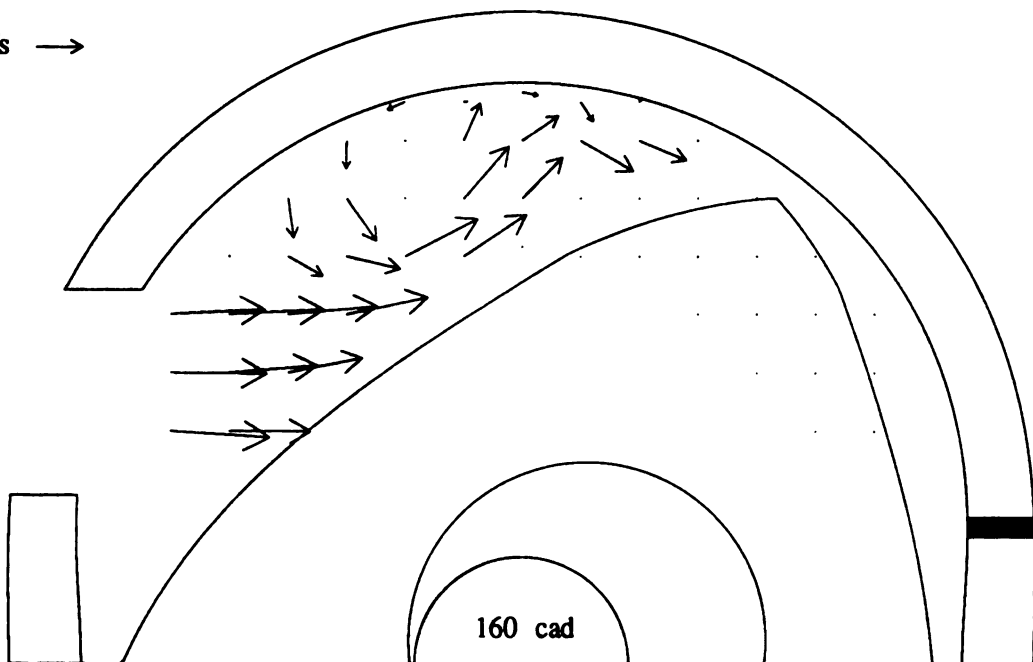
Symmetric Recess - Mean Velocity

Figure 8 Comparison of the Mean Velocity Flow Fields for the LDR and SMR rotors

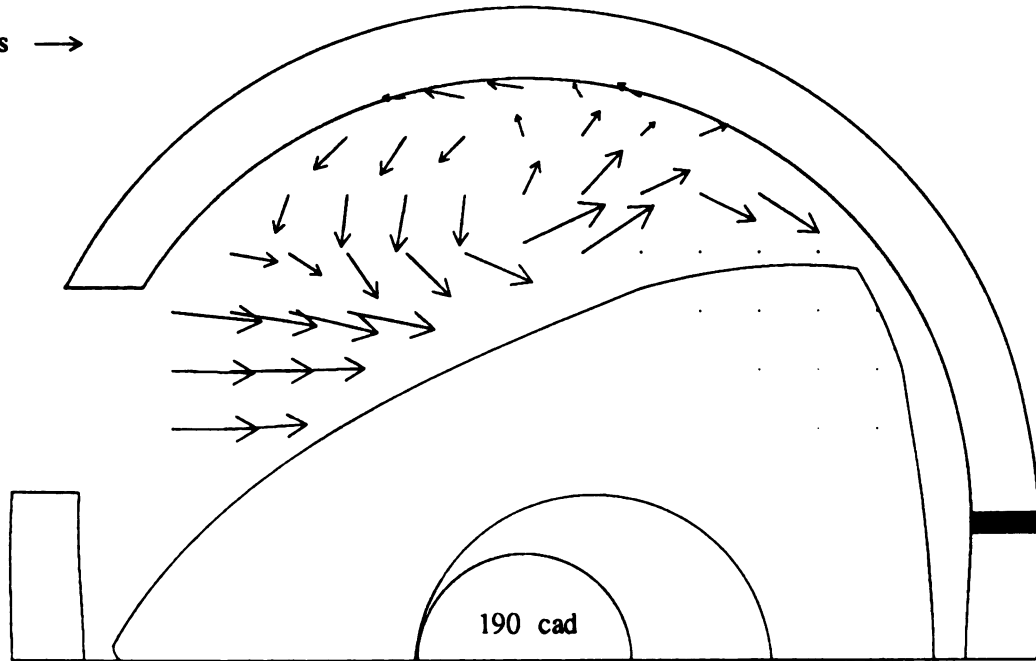
10 m/s →

**Mazda Leading Deep Recess - Mean Velocity**

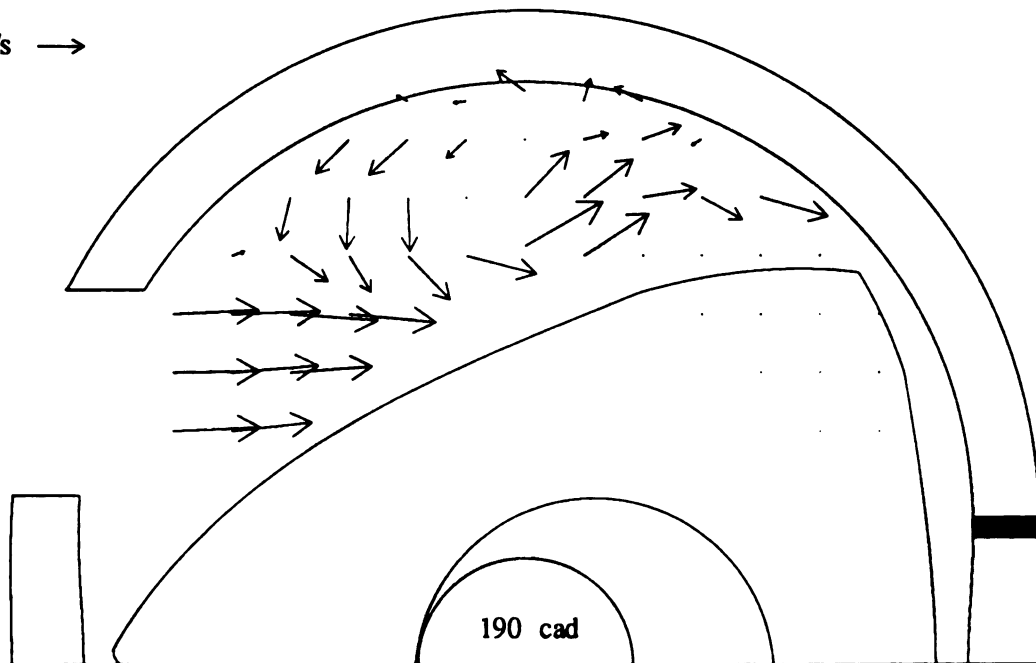
10 m/s →

**Symmetric Recess - Mean Velocity****Figure 8 cont. Comparison of the Mean Velocity Flow Fields for the LDR and SMR rotors**

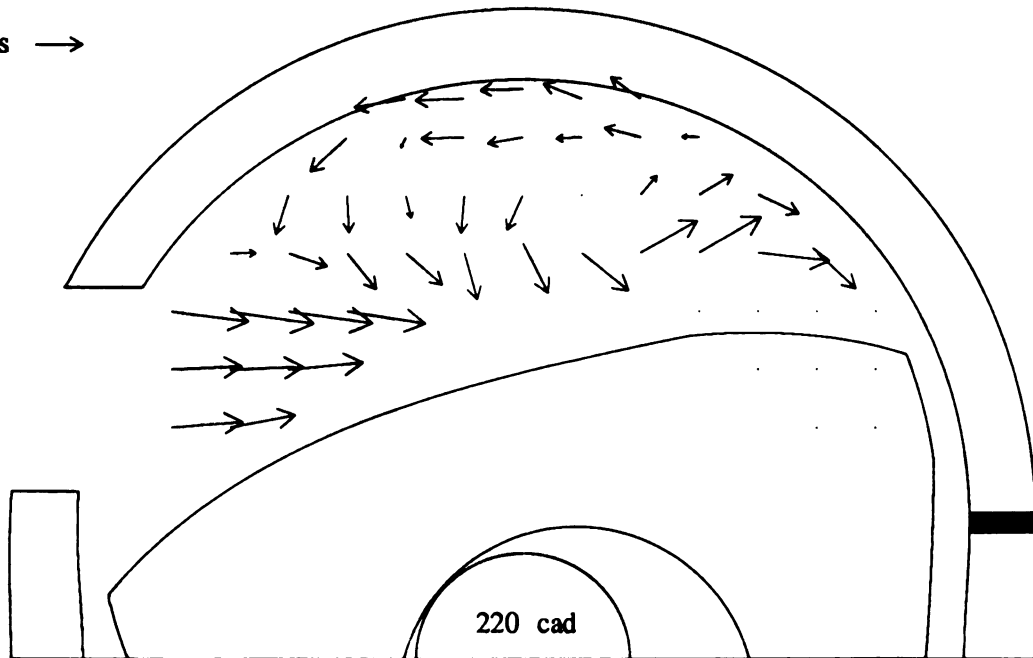
10 m/s →

**Mazda Leading Deep Recess - Mean Velocity**

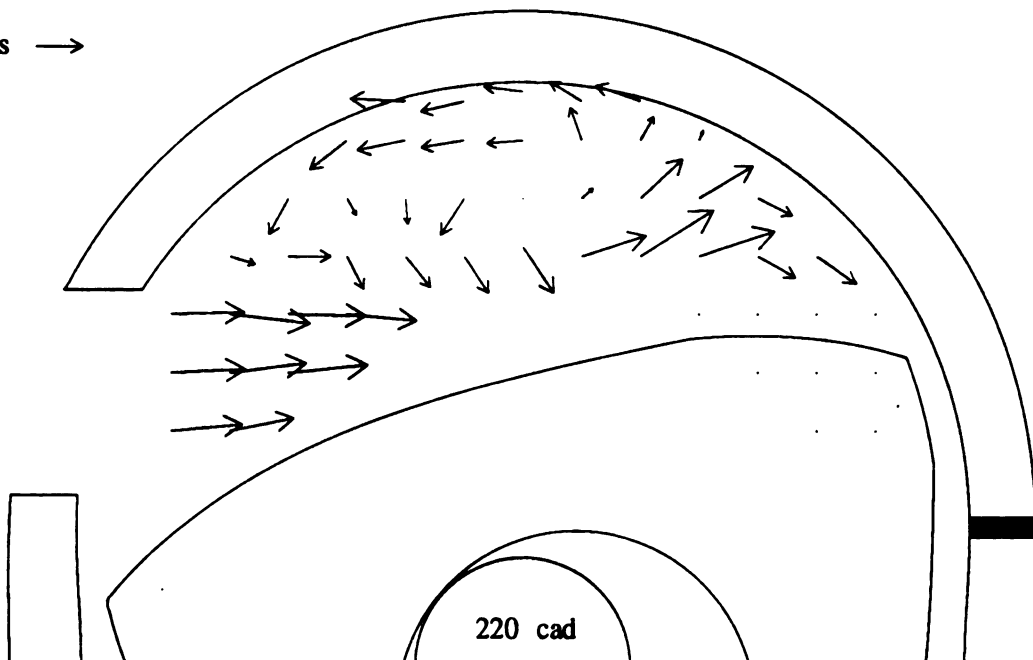
10 m/s →

**Symmetric Recess - Mean Velocity****Figure 8 cont. Comparison of the Mean Velocity Flow Fields for the LDR and SMR rotors**

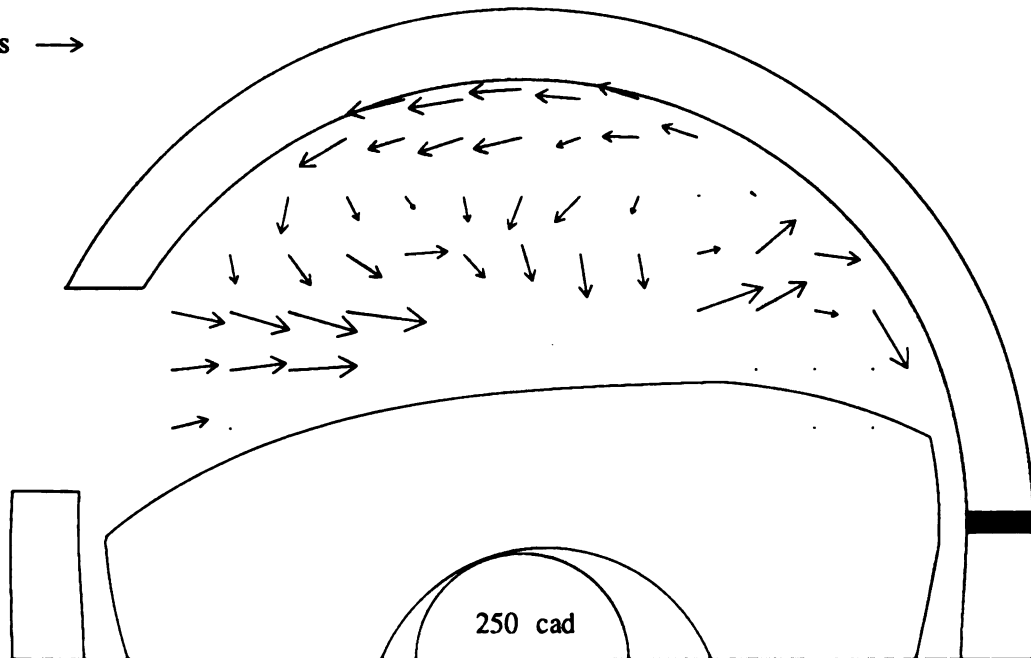
10 m/s →

**Mazda Leading Deep Recess - Mean Velocity**

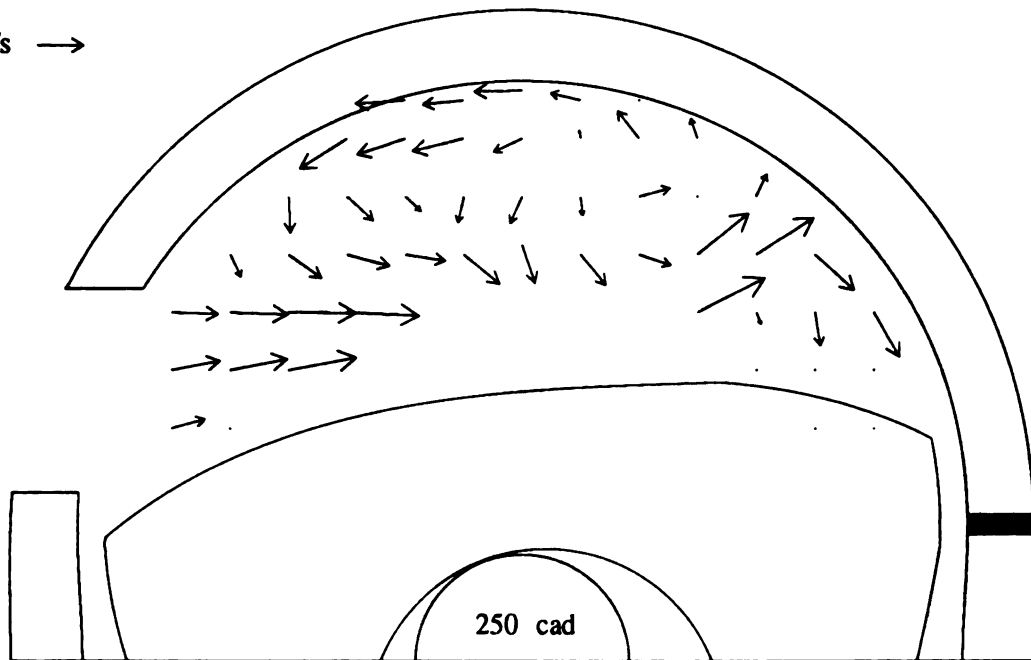
10 m/s →

**Symmetric Recess - Mean Velocity****Figure 8 cont. Comparison of the Mean Velocity Flow Fields for the LDR and SMR rotors**

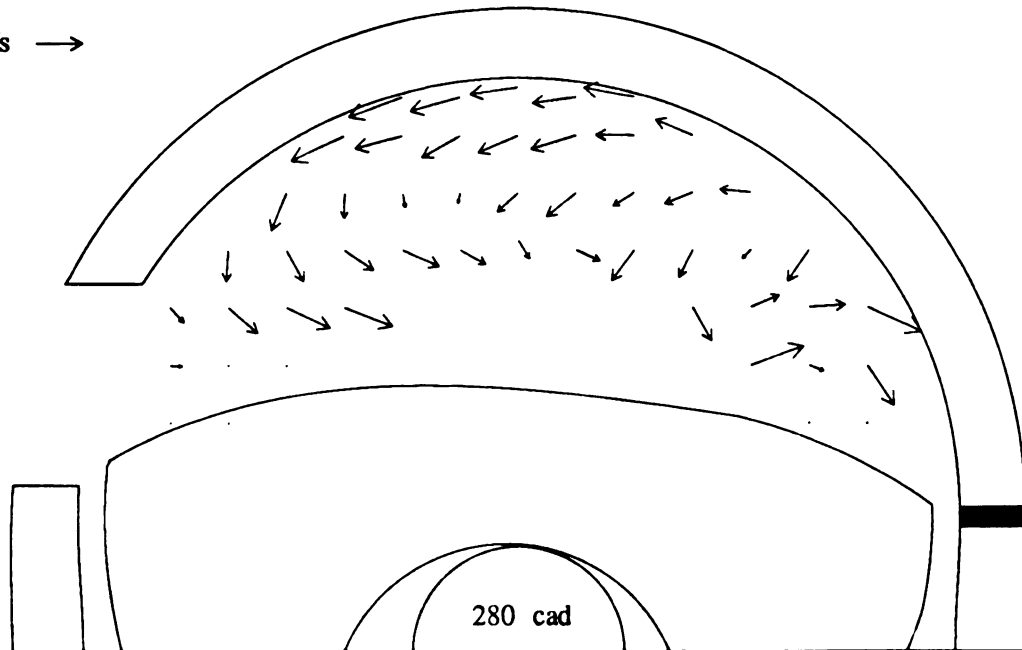
10 m/s →

**Mazda Leading Deep Recess - Mean Velocity**

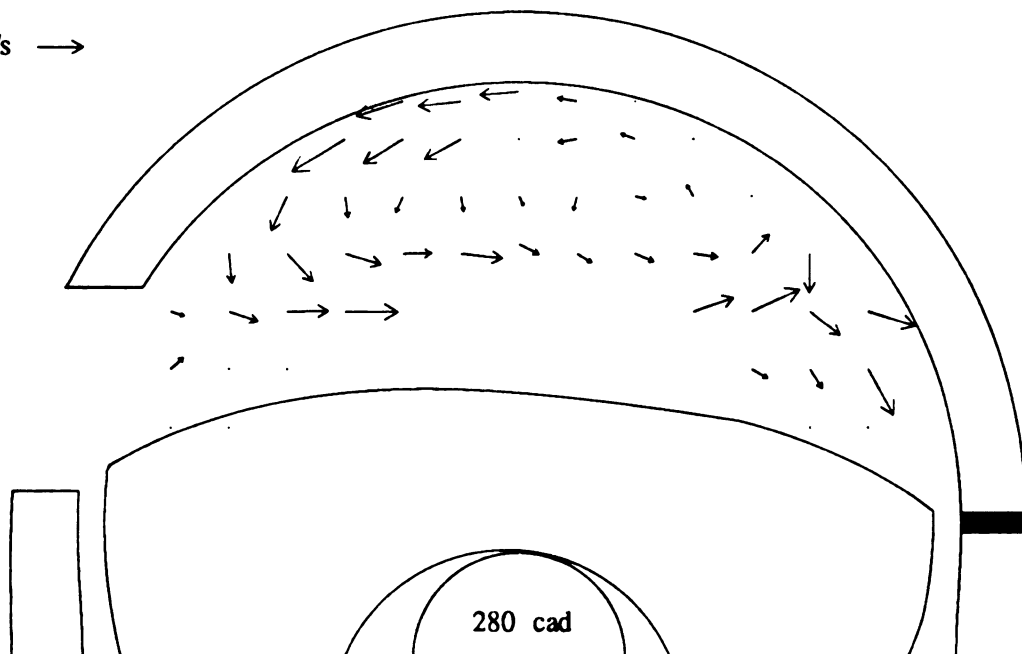
10 m/s →

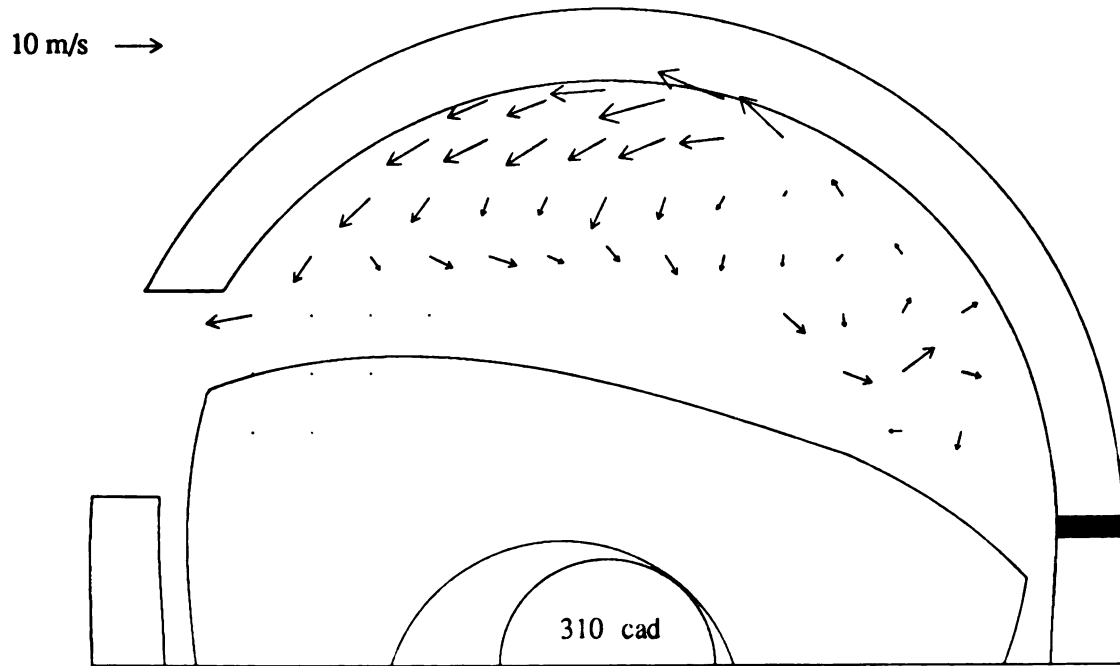
**Symmetric Recess - Mean Velocity****Figure 8 cont. Comparison of the Mean Velocity Flow Fields for the LDR and SMR rotors**

10 m/s →

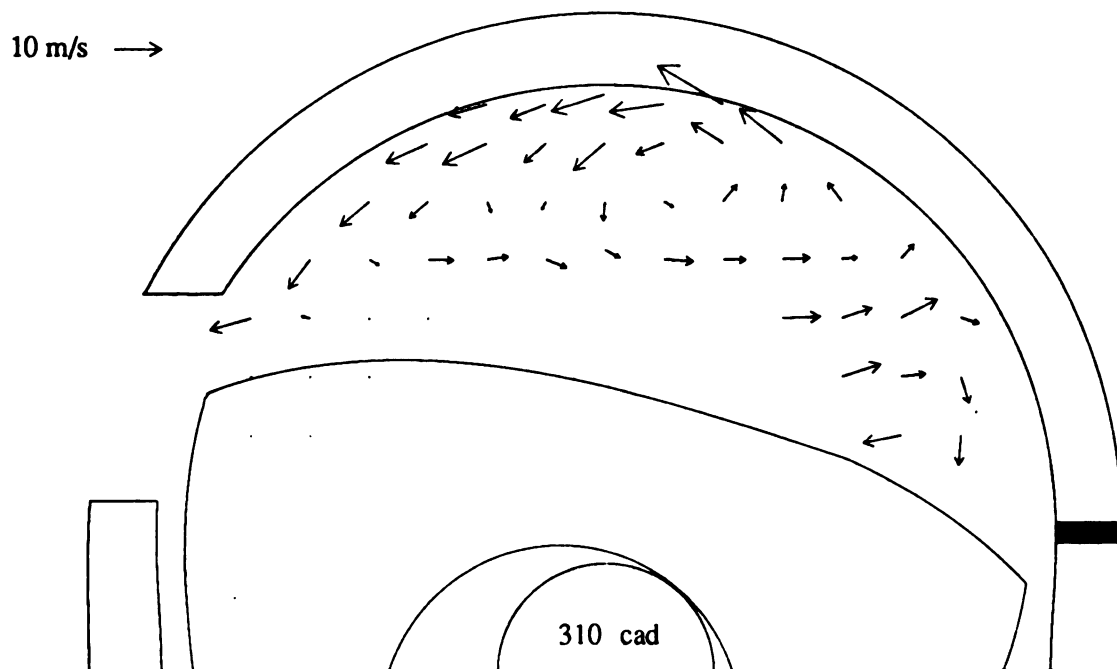
**Mazda Leading Deep Recess - Mean Velocity**

10 m/s →

**Symmetric Recess - Mean Velocity****Figure 8 cont. Comparison of the Mean Velocity Flow Fields for the LDR and SMR rotors**



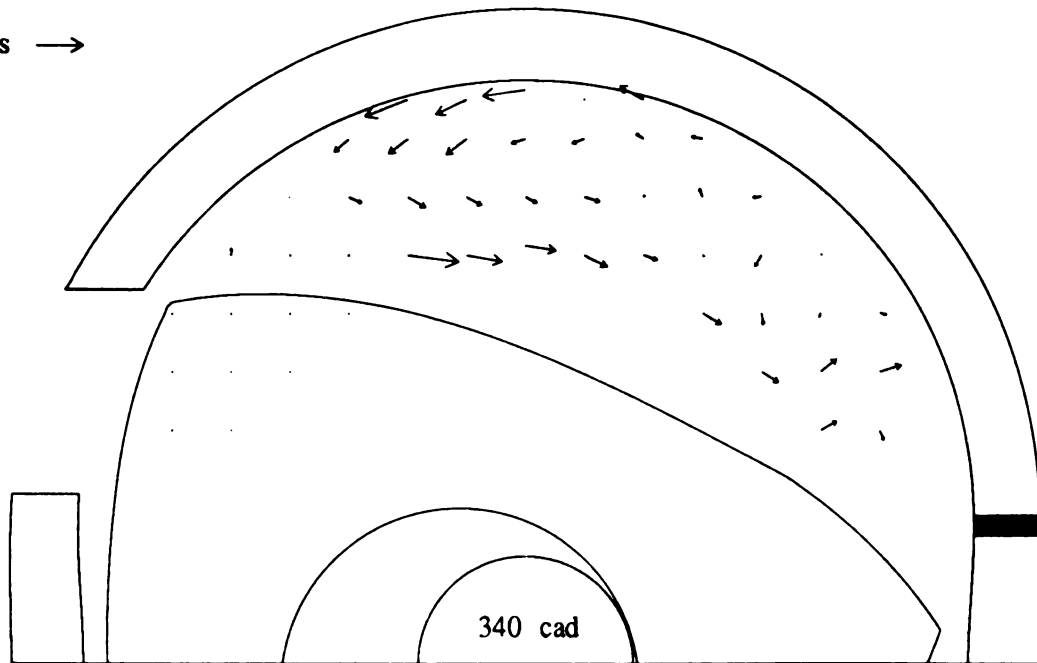
Mazda Leading Deep Recess - Mean Velocity



Symmetric Recess - Mean Velocity

Figure 8 cont. Comparison of the Mean Velocity Flow Fields for the LDR and SMR rotors

10 m/s →

**Mazda Leading Deep Recess - Mean Velocity**

10 m/s →

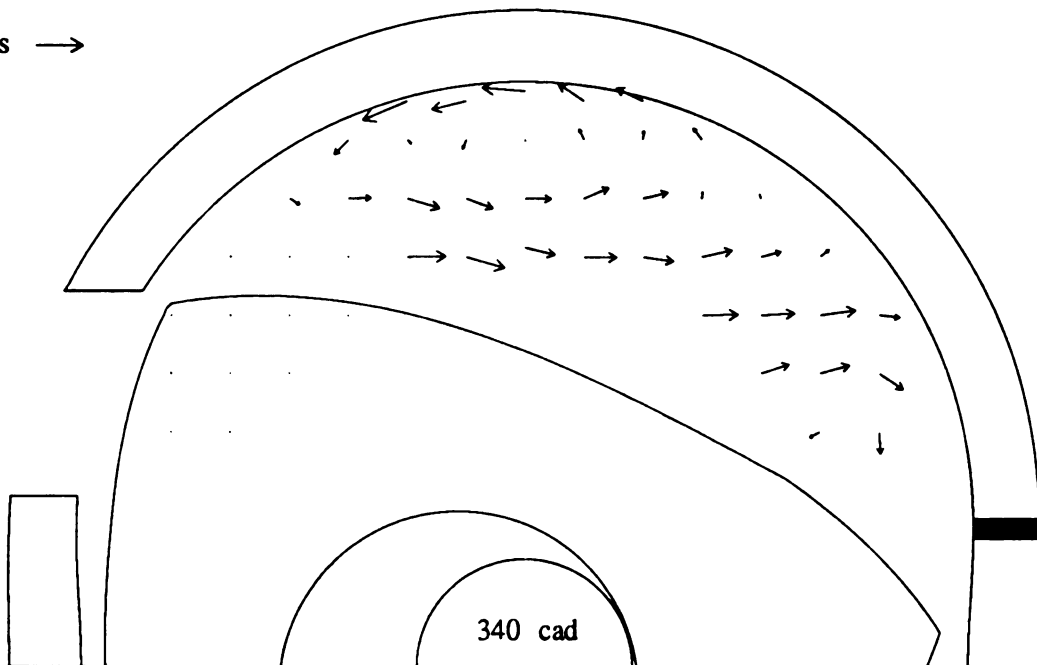
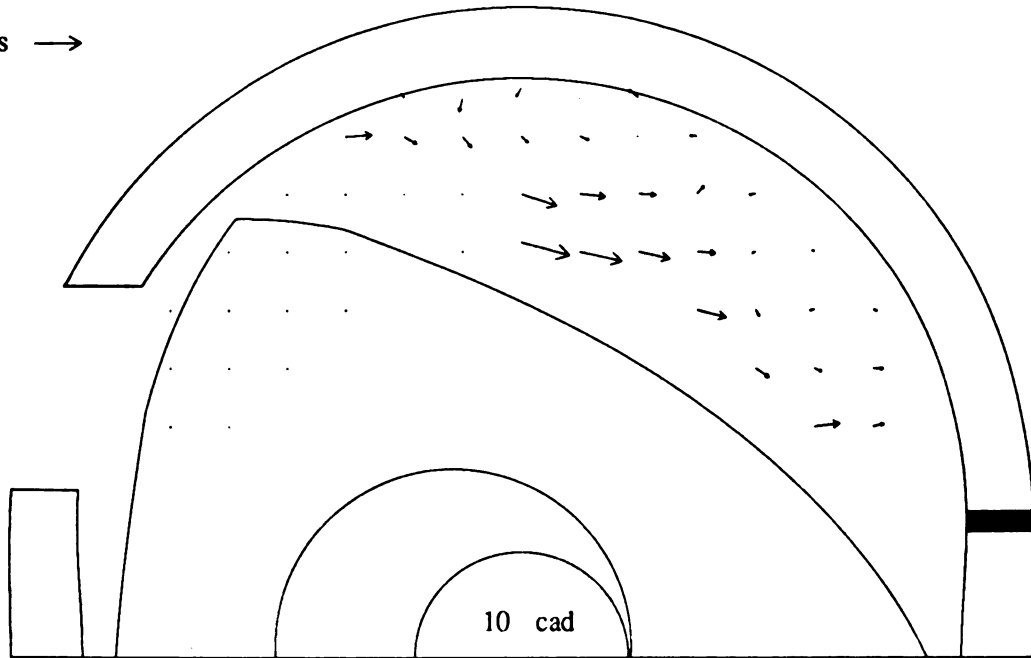
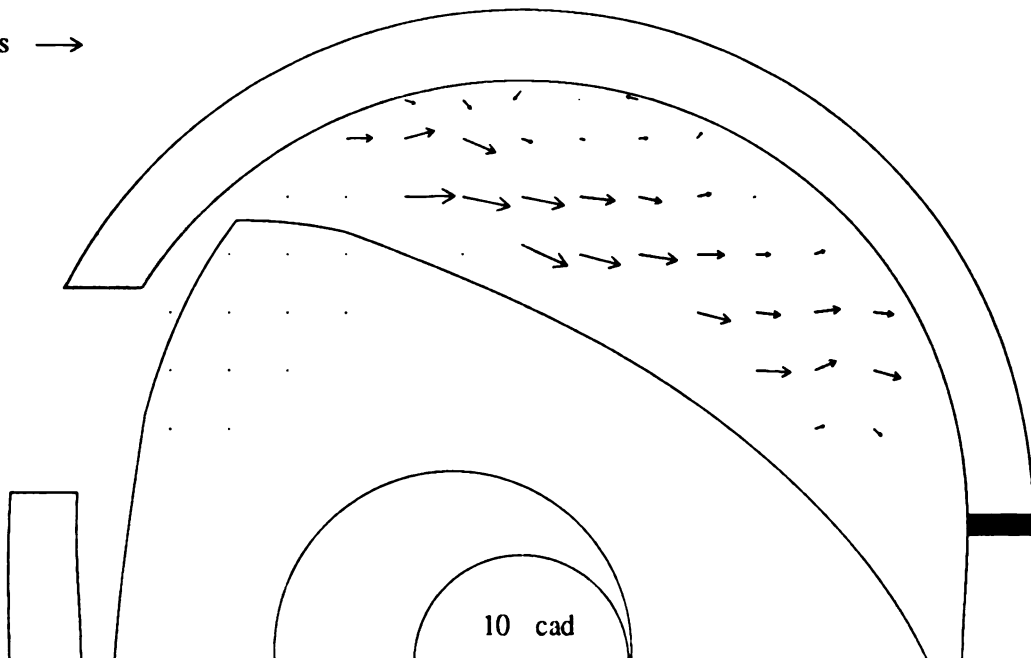
**Symmetric Recess - Mean Velocity**

Figure 8 cont. Comparison of the Mean Velocity Flow Fields for the LDR and SMR rotors

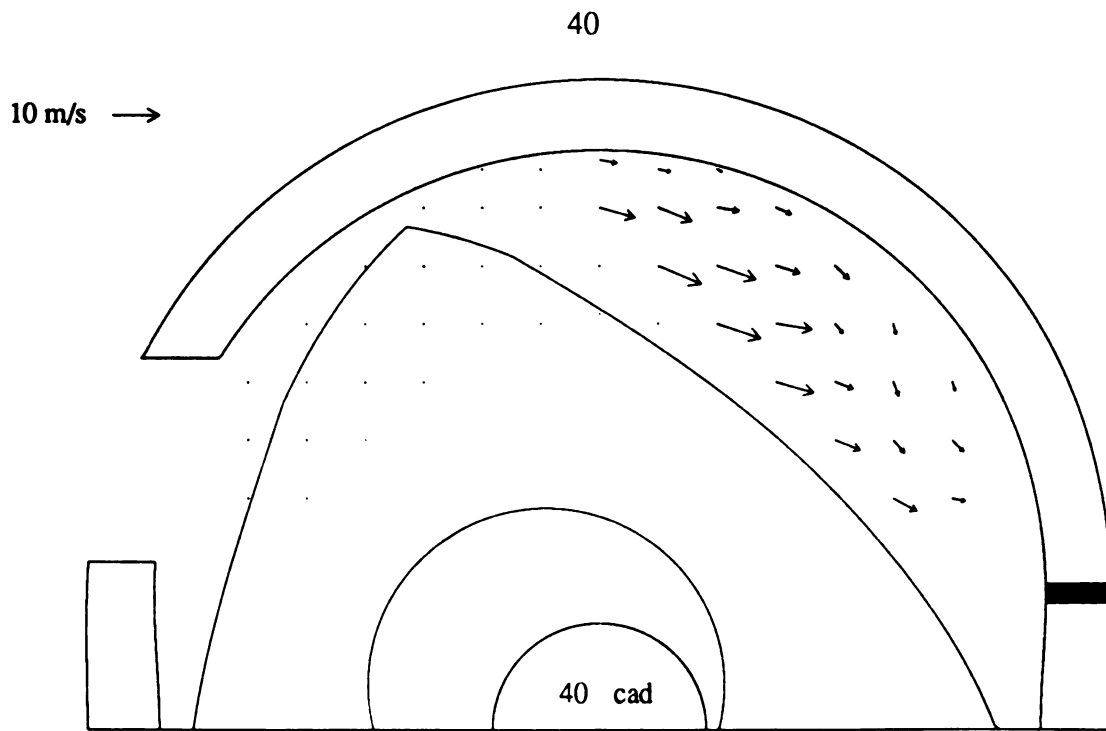
10 m/s →

**Mazda Leading Deep Recess - Mean Velocity**

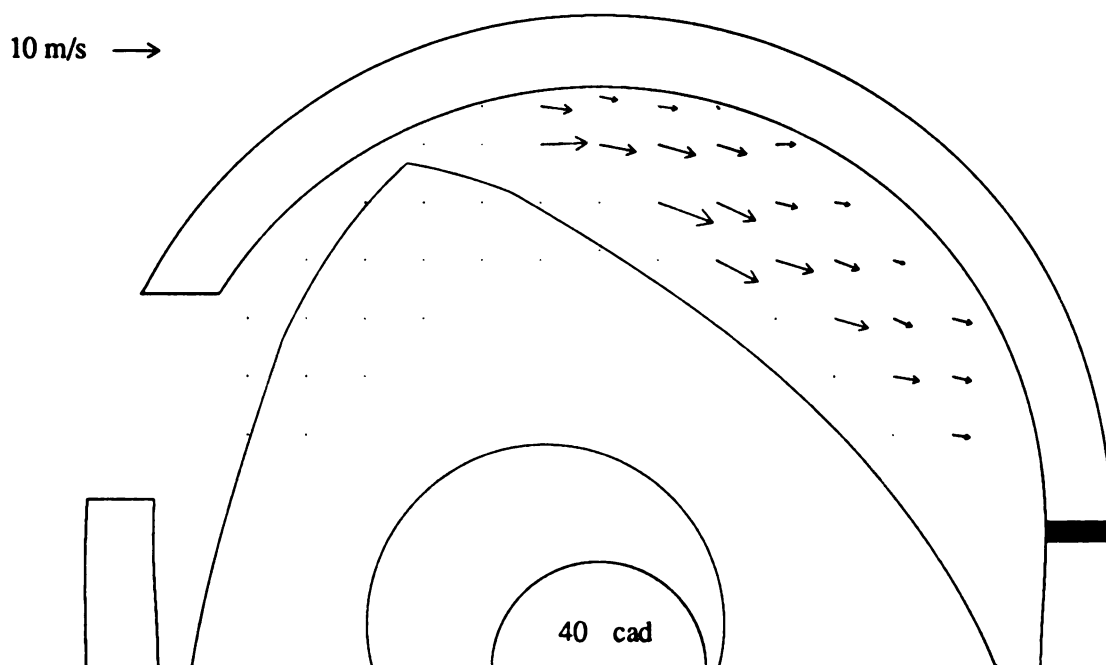
10 m/s →

**Symmetric Recess - Mean Velocity**

**Figure 8 cont. Comparison of the Mean Velocity Flow Fields for
the LDR and SMR rotors**



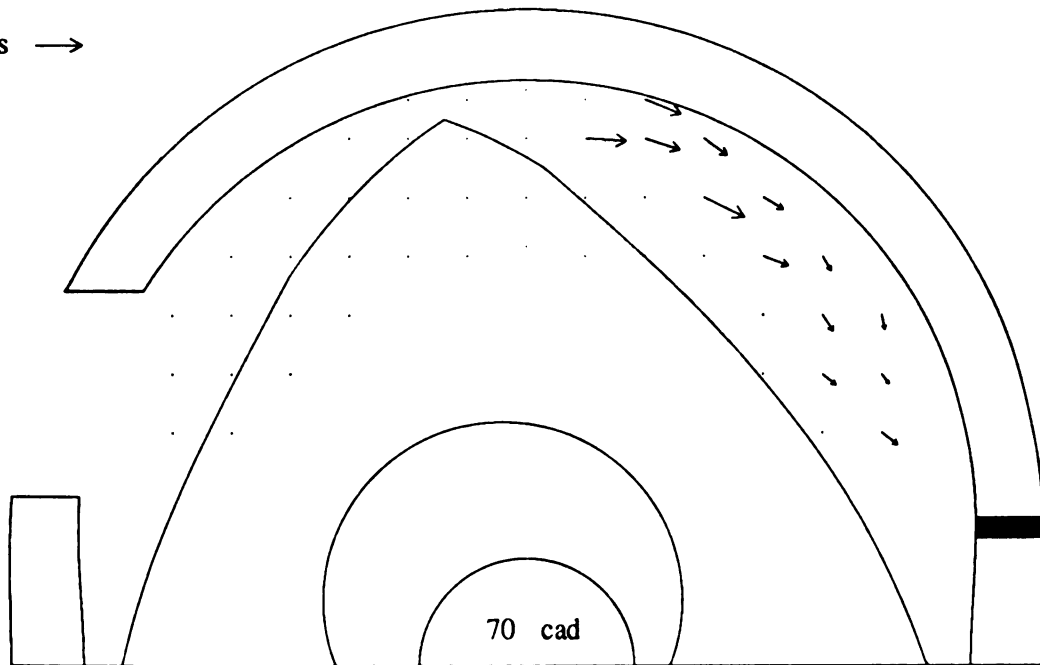
Mazda Leading Deep Recess - Mean Velocity



Symmetric Recess - Mean Velocity

Figure 8 cont. Comparison of the Mean Velocity Flow Fields for the LDR and SMR rotors

10 m/s →

**Mazda Leading Deep Recess - Mean Velocity**

10 m/s →

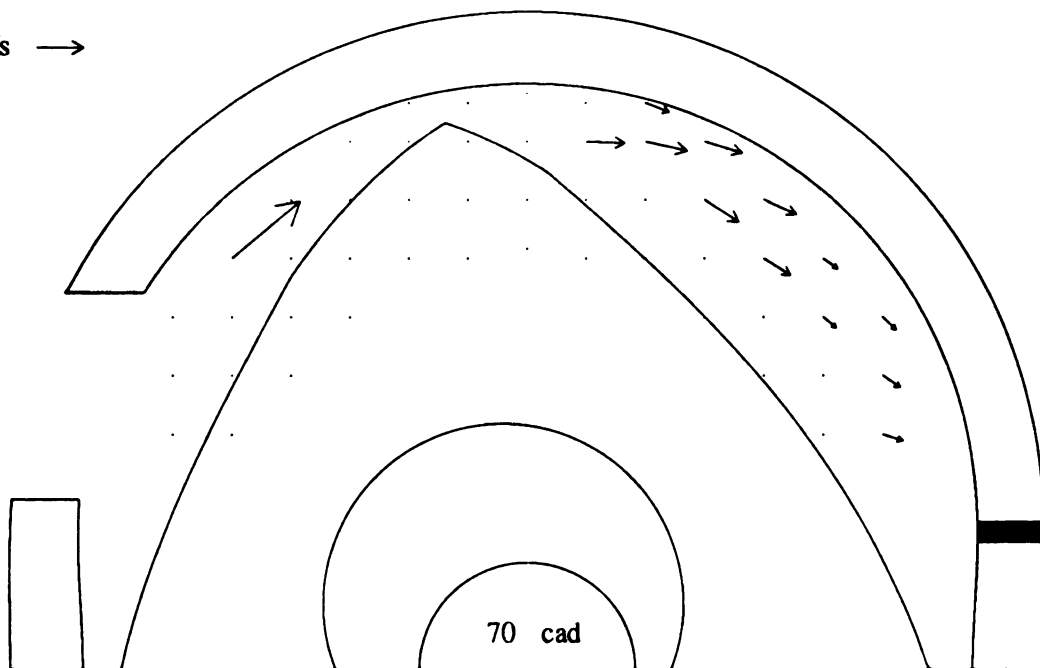
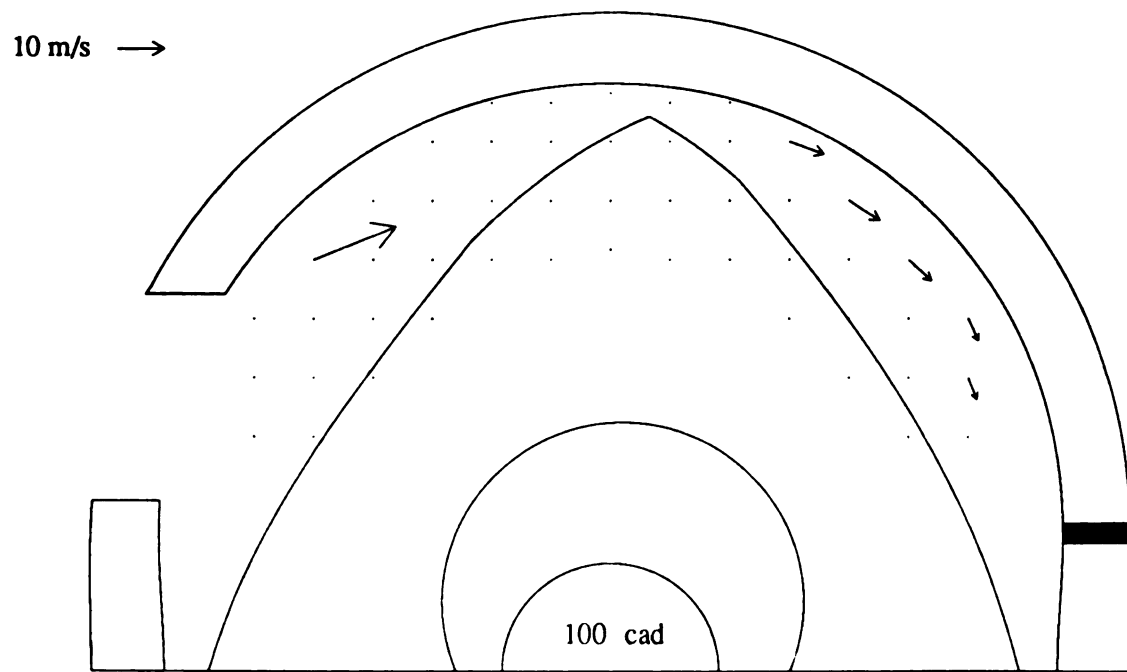
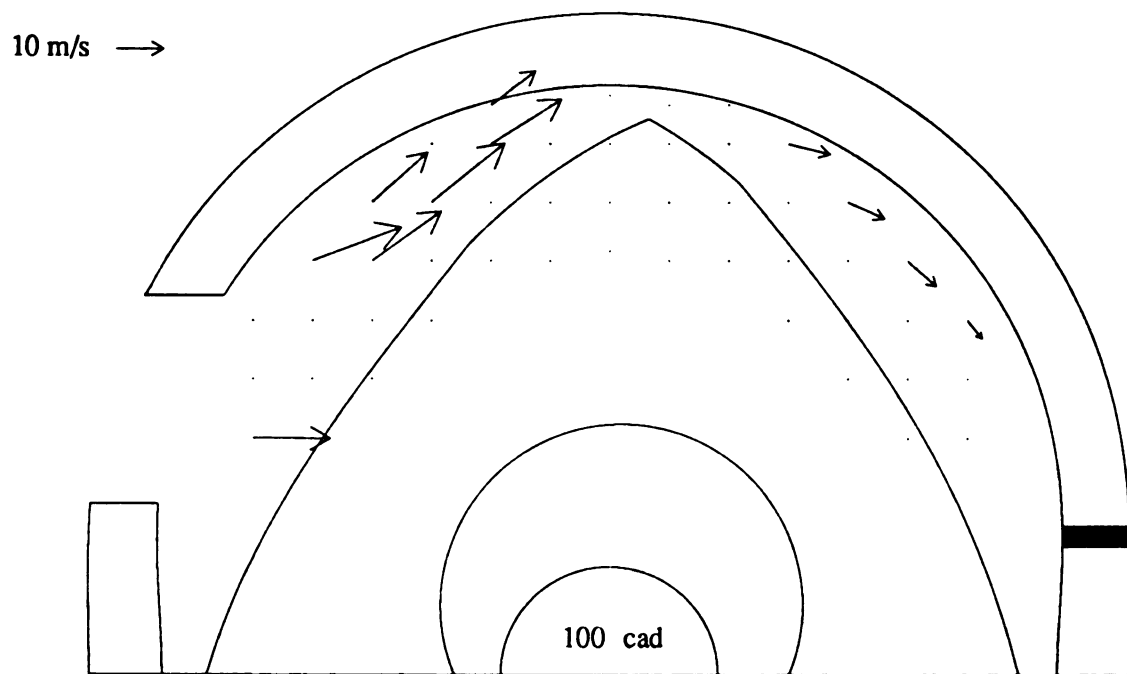
**Symmetric Recess - Mean Velocity**

Figure 8 cont. Comparison of the Mean Velocity Flow Fields for the LDR and SMR rotors



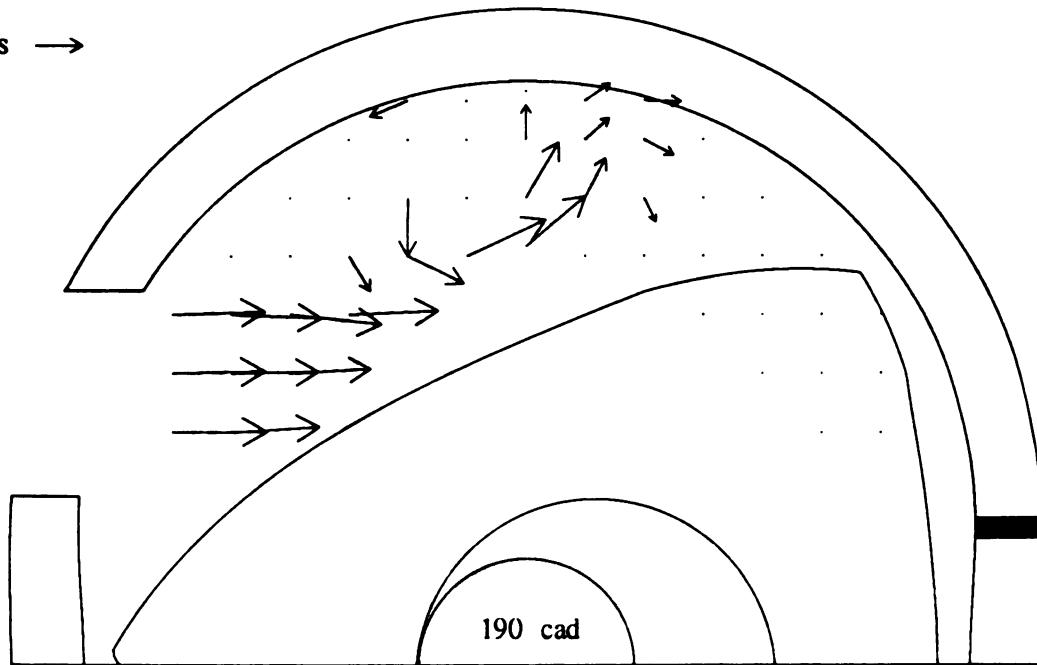
Mazda Leading Deep Recess - Mean Velocity



Symmetric Recess - Mean Velocity

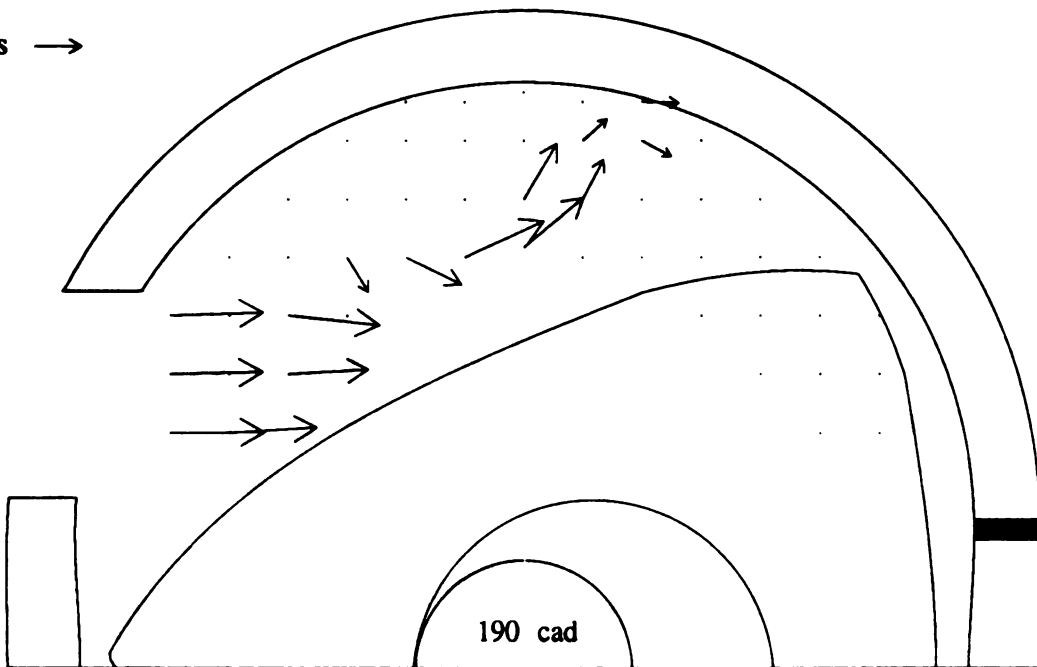
Figure 8 cont. Comparison of the Mean Velocity Flow Fields for the LDR and SMR rotors

10 m/s →



Symmetric Recess, No Compression - Mean Velocity
30 minimum

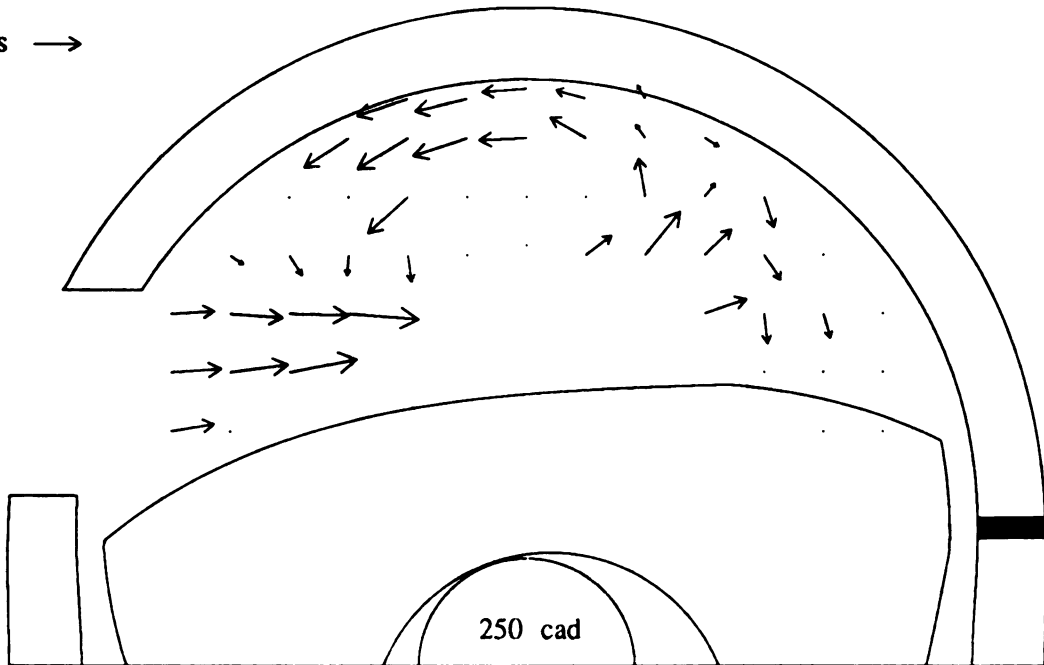
10 m/s →



Symmetric Recess, No Compression - Mean Velocity
50 minimum

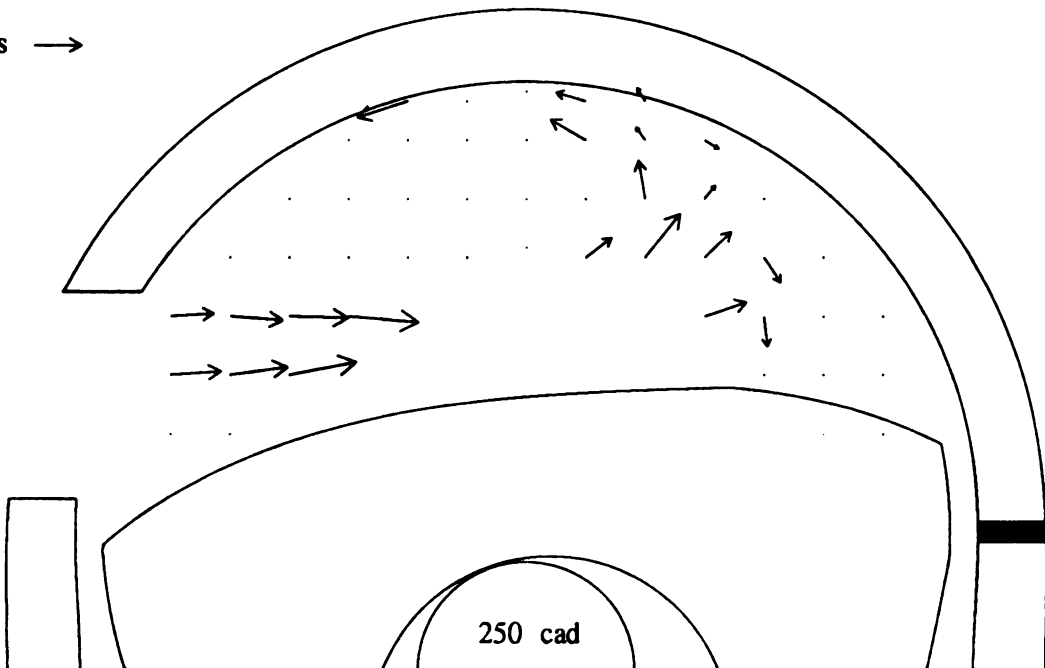
Figure 9 Comparison of 30 and 50 Count Minimums

10 m/s →



Symmetric Recess, No Compression - Mean Velocity
30 minimum

10 m/s →



Symmetric Recess, No Compression - Mean Velocity
50 minimum

Figure 9 Comparison of 30 and 50 Count Minimums

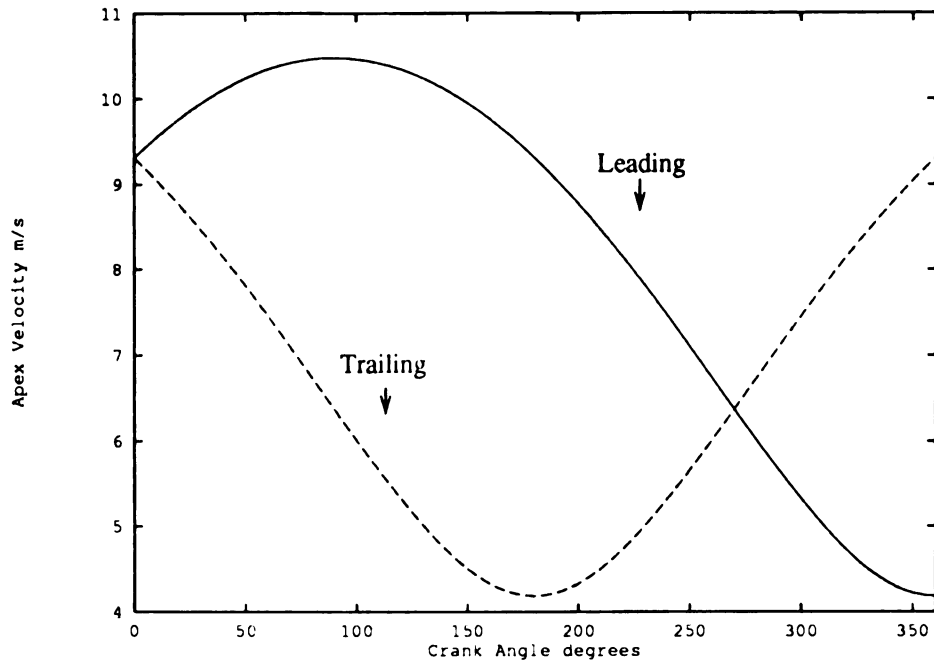


Figure 10 Velocities of the Leading and Trailing Apex Seals

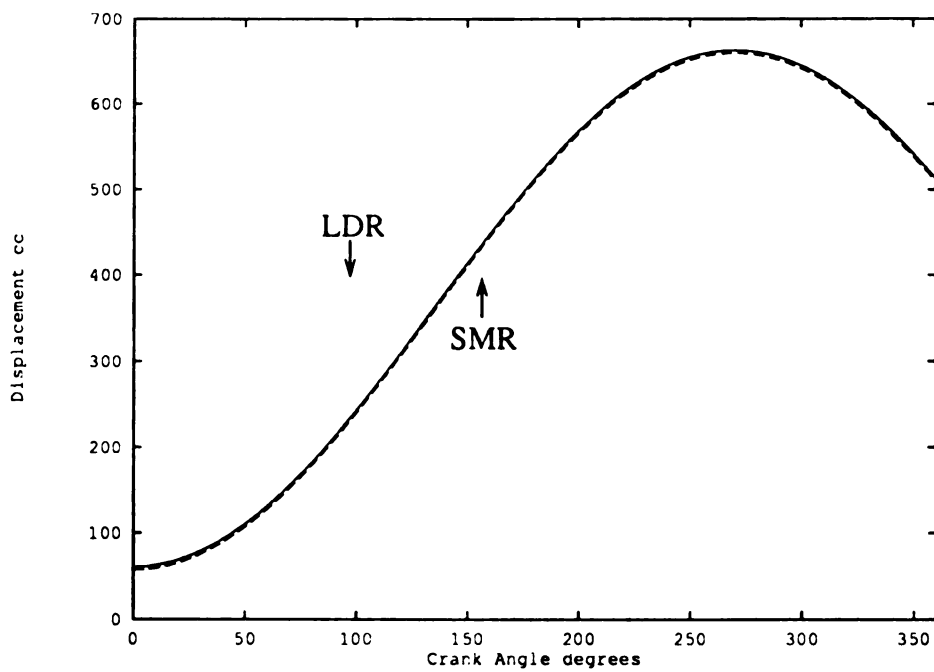
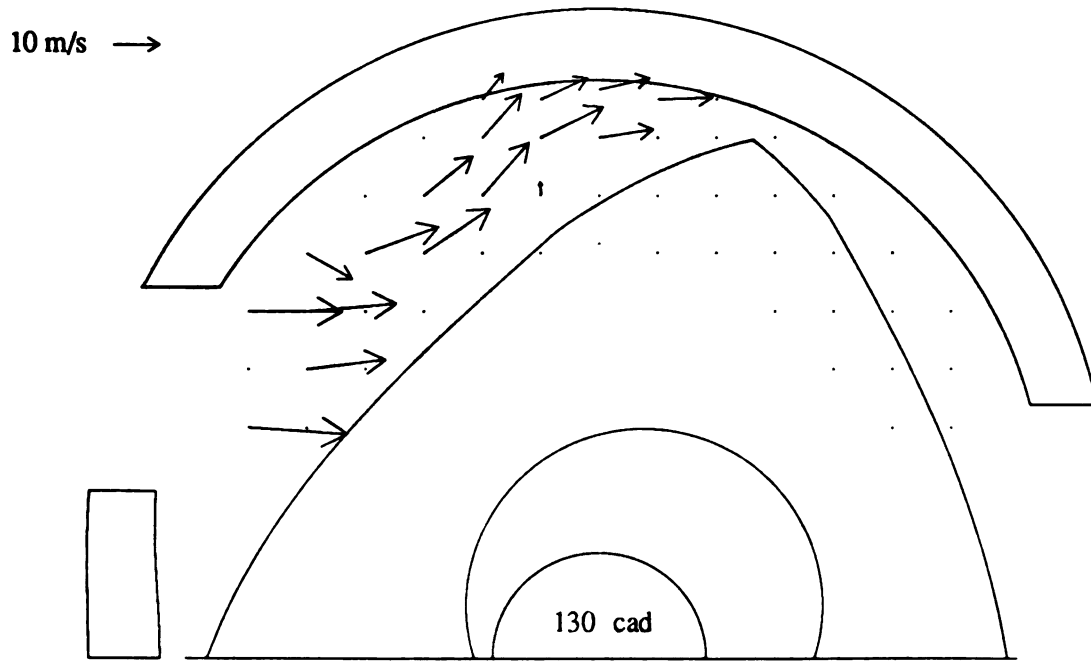
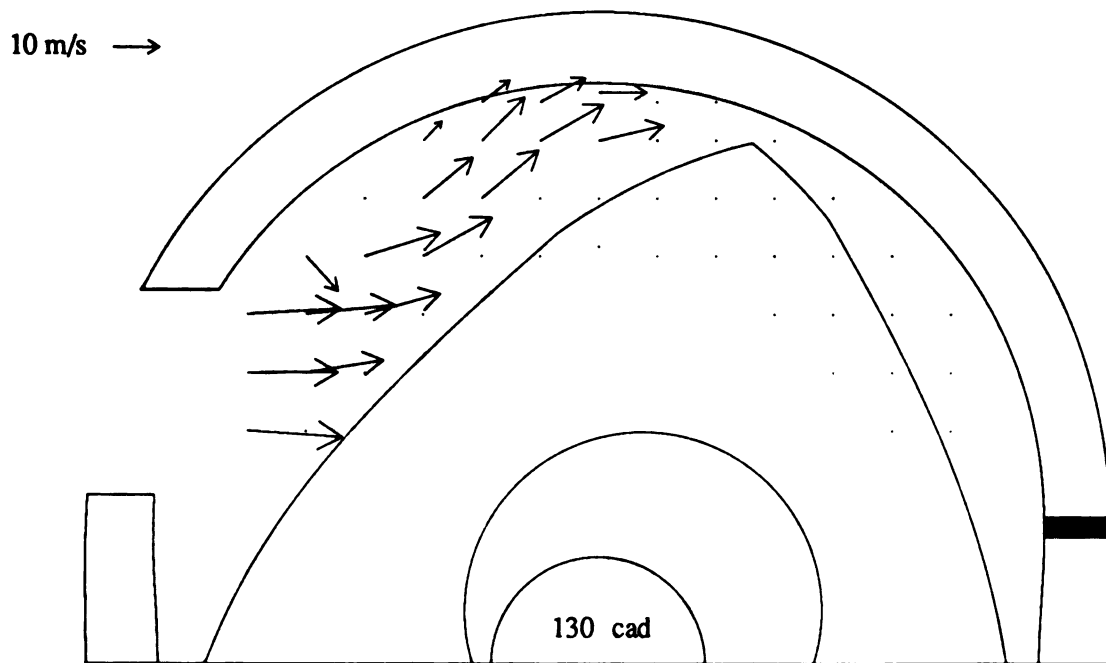


Figure 11 Volume of Working Chamber Versus Crank Angle



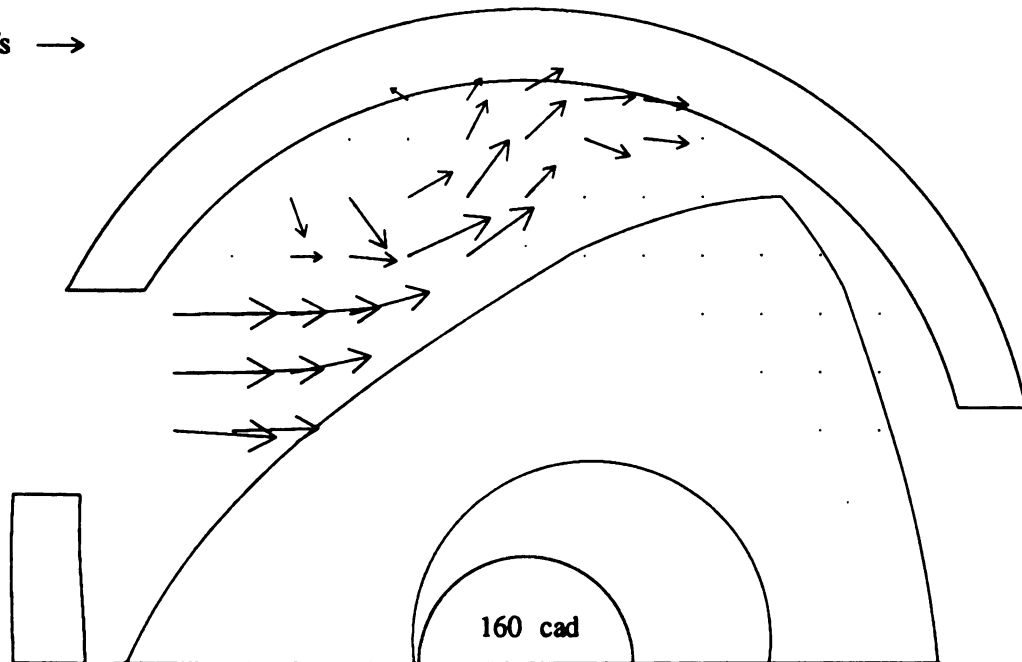
Symmetric Recess, No Compression - Mean Velocity



Symmetric Recess - Mean Velocity

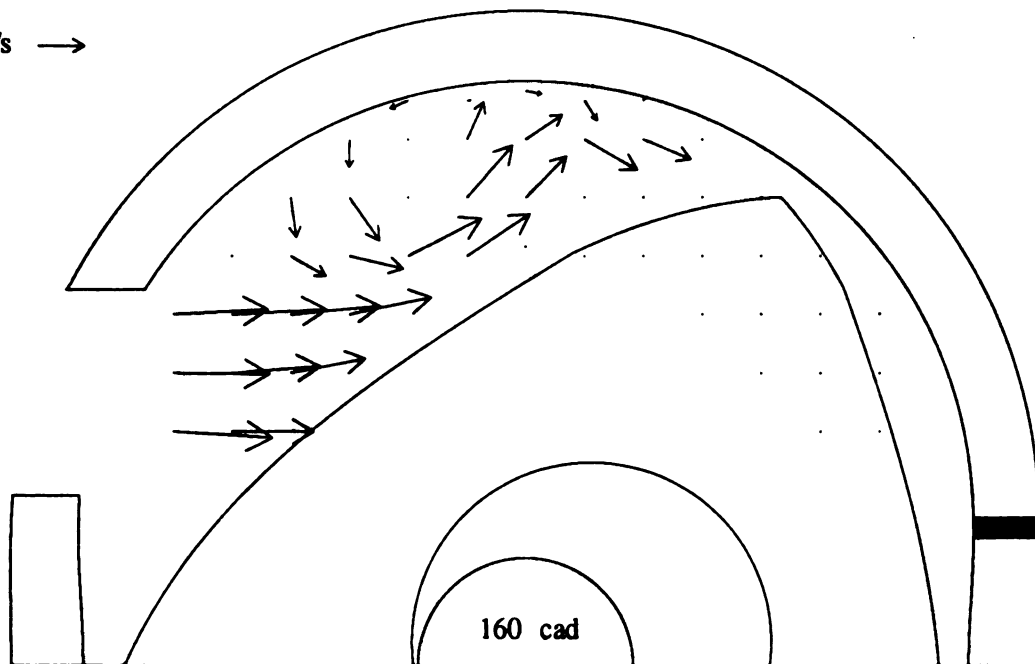
Figure 12 Comparison of the Mean Velocity Flow Fields for the SMR Rotor With and Without Compression

10 m/s →



Symmetric Recess, No Compression - Mean Velocity

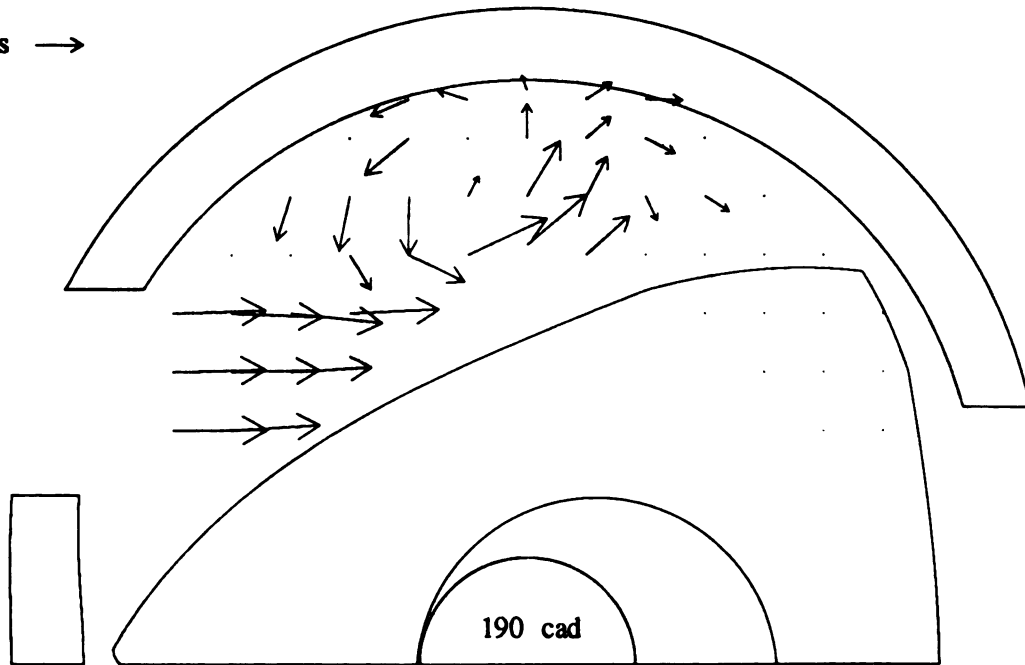
10 m/s →



Symmetric Recess - Mean Velocity

Figure 12 cont. Comparison of the Mean Velocity Flow Fields for the SMR Rotor With and Without Compression

10 m/s →

**Symmetric Recess, No Compression - Mean Velocity**

10 m/s →

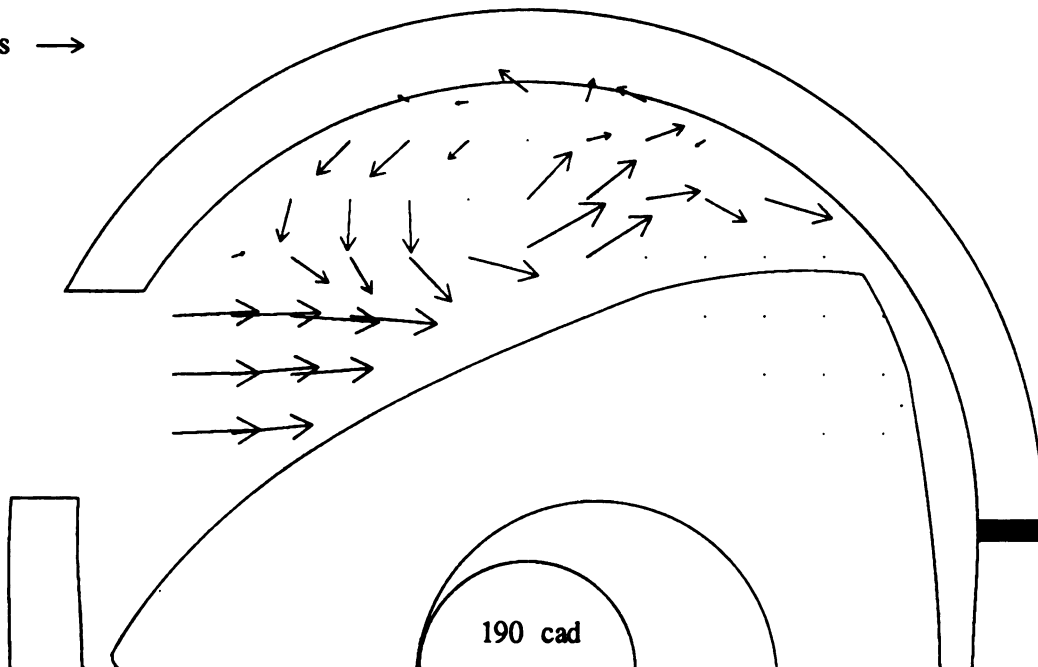
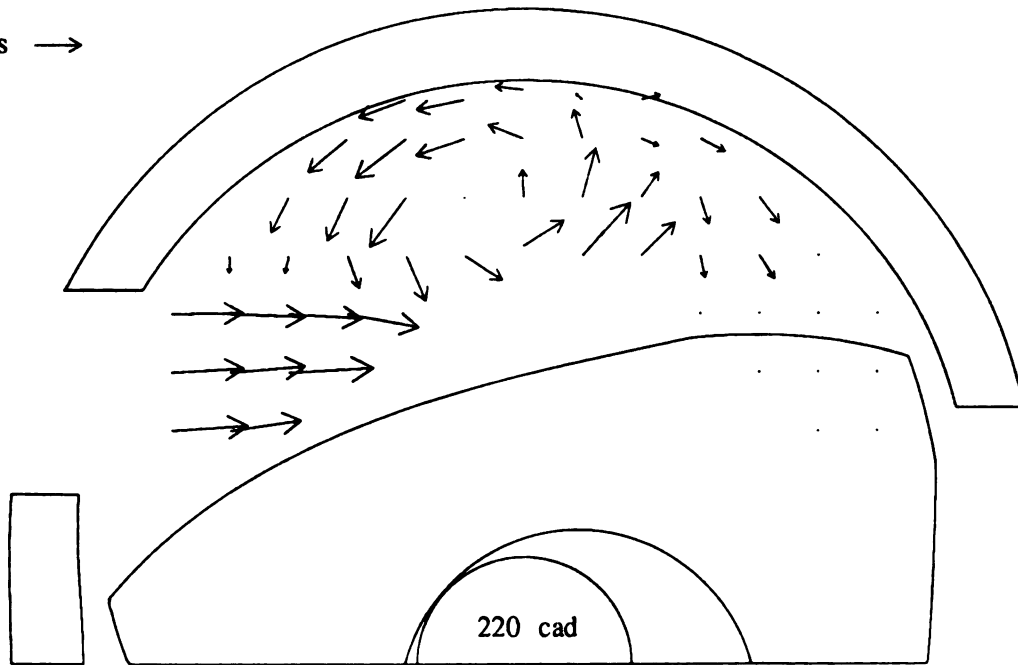
**Symmetric Recess - Mean Velocity**

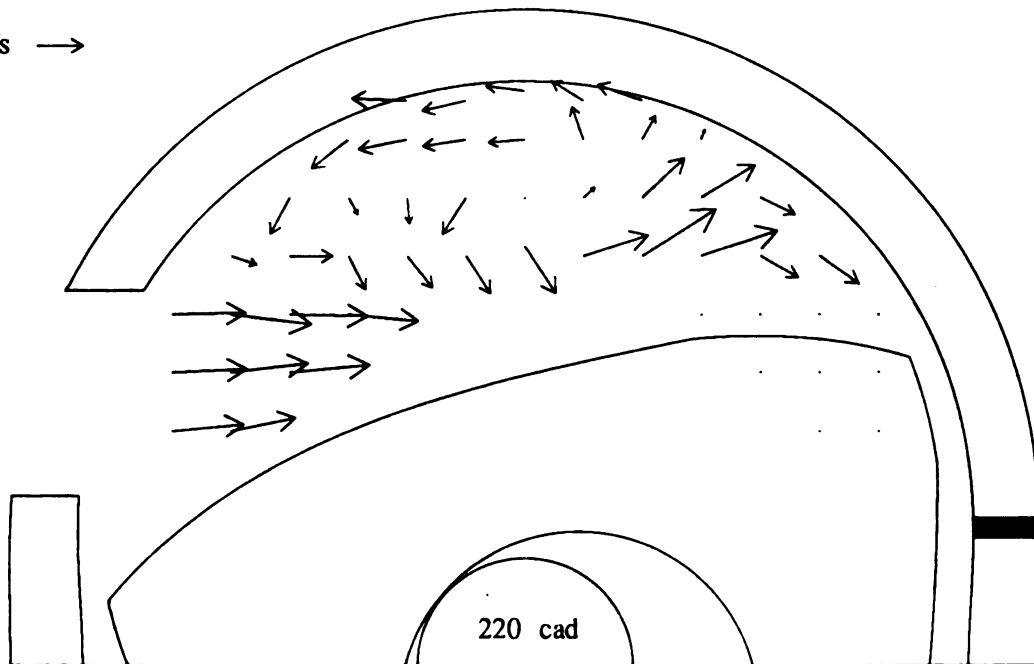
Figure 12 cont. Comparison of the Mean Velocity Flow Fields for the SMR Rotor With and Without Compression

10 m/s →



Symmetric Recess, No Compression - Mean Velocity

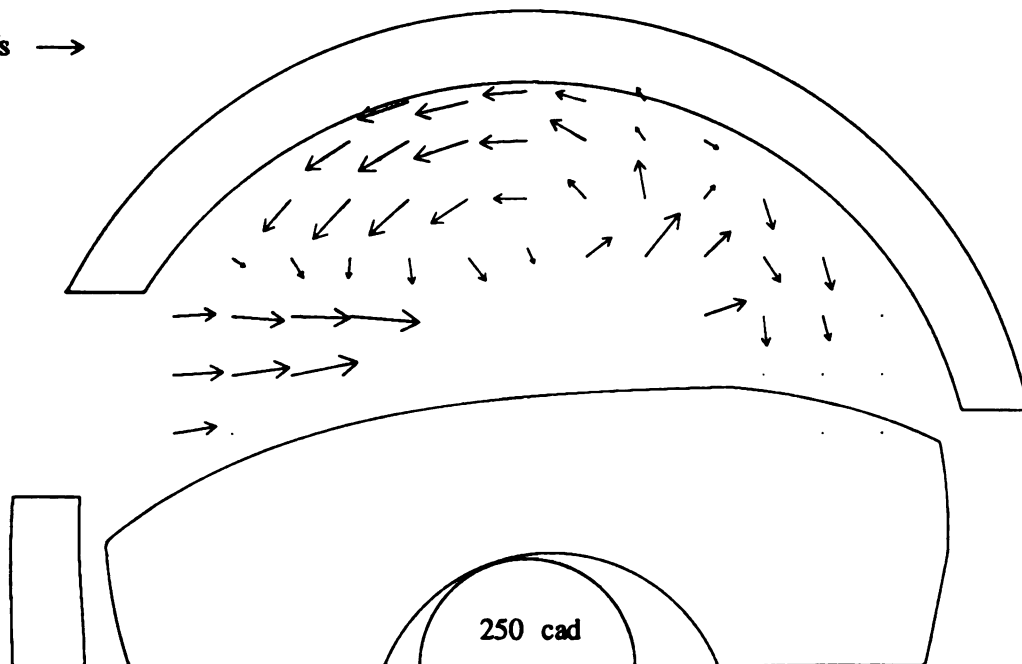
10 m/s →



Symmetric Recess - Mean Velocity

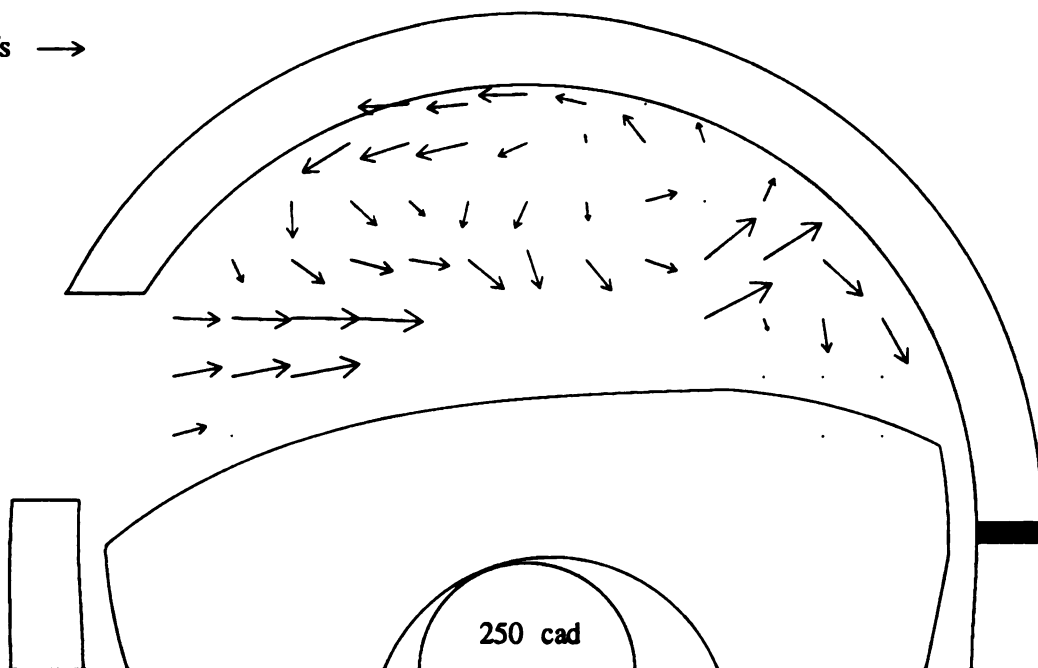
Figure 12 cont. Comparison of the Mean Velocity Flow Fields for the SMR Rotor With and Without Compression

10 m/s →



Symmetric Recess, No Compression - Mean Velocity

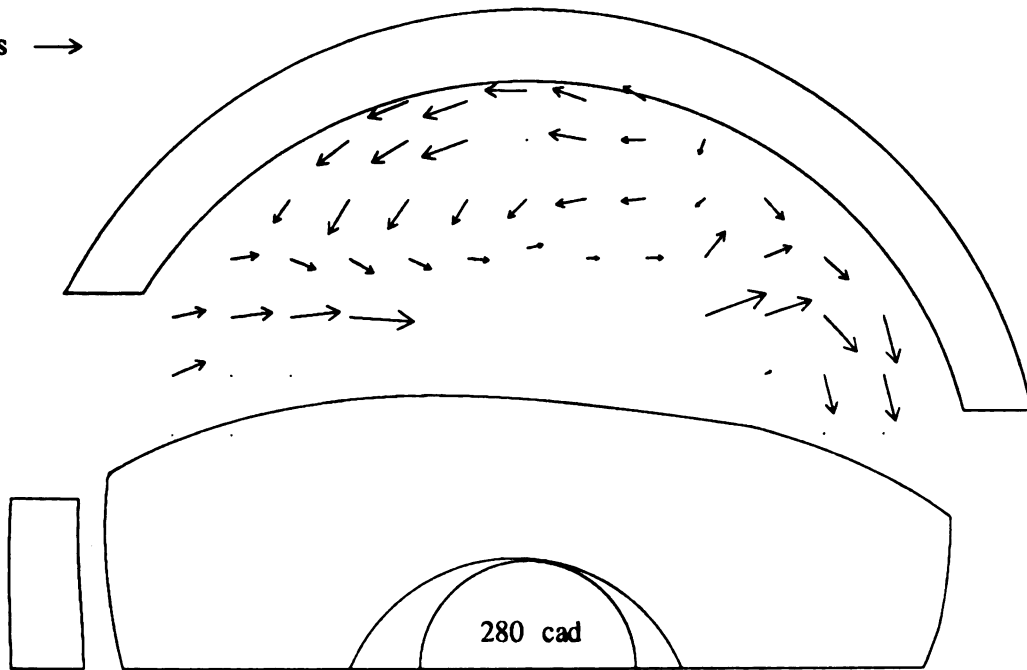
10 m/s →



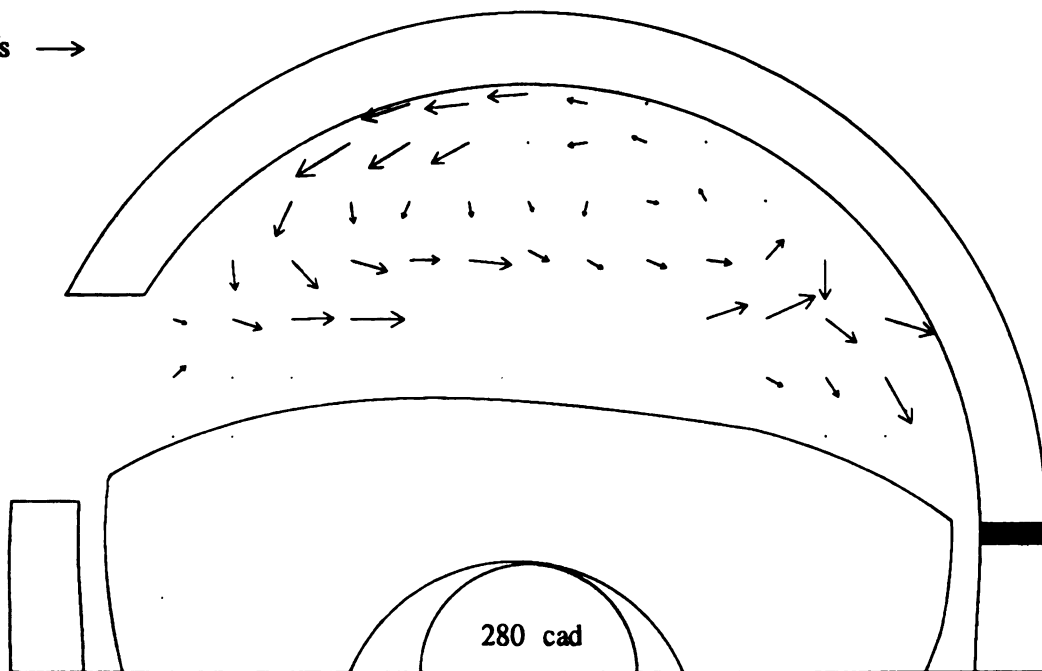
Symmetric Recess - Mean Velocity

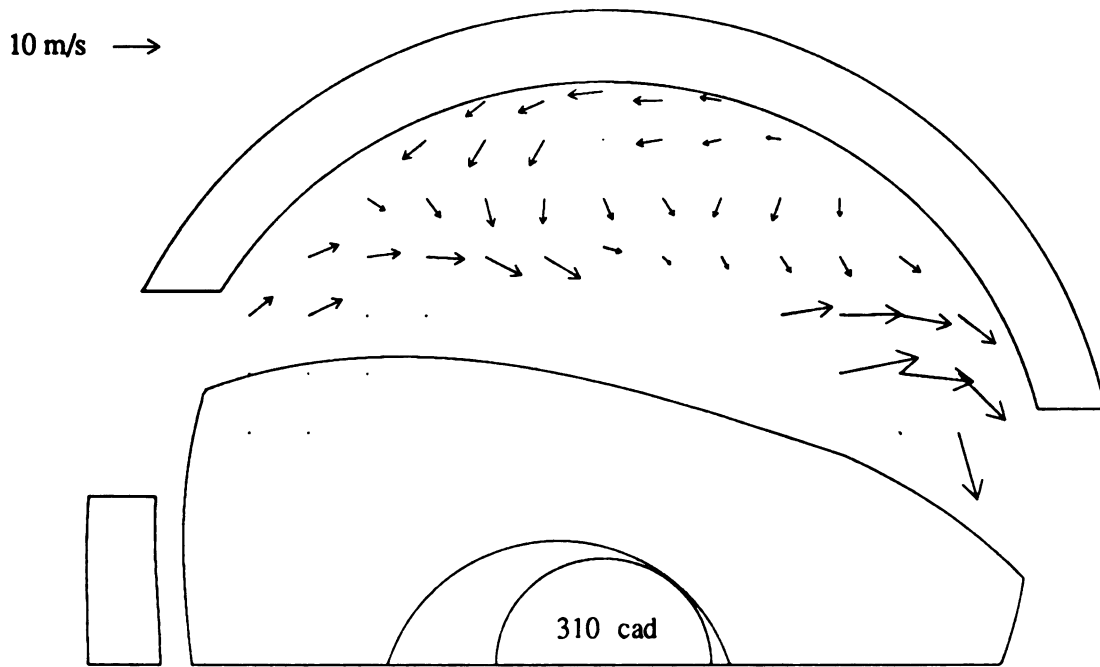
Figure 12 cont. Comparison of the Mean Velocity Flow Fields for the SMR Rotor With and Without Compression

10 m/s →

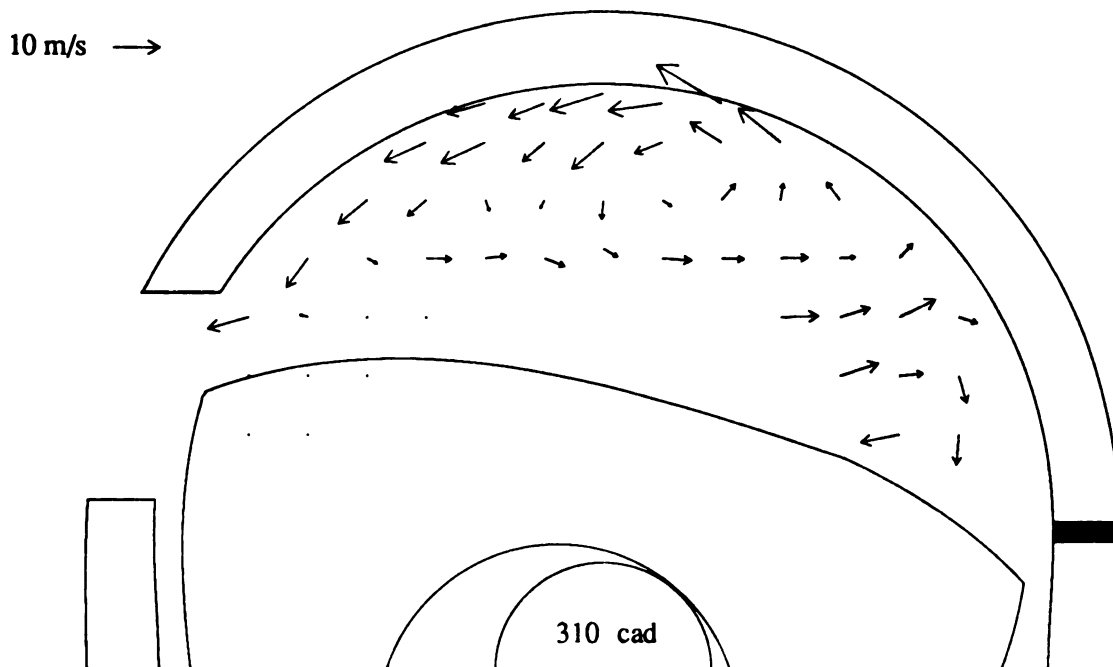
**Symmetric Recess, No Compression - Mean Velocity**

10 m/s →

**Symmetric Recess - Mean Velocity****Figure 12 cont. Comparison of the Mean Velocity Flow Fields for the SMR Rotor With and Without Compression**

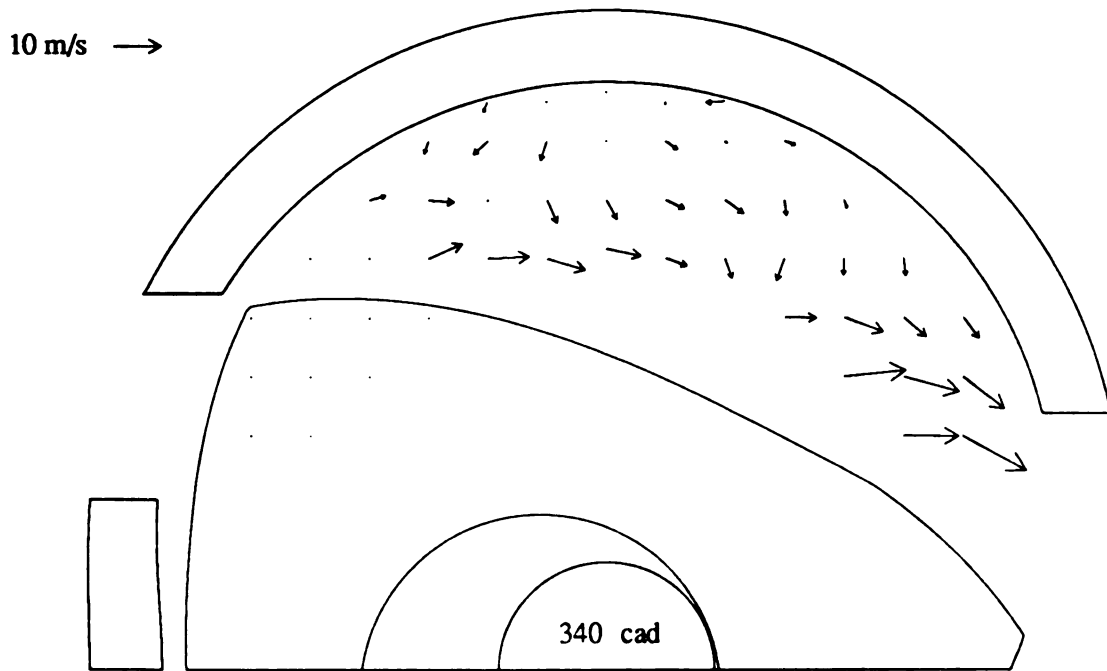


Symmetric Recess, No Compression - Mean Velocity

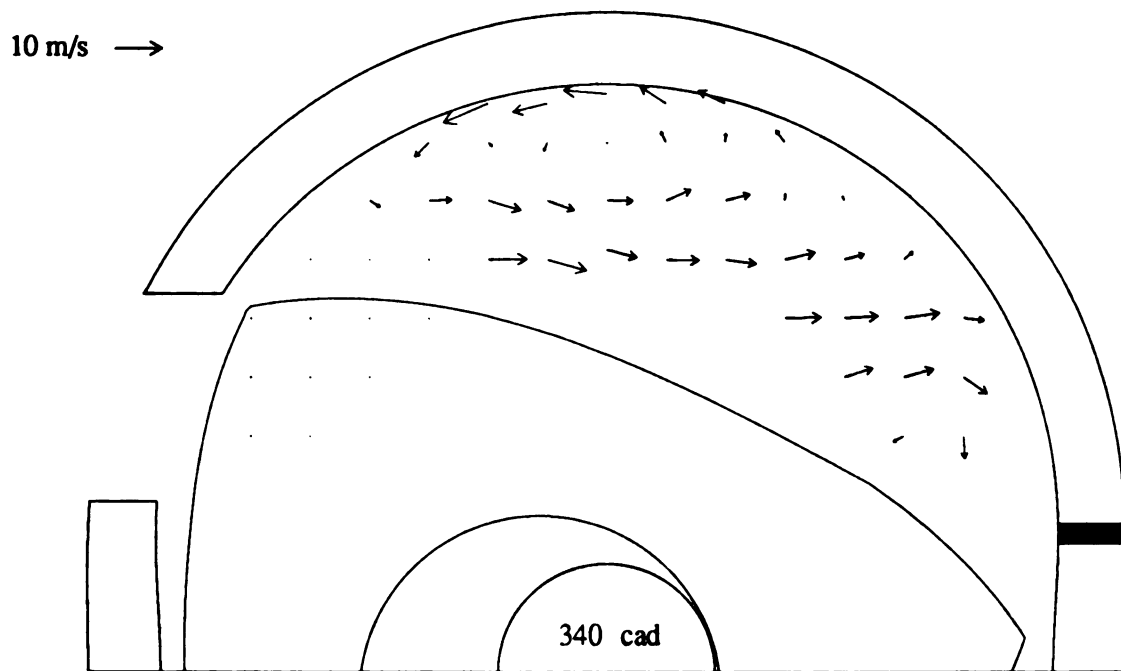


Symmetric Recess - Mean Velocity

Figure 12 cont. Comparison of the Mean Velocity Flow Fields for the SMR Rotor With and Without Compression

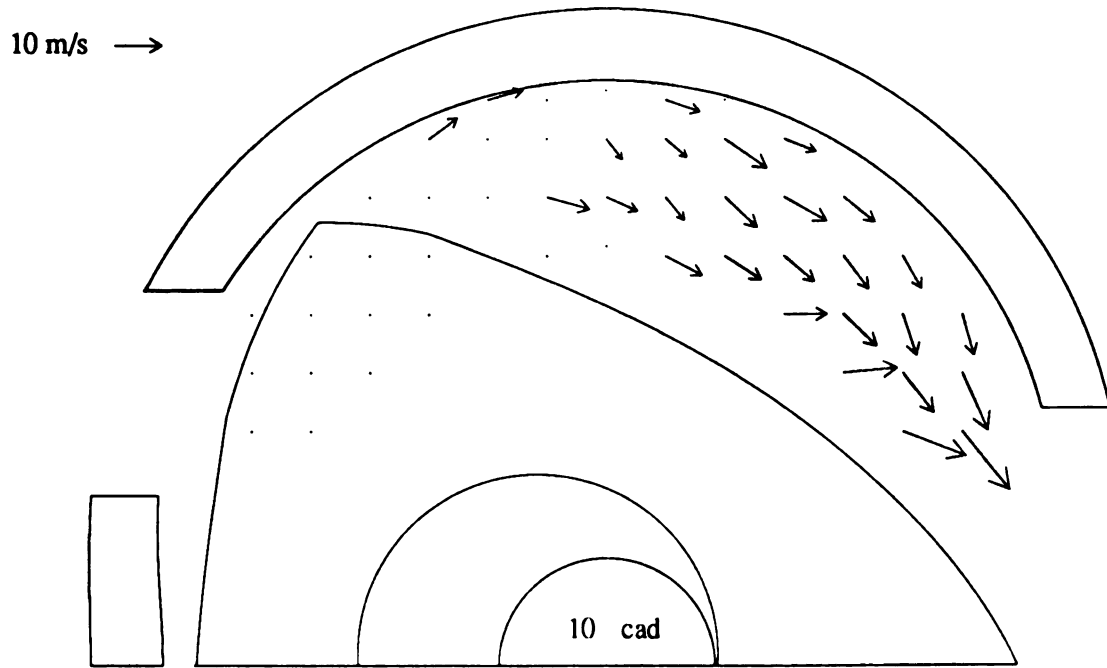


Symmetric Recess, No Compression - Mean Velocity

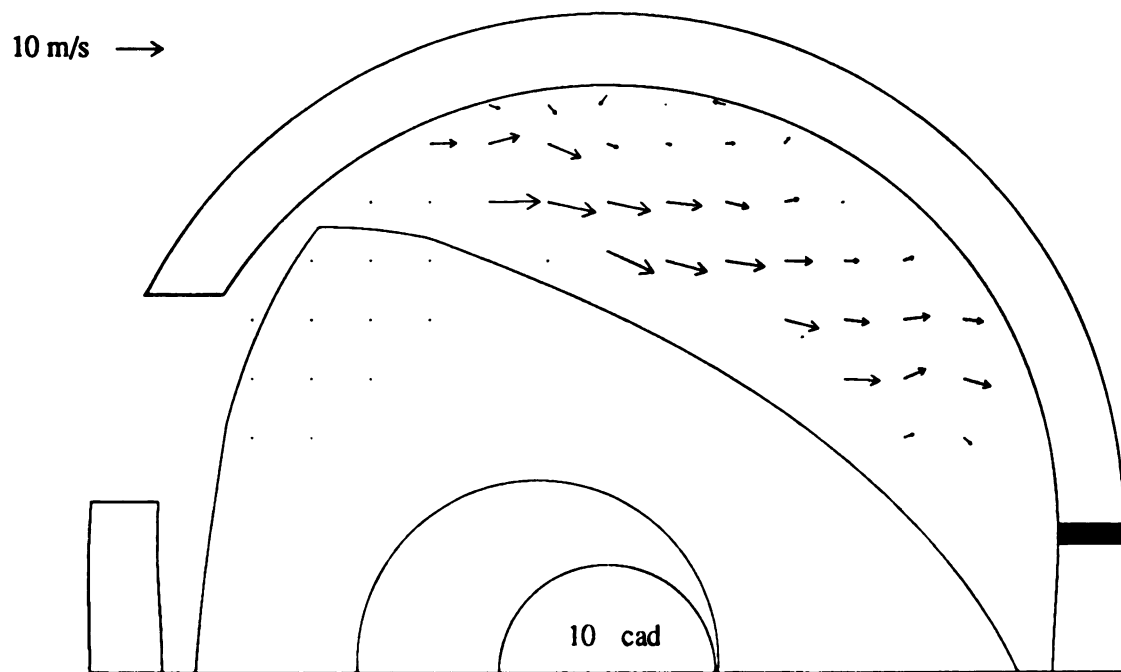


Symmetric Recess - Mean Velocity

Figure 12 cont. Comparison of the Mean Velocity Flow Fields for the SMR Rotor With and Without Compression

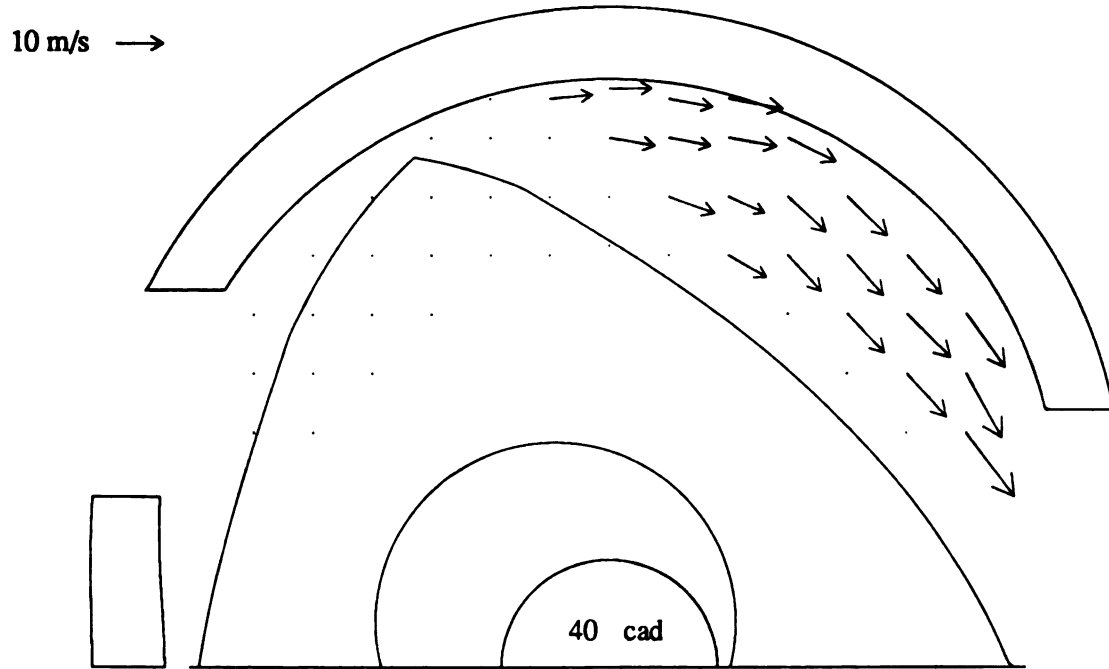


Symmetric Recess, No Compression - Mean Velocity

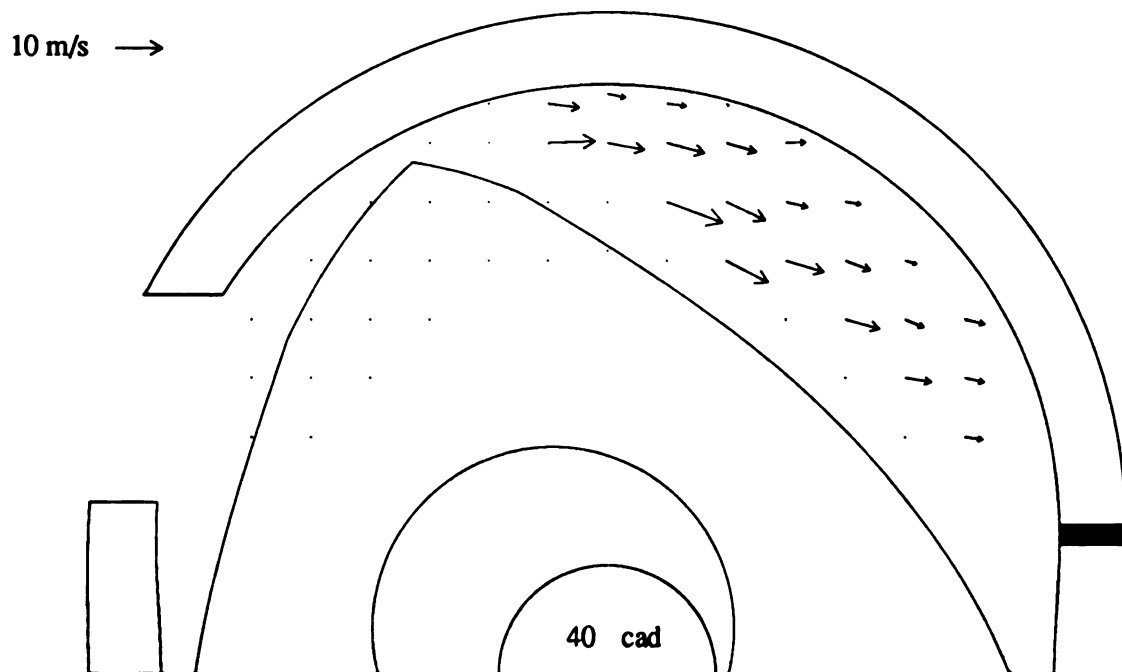


Symmetric Recess - Mean Velocity

Figure 12 cont. Comparison of the Mean Velocity Flow Fields for the SMR Rotor With and Without Compression

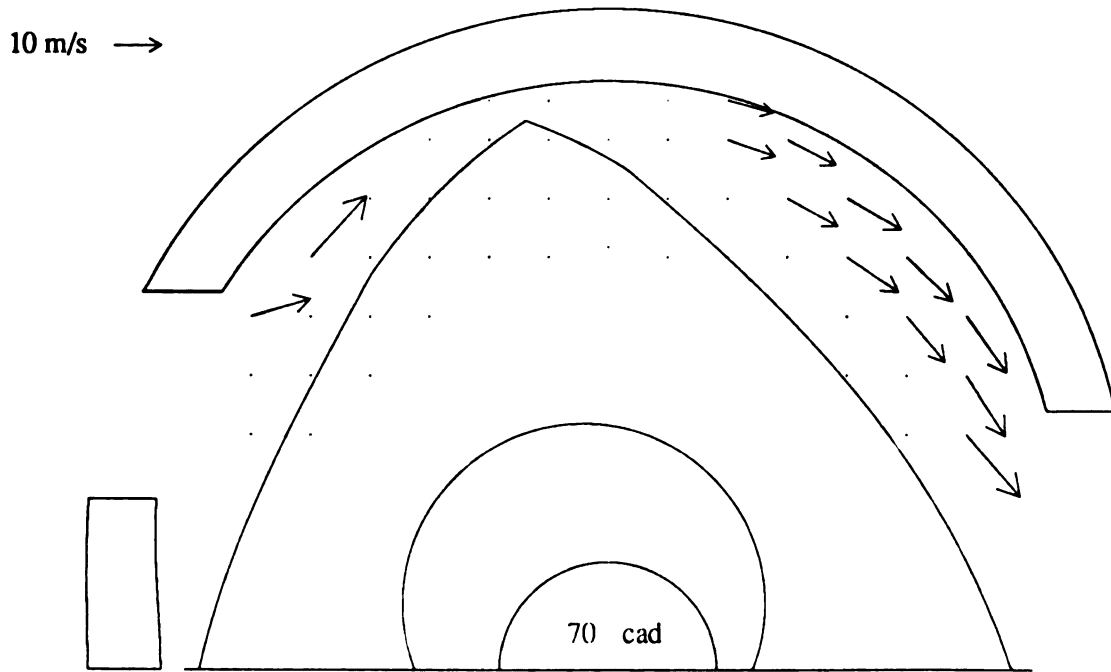


Symmetric Recess, No Compression - Mean Velocity

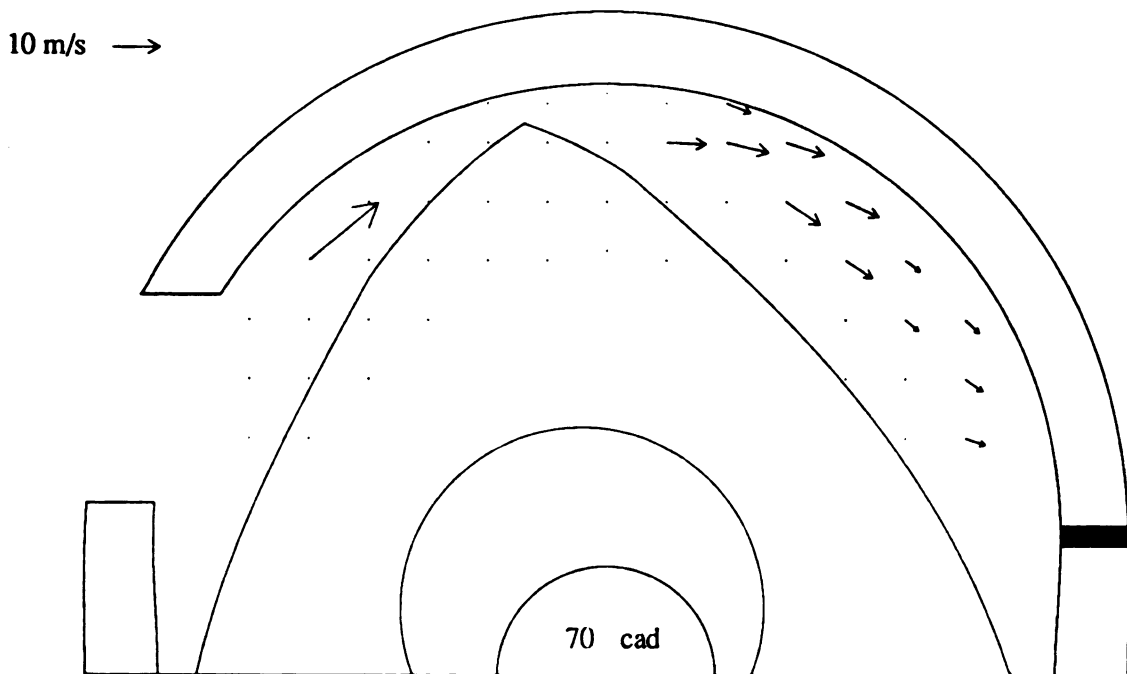


Symmetric Recess - Mean Velocity

Figure 12 cont. Comparison of the Mean Velocity Flow Fields for the SMR Rotor With and Without Compression



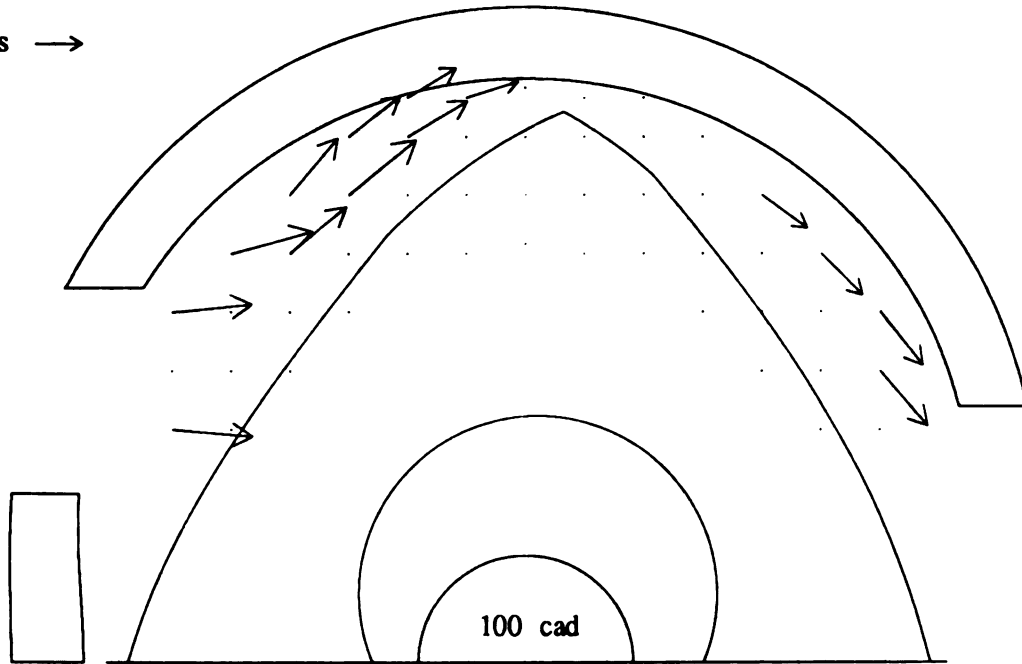
Symmetric Recess, No Compression - Mean Velocity



Symmetric Recess - Mean Velocity

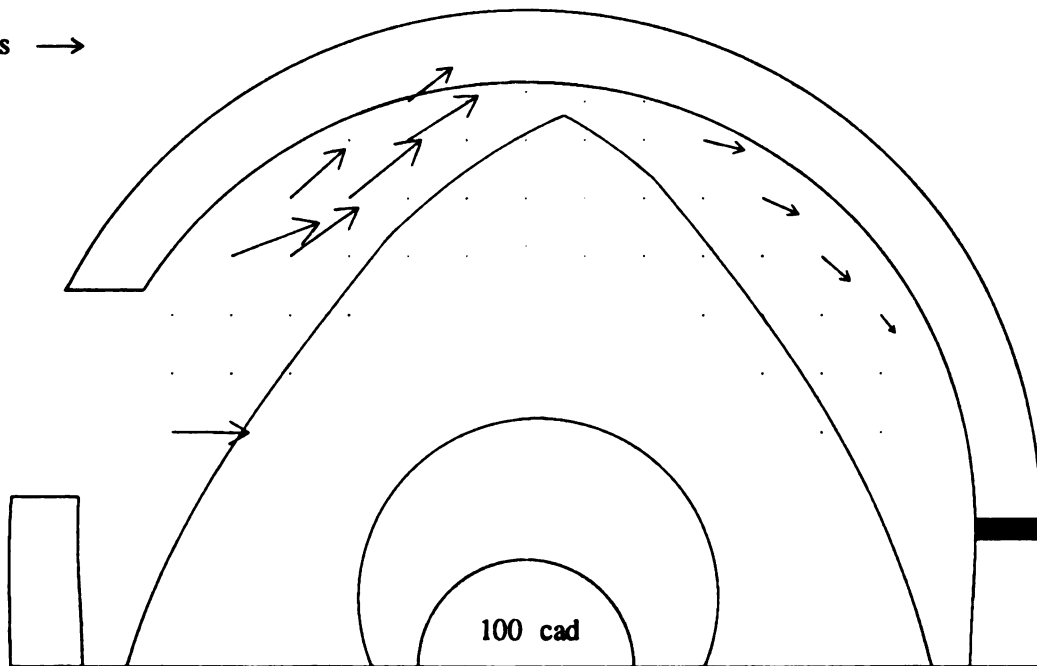
Figure 12 cont. Comparison of the Mean Velocity Flow Fields for the SMR Rotor With and Without Compression

10 m/s →



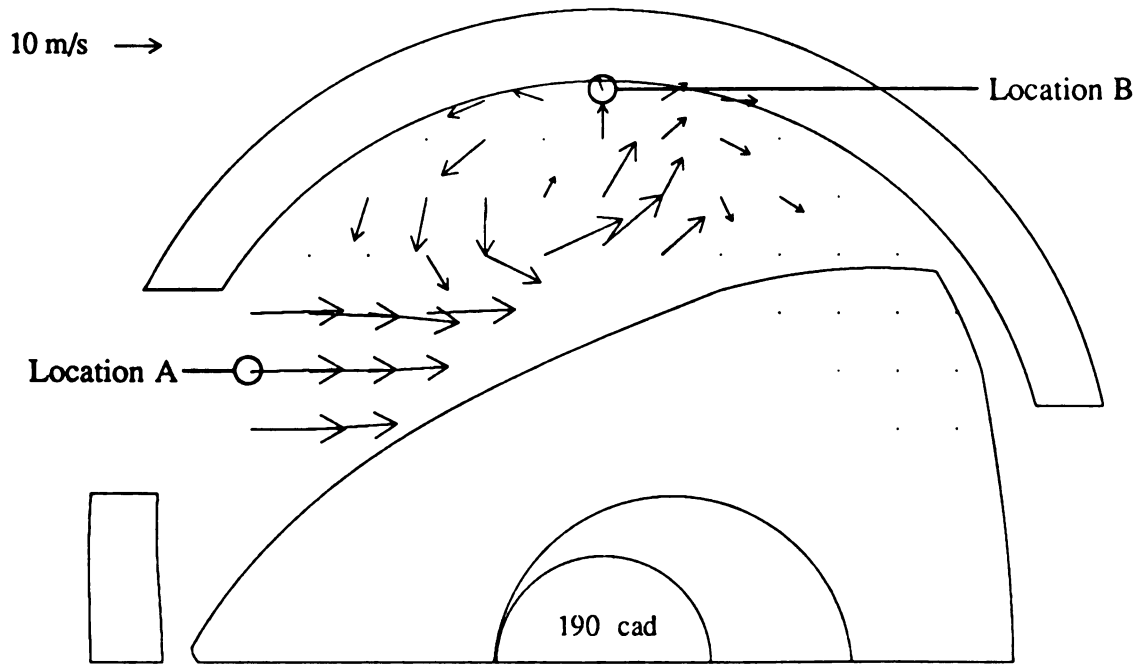
Symmetric Recess, No Compression - Mean Velocity

10 m/s →

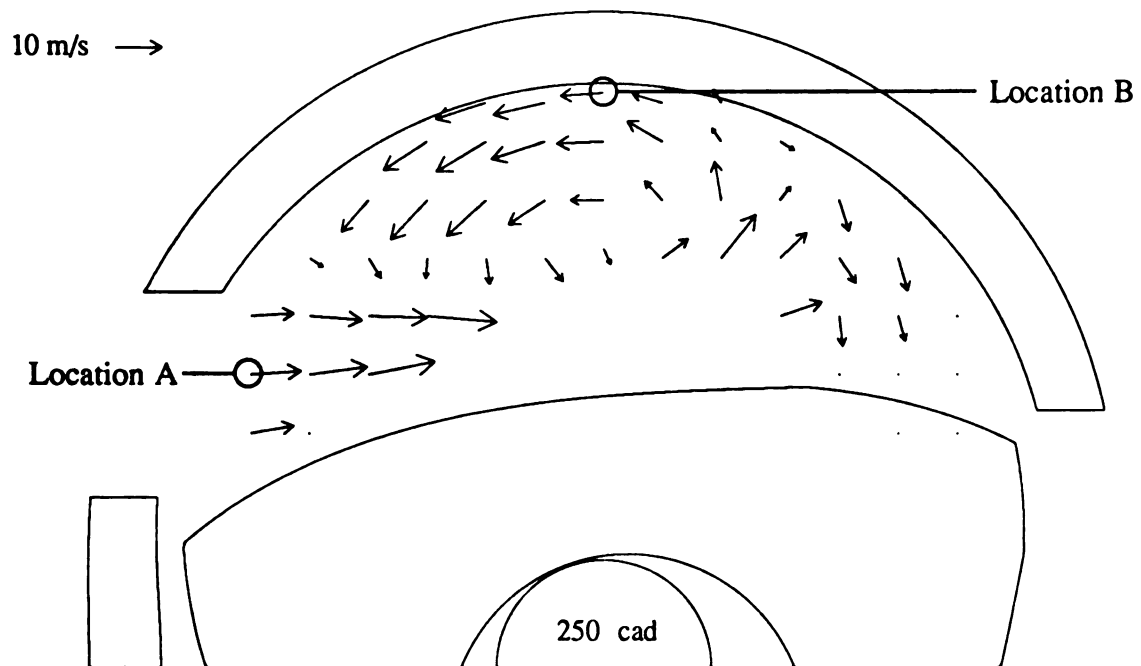


Symmetric Recess - Mean Velocity

Figure 12 cont. Comparison of the Mean Velocity Flow Fields for the SMR Rotor With and Without Compression

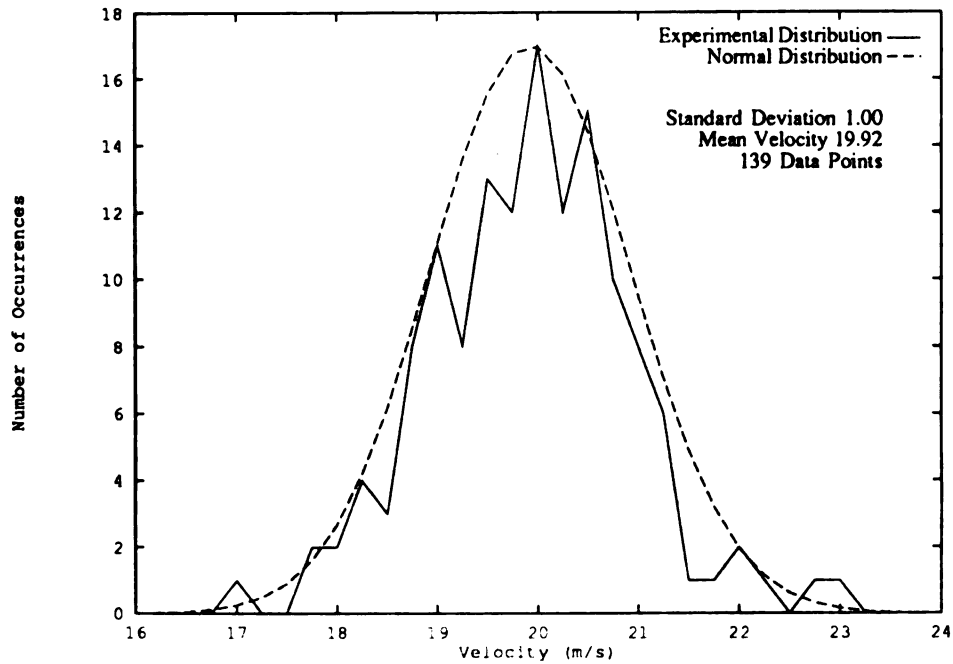


Symmetric Recess, No Compression - Mean Velocity

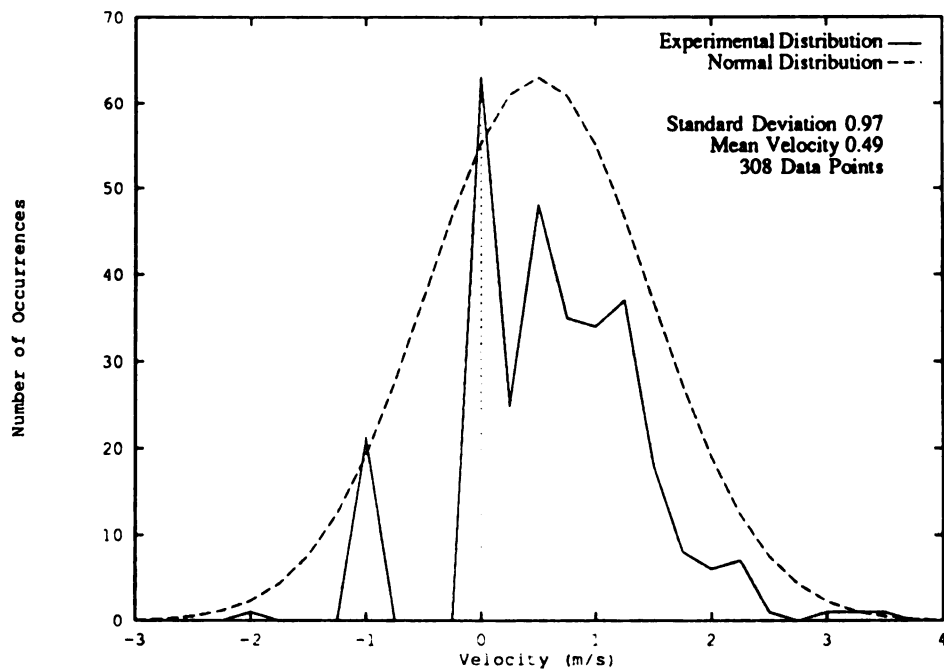


Symmetric Recess, No Compression - Mean Velocity

Figure 13 Locations and Crank Angles used for Figures 14 and 15

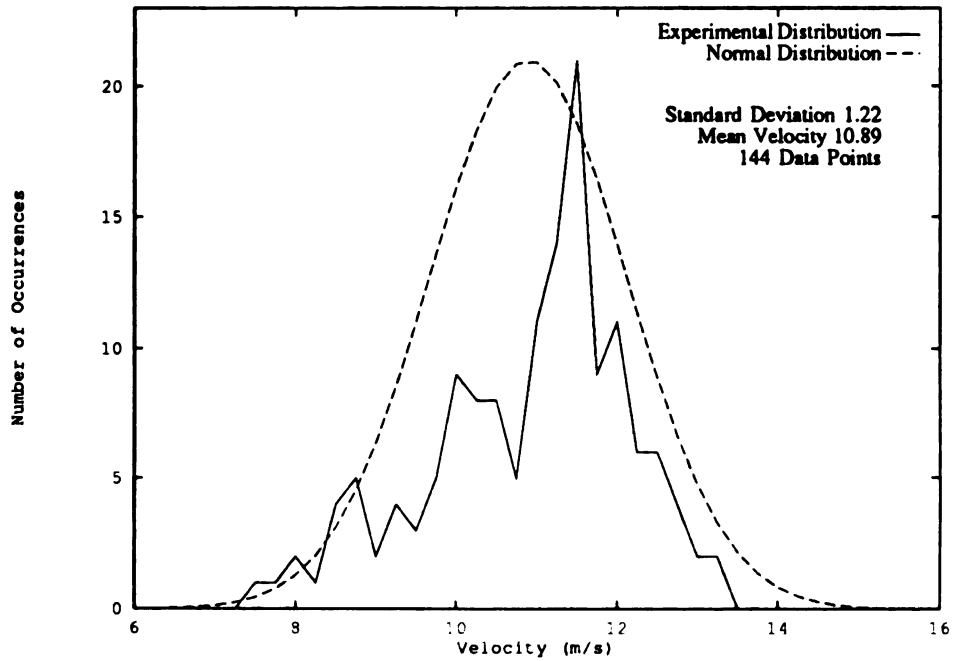


Normal Distribution and Experimental Data Distribution
for Location A, 190 cad, U Velocity Component

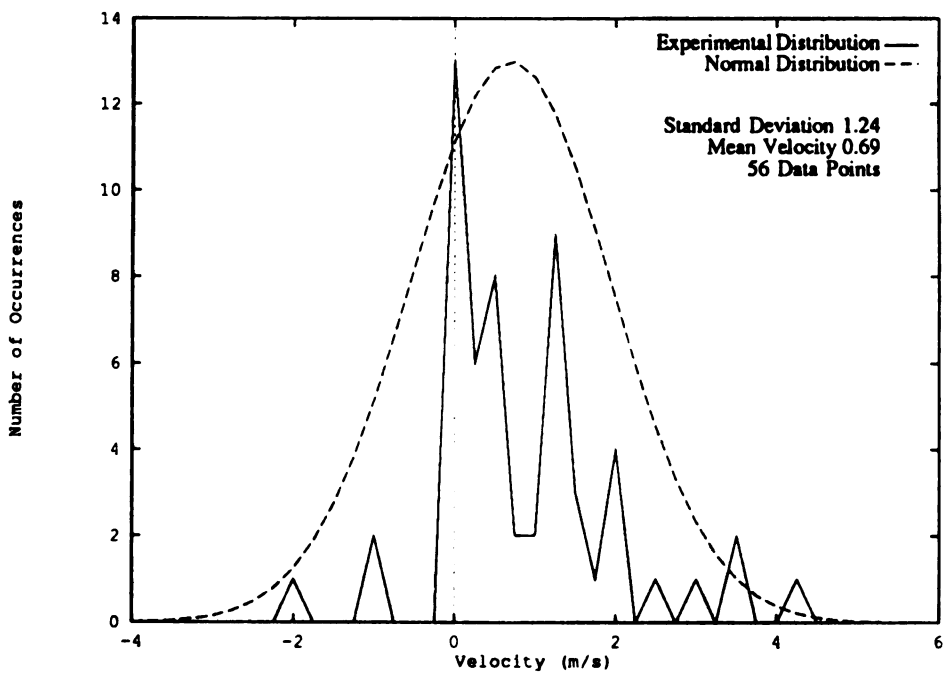


Normal Distribution and Experimental Data Distribution
for Location A, 190 cad, V Velocity Component

Figure 14 Data Distributions for Location A

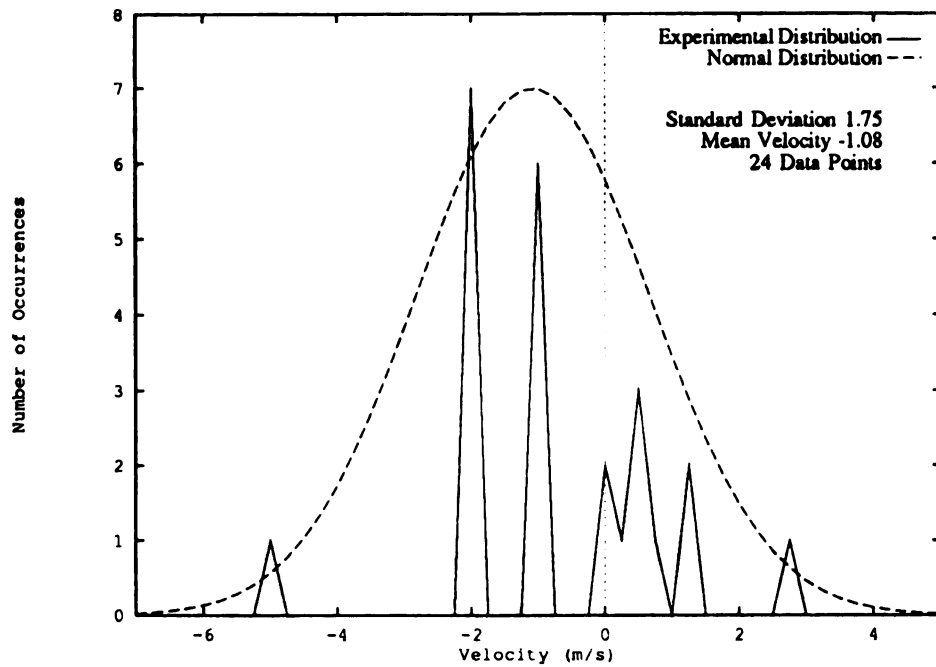


Normal Distribution and Experimental Data Distribution
for Location A, 250 cad, U Velocity Component

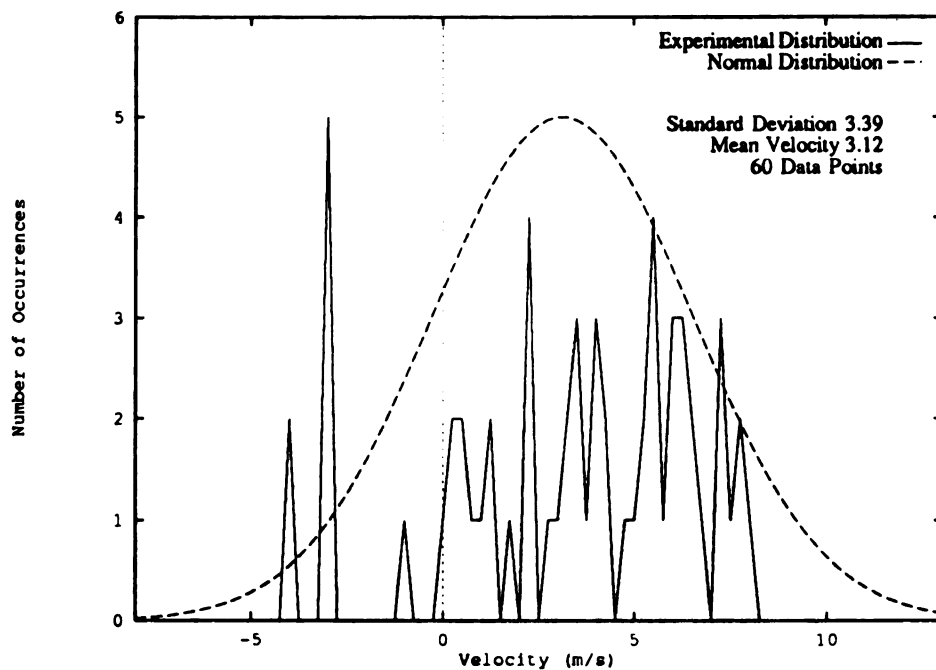


Normal Distribution and Experimental Data Distribution
for Location A, 250 cad, V Velocity Component

Figure 14 cont. Data Distributions for Location A

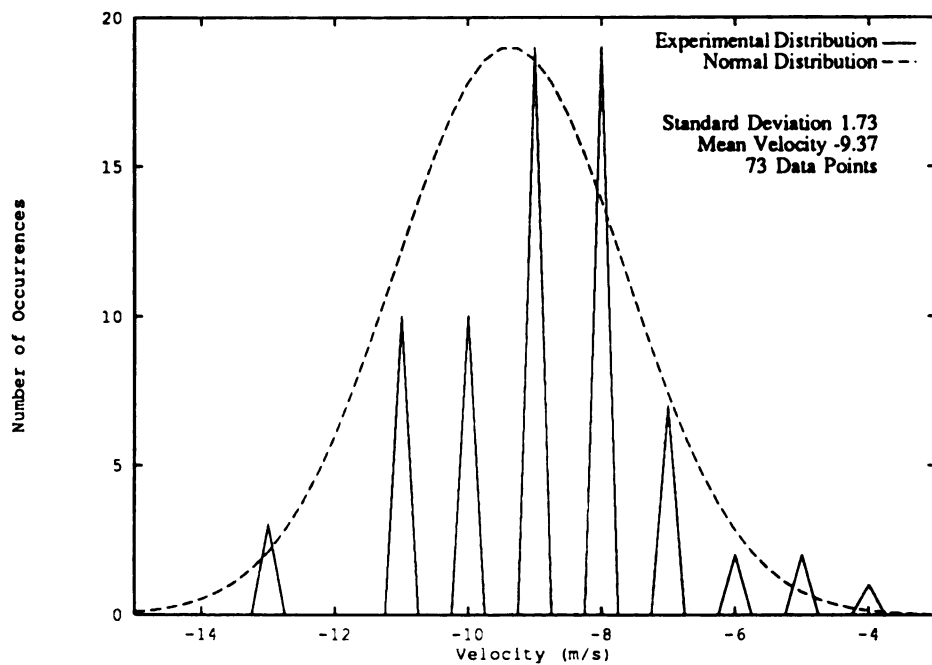


Normal Distribution and Experimental Data Distribution
for Location B, 190 cad, U Velocity Component

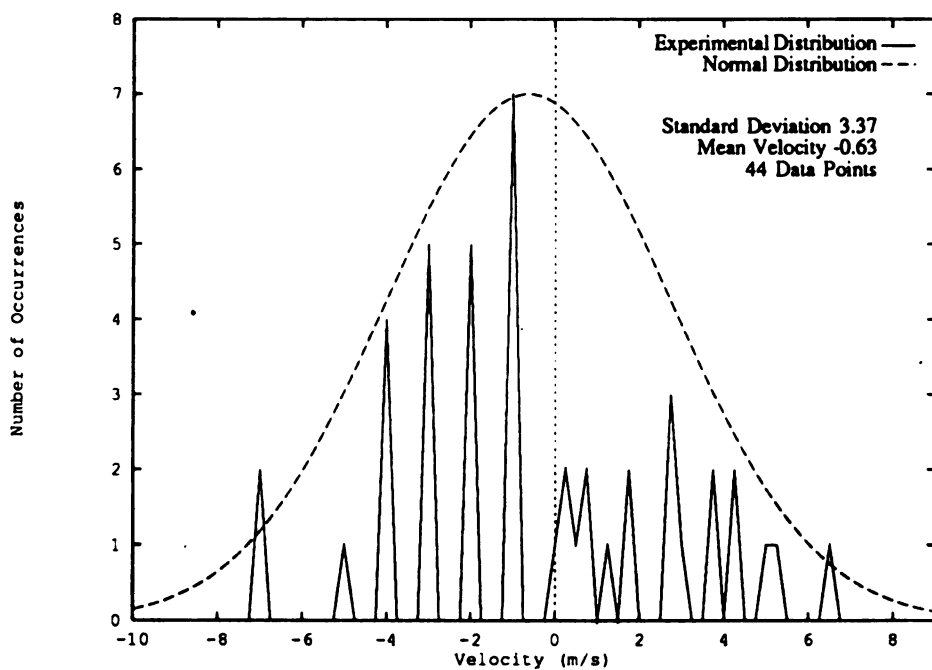


Normal Distribution and Experimental Data Distribution
for Location B, 190 cad, V Velocity Component

Figure 15 Data Distributions for Location B



Normal Distribution and Experimental Data Distribution
for Location B, 250 cad, U Velocity Component



Normal Distribution and Experimental Data Distribution
for Location B, 250 cad, V Velocity Component

Figure 15 cont. Data Distributions for Location B

APPENDIX A
RTOVEL Program

```

/*
 *   This program was developed to take TSI Phase ldv data
 *   output ( the velocity files) and convert them into the
 *   appropriate data files for use with PVwave.
 *
 *   History:
 *
 *
 */
#include <stdio.h> #include <stdlib.h> #include <string.h>
#include <math.h> #define FN 2 #define FILES 50 #define MIN
(int) 15

/*****

        This is the data file list for the inputs
*****/
char *filelist[] = {  "mld_b48u.v02", "mld_b48v.v01",
    "mld_b60u.v01", "mld_b60v.v01",
    "mld_b72u.v01", "mld_b72v.v01",
    "mld_c48u.v01", "mld_c48v.v01",
    "mld_c60u.v01", "mld_c60v.v01",
    "mld_c72u.v01", "mld_c72v.v01",
    "mld_c84u.v01", "mld_c84v.v01",
    "mld_d60u.v01", "mld_d60v.v01",
    "mld_d72u.v01", "mld_d72v.v01",
    "mld_d84u.v01", "mld_d84v.v01",
    "mld_d96u.v02", "mld_d96v.v01",
    "mld_e72u.v01", "mld_e72v.v01",
    "mld_e84u.v01", "mld_e84v.v01",
    "mld_e96u.v01", "mld_e96v.v01",
    "junke08u.v01", "mld_e08v.v03",
    "mld_f84u.v01", "mld_f84v.v01",
    "mld_f96u.v01", "mld_f96v.v01",
    "mld_f08u.v02", "mld_f08v.v01",
    "mld_f16u.v01", "mld_f16v.v01",
    "mld_g84u.v01", "mld_g84v.v01",
    "mld_g96u.v01", "mld_g96v.v01",
    "mld_g08u.v01", "mld_g08v.v01",
    "mld_g16u.v01", "mld_g16v.v01",
    "mld_h86u.v01", "mld_h86v.v01",
    "mld_h96u.v01", "mld_h96v.v01",
    "mld_h08u.v01", "mld_h08v.v01",

```

```

"mld_h18u.v01", "mld_h18v.v01",
"mld_i84u.v01", "mld_i84v.v01",
"mld_i96u.v01", "mld_i96v.v01",
"mld_i08u.v01", "mld_i08v.v01",
"mld_i16u.v01", "mld_i16v.v01",
"mld_j84u.v01", "mld_j84v.v01",
"mld_j96u.v01", "mld_j96v.v01",
"mld_j08u.v01", "mld_j08v.v01",
"mld_j16u.v01", "mld_j16v.v01",
"mld_k72u.v01", "mld_k72v.v01",
"mld_k84u.v01", "mld_k84v.v01",
"mld_k96u.v02", "mld_k96v.v01",
"mld_k08u.v01", "mld_k08v.v01",
"mld_l60u.v01", "mld_l60v.v01",
"mld_l72u.v01", "mld_l72v.v01",
"mld_l84u.v01", "mld_l84v.v01",
"mld_l96u.v01", "mld_l96v.v01",
"mld_m48u.v01", "mld_m48v.v01",
"mld_m60u.v01", "mld_m60v.v01",
"mld_m72u.v01", "mld_m72v.v01",
"mld_m84u.v01", "mld_m84v.v01",
"mld_n48u.v01", "mld_n48v.v01",
"mld_n60u.v01", "mld_n60v.v01",
"mld_n72u.v01", "mld_n72v.v01"
};

```

```

/*****

```

The pattern for the Phase velocity files with
the processor in random mode and tbd off is:

for i=1, number_of_data_points, increment by 1

record(i) = address of procesor 2byte

int

```

velocity from procesor 4byte real
1-15 cwords optional 2byte int
grouped in blocks of 3 2byte int
2byte int
encoder angle 2byte int
cycle number 2byte int
window number 2byte int
dummy value -2 2byte int
tau 4byte real

```

```

*****/

```

```

struct table {
int address;
float velocity;

```



```

/*****

opening output files
*****/

if ((vmeanf=fopen(vmeanfn,"w"))==NULL) {

    printf("error opening %s\n",vmeanfn);
    exit(1);
}
if ((vstdf=fopen(vstdfn,"w"))==NULL) {

    printf("error opening %s\n",vstdfn);
    exit(1);
}
if ((vtrbf=fopen(vtrbfn,"w"))==NULL) {

    printf("error opening %s\n",vtrbfn);
    exit(1);
}
printf(" output files opened\n");

/*****

Start loop to go through data files in sets of 2
for this to work properly the data file list must
be set up so that the u and v component data files
for one location follow each other. eg.
    ldrcu_a6.v01
    ldrcv_a6.v01
    ldrcu_b3.v01 .etc .....
*****/
m = 0;

for ( z = 0; z < (FILES*2); z = z+2) {

/*****

initialize data arrays to zero
*****/

xtempn = (float) 0.000;

ytempn = (float)0.000;

    for (j=0;j<=360;j++) {
        theta[m][j] = j;
        xcoord[m][j] = (float)0;
    }
}

```

```

        ycoord[m][j] = (float)0;
        number[m][j] = (float)0.000;
        vxtotal[m][j] = (float)0.000;
        vytotal[m][j] = (float)0.000;
        vxsqrd[m][j] = (float)0.000;
        vysqrd[m][j] = (float)0.000;
        vxtrb[m][j] = (float)0.000;
        vytrb[m][j] = (float)0.000;
    }
    printf(" data arrays set to zero \n");

    /*****

Begin large for loop to shuffle pair of through

Phase velocity files.
*****/

    /*      n = 0; */
    /*      m = m+1; */
    for (k=z;k<(FN+z);k++)

        { /***** open
Kth input file in char array filelist
*****/
        if ((infile = fopen(filelist[k],"rb")) == NULL) {

            printf("error opening %s \n",filelist[k]);
            exit (1);
        }

        /***** read header
of velocity file and check number of data points also get x
and y coordinates.
*****/

        printf("about to read header info\n");

        /*****

        read in # of data points
        line #10 in phase header file
*****/
        for (i=0;i<9;i++) {
            fgets(line,80,infile);
        }
        fscanf(infile,"%d",&datapts);
        printf("%d k = %d \n",datapts,k);

```



```

/*****

read in x,y,z coordinates
lines 79, 82 and 85 respectively
The x,y,z coords. are the traverse
table coords. When they are read in
they are switched to graphical output
coords. x in the header file is z on the
graph, y is x and z is y.
*****/
for (i=0;i<69;i++) {
    fgets(line,80,infile);
    }
    fscanf(infile,"%f",&ztemp);
    printf("%f %d \n",ztemp,k);
    for (i=0;i<3;i++) {
        fgets(line,80,infile);
        }
        fscanf(infile,"%f",&xtemp);
        printf("%f %d \n",xtemp,k);
        xtemp = -xtemp;
        for (i=0;i<3;i++) {
            fgets(line,80,infile);
            }
            fscanf(infile,"%f",&ytemp);
            printf("%f %d \n",ytemp,k);
/***** read in which
velocity component is being read in. Line 88 in header file.
*****/

for (i=0;i<3;i++) {

    fgets(line,80,infile);
    }
    fscanf(infile,"%c",&compchar);
    printf("%c %d \n",compchar,k);
    if ((compchar != 'u') && (compchar != 'v')) {
        printf(" \n");
        printf(" Undeclared or unrecognized velocity
component! \n");
        exit(1);
    }
/***** read out the rest
of the header, Phase header has a total of 230 lines
*****/

for (i=0;i<143;i++) {

```

```

        fgets(line,80,infile);
    }
    printf("header read for %s \n",filelist[k]);

    /***** check to see
    if one component has already been read in for this location,
    if x,y = a previous x,y then one component has already been
    read in. In this case the new x,y location will be given the
    same counter as the matching previous so that the second
    velocity component can be recorded at the same location.

    x y Vx Vy theta Prs  instead of
    x y Vx 0  theta Prs and
    x y 0  Vy theta Prs
    *****/
    for (i=0;i<=n;i++) {
        if ((xtemp==xtempn)&&(ytemp==ytempn)) {
            m = i;
        }
        else {
            xtempn = xtemp;
            ytempn = ytemp;
            if (n != 0) {
                n = n + 1;
                m = n;
            }
        }
    }
    printf(" m = %d n = %d \n",m,n); */
    for (i=0;i<=360;i++) {
        number[m][i] = (float)0.0000;
    }
    /***** read through
    file - sum velocities -

    count the number of entries, calculate
    mean velocity and sum of the squares
    *****/
    for (i=0;i<(datapts*1000);i++) {
        fread(mem.record,1,18,infile);
        angle = (int)(mem.info.angle*360.0/2048.0);
        remain = (float)
fmod((double)(mem.info.angle*360.0),(double)(2048.0));
        if (remain > (float)0.5) {
            angle = angle + 1;
        }
    }

```

```

        theta[m][angle] = angle;
        xcoord[m][angle] = (xtemp*0.00351783) + 0.500;
        ycoord[m][angle] = (ytemp*0.00349493) + 0.500;
        number[m][angle] = number[m][angle] + 1.000;
/***** sorting v components from u components
*****/

if (compchar == 'u') {

        vxtotal[m][angle] = vxtotal[m][angle] +
mem.info.velocity;
vxsqrd[m][angle]=vxsqrd[m][angle]+((mem.info.velocity)*(mem.i
nfo.velocity));
        }
        if (compchar == 'v') {
                vytotal[m][angle] = vytotal[m][angle] +
mem.info.velocity;
vysqrd[m][angle]=vysqrd[m][angle]+((mem.info.velocity)*(mem.i
nfo.velocity));
        }
        } /* this line is the end of the loop for reading
in data */
fclose(infile);

/***** check for division
by zero and inform user of zero detection
*****/

        for(i=0;i<=360;i++) {
                check = check + number[m][i];
                xcoord[m][i] = (xtemp*0.00351783) + 0.500;
                ycoord[m][i] = (ytemp*0.00349493) + 0.500;
        }
        if (check<=(float)0.0) {
                printf("No data points were recorded for %s
\n",filelist[k]);
                exit (1);
        }
/***** mean velocity for mth location *****/

and

std of the velocity

```

Equation for standard deviation taken from EIT Reference Manual

7th edition, by Michael R. Lindeburg, Professional

Publications,

INC. Belmont CA 1990 page 11-10

std = square root of the sum of the squares divided by
the number of measurements minus the mean squared

*****/

if (compchar == 'u') {

for (i=0;i<=360;i++) {

if ((int) number[m][i] < MIN) {

vxmean[m][i] = (float)0.0000;

}

else {

vxmean[m][i] = (vxtotal[m][i])/(number[m][i]);

}

}

for (i=0;i<=360;i++) {

if ((int)number[m][i] > MIN) {

vxsqmean = vxsqrd[m][i]/number[m][i];

xmeansqrd = vxmean[m][i]*vxmean[m][i];

}

else {

vxsqmean = (float)0.000;

xmeansqrd = (float)0.000;

}

if ((vxsqmean-xmeansqrd)<=(float)0.000)

{

vxstd[m][i] = (double)0.0;

}

else {

vxstd[m][i]= sqrt(vxsqmean-xmeansqrd);

}

}

for (i=0;i<=360;i++) {

if ((float)vxmean[m][i] == (float)0.000)

{

vxtrb[m][i] =(float)0.000;

}

else {

vxtrb[m][i] =

((float)vxstd[m][i]*100.00)/vxmean[m][i];

}

} } /* end of if loop for u component */

if (compchar == 'v') {

for (i=0;i<=360;i++) {

if ((int)number[m][i] > MIN) {

```

    vymeansqr[m][i] = (vysqr[m][i]) / (number[m][i]);
}
else {
    vymeansqr[m][i] = (float)0.000;
}
}
for (i=0; i<=360; i++) {
    if ((int)number[m][i] > MIN) {
        vysqrmean = vysqr[m][i] / number[m][i];
        vymeansqr = vymeansqr[m][i] * vymeansqr[m][i];
    }
    else {
        vysqrmean = (float)0.000;
        vymeansqr = (float)0.000;
    }
    if ((vysqrmean - vymeansqr) < (float)0.000)
    {
        vystd[m][i] = (double) 0.0;
    }
    else {
        vystd[m][i] = sqrt(vysqrmean - vymeansqr);
    }
}
for (i=0; i<=360; i++) {
    if ((float)vymeansqr[m][i] == (float)0.000)
    {
        vytrb[m][i] = (float)0.000;
    }
    else {
        vytrb[m][i] =
((float)vystd[m][i] * 100.00) / vymeansqr[m][i];
    }
}
/* end of if loop for v component */
/***** close for loop for shuffling
through data files *****/
}

printf(" data file loop closed \n");

for (j=0; j<=360; j++) {
    if ((vxmean[m][j] == (float)0.000) || (vymeansqr[m][j] ==
(float)0.000)) {
        vxmean[m][j] = (float)0.000;
        vymeansqr[m][j] = (float)0.000;
    }
}

```

```

    }
    if ((vxstd[m][j] == (double)0.000) || (vystd[m][j] ==
(double)0.000)) {
        vxstd[m][j] = (float)0.000;
        vystd[m][j] = (float)0.000;
    }
    if ((vxtrb[m][j] == (float)0.000) || (vytrb[m][j] ==
(float)0.000)) {
        vxtrb[m][j] = (float)0.000;
        vytrb[m][j] = (float)0.000;
    }
}

printf("means, stds and trbs calculated.\n");
for (j=0;j<=360;j++) {
    for (i=0;i<=m;i++) {
        fprintf(vmeanf,"%f %f %f %f %d \n",xcoord[i][j],
ycoord[i][j],vxmean[i][j],vymean[i][j],theta[i][j]);
        fprintf(vstdf,"%f %f %f %f %d \n",xcoord[i][j],
ycoord[i][j],vxstd[i][j],vystd[i][j],theta[i][j]);
        fprintf(vtrbf,"%f %f %f %f %d \n",xcoord[i][j],
ycoord[i][j],vxtrb[i][j],vytrb[i][j],theta[i][j]);
    }
}

fflush(vmeanf);
fflush(vstdf);
fflush(vtrbf);
/***** close for
loop for shuffling through data files
*****/ }

fclose(vmeanf);
fclose(vstdf);
fclose(vtrbf); }

```

APPENDIX B

ROTOR_DOUBLE Program

```

;
;          ***   ROTOR DOUBLE IMAGE   ***
;
;          Developed by: Mark Novak and Mike DeFilippis
;
points = 51
stdeg = 0
endeg = 360
rellen = 15
xpixst = 65
ypixst = 42
;
;   *** for sun output ***
;
set_plot,'sun'
window,0, xsize = 640, ysize = 600
rotormovie = bytarr(512,512,20)
;
!order = 0
angle = intarr(361)
xpos = fltarr(points,361)
ypos = fltarr(points,361)
vx = fltarr(points,361)
vy = fltarr(points,361)
vel = fltarr(points,361)
degr = fltarr(points,361)
x = fltarr(points)
y = fltarr(points)
;
; read in velocity position and calculate vector length data
;
openr,15,'nasa50.vel'
for p = 0, points-2 do begin
  for i = 0, 360 do begin
    readf,15,tempxpos,tempypos,tempvx,tempvy,tempdeg
    xpos(p,i) = tempxpos
    ypos(p,i) = tempypos - 0.5
    vx(p,i) = tempvx
    vy(p,i) = tempvy
    degr(p,i) = tempdeg
    vel(p,i) = ((vx(p,i)^2) + (vy(p,i)^2)) ^ .5
  
```



```

    endfor
endfor
close,15
;
angle2 = intarr(361)
xpos2 = fltarr(50,361)
ypos2 = fltarr(50,361)
vx2 = fltarr(50,361)
vy2 = fltarr(50,361)
vel2 = fltarr(50,361)
degr2 = fltarr(50,361)
x2 = fltarr(50)
y2 = fltarr(50)
;
; read in velocity position and calculate vector length data
;
openr,45,'final.vel'
for p = 0, points-2 do begin
    for i = 0, 360 do begin
        readf,45,tempxpos,tempypos,tempvx,tempvy,tempdeg
        xpos2(p,i) = tempxpos
        ypos2(p,i) = tempypos -0.07
        vx2(p,i) = tempvx
        vy2(p,i) = tempvy
        degr2(p,i) = tempdeg
        vel2(p,i) = ((vx(p,i)^2) + (vy(p,i)^2)) ^ .5
    endfor
endfor
close,45
;
; This routine automatically adds the key vector to the end
; of each array controlling the vector arrows, at (xpos,
; ypos), and equalling 10 m/s, and xyouts' coordinates
;control the placement of the "10 m/s" velocity key script
;placement
;
xpos(points-1,*) = 0.245
ypos(points-1,*) = 0.445
vx(points-1,*) = 10
vy(points-1,*) = 0
vel(points-1,*) = 10
;
;   create top rotor image
;
c = 0 for cr_ang = stdeg, endeg do begin
    crang = cr_ang - stdeg

```

```

;
;   *** housing ***
;
t3d, /reset & house_double
;
;   *** rotor rotation ***
;
rot_ang = cr_ang / 3
ca_rad = (cr_ang*3.1415927)/180
;
t3d, /reset, tr=[-.44984,-0.43,0], rot=[0,0,-rot_ang]
t3d, tr=[.44984,0.43,0]
ecc = .050162
dy = ecc*(sin(ca_rad))
dx = ecc - ecc*(cos(ca_rad))
t3d, tr=[dx,dy,0] & rotor2_double
;
t3d, /reset, tr=[-0.5,-0.43,0], rot=[0,0,-cr_ang]
t3d, tr=[0.5,0.43,0] & rotor1_double
t3d, /reset
;
;   *** velocity vectors ***
;
for j = 0, 49 do begin
  shaftrat = vel2(j,cr_ang) / relen
  ;
  ;Create "points" # of vector shafts with their relative
;lengths
  ;           controlled by "relen"
  ;
  shaftlen = shaftrat * .05
  theta = atan(vy2(j,cr_ang),vx2(j,cr_ang))
  dxvel = shaftlen * (cos(theta))
  dyvel = shaftlen * (sin(theta))
  xshaft = xpos2(j,cr_ang) + dxvel
  yshaft = ypos2(j,cr_ang) + dyvel
  x2 = [(xpos2(j,cr_ang)), (xshaft)]
  y2 = [(ypos2(j,cr_ang)), (yshaft)]
  shaft = [indgen(2),0]
  plots, x2(shaft), y2(shaft), /normal
  ;
  ;   Create the vector arrow heads
  ;
  headlen = shaftlen * .3
  beta = theta - .5236
  alpha = theta - 1.0472

```

```

dxheadl = headlen * (cos(beta))
dyheadl = headlen * (sin(beta))
dxheadr = headlen * (sin(alpha))
dyheadr = headlen * (cos(alpha))
xheadl = xpos2(j,cr_ang) + dxvel - dxheadl
yheadl = ypos2(j,cr_ang) + dyvel - dyheadl
xheadr = xpos2(j,cr_ang) + dxvel + dxheadr
yheadr = ypos2(j,cr_ang) + dyvel - dyheadr
xhead = [(xheadl), (xshaft), (xheadr)]
yhead = [(yheadl), (yshaft), (yheadr)]
head = [indgen(3)]
plots, xhead(head), yhead(head), /normal
endfor
;
xbox = [0,1.0,1.0,0]
ybox = [0.495,0.495,0.2,0.2]
polyfill, xbox, ybox, color=0, /normal
xline = [0.1316,0.868]
yline = [0.495,0.495]
sep = [indgen(2)]
plots, xline(sep), yline(sep), /normal
;
;   create bottom rotor image
;
;   *** housing ***
;
t3d, /reset & house
;
;   *** rotor rotation ***
;
rot_ang = cr_ang / 3
ca_rad = (cr_ang*3.1415927)/180
;
t3d, /reset, tr=[-.44984,0,0], rot=[0,0,-rot_ang]
t3d, tr=[.44984,0,0]
ecc = .050162
dy = ecc*(sin(ca_rad))
dx = ecc - ecc*(cos(ca_rad))
t3d, tr=[dx,dy,0] & rotor2
;
t3d, /reset, tr=[-.5,0,0], rot=[0,0,-cr_ang]
t3d, tr=[.5,0,0] & rotor1
t3d, /reset
;
;   *** velocity vectors ***
;

```

```

for j = 0, points-1 do begin
  shaftrat = vel(j,cr_ang) / rellen
  ;
  ;      Create "points" # of vector shafts with their
;relative lengths controlled by "rellen"
  ;
  shaftlen = shaftrat * .05
  theta = atan(vy(j,cr_ang),vx(j,cr_ang))
  dxvel = shaftlen * (cos(theta))
  dyvel = shaftlen * (sin(theta))
  xshaft = xpos(j,cr_ang) + dxvel
  yshaft = ypos(j,cr_ang) + dyvel
  x = [(xpos(j,cr_ang)), (xshaft)]
  y = [(ypos(j,cr_ang)), (yshaft)]
  ;
  x = [(xpos(j,cr_ang)), (xpos(j,cr_ang))]
  ;
  y = [(ypos(j,cr_ang)), (ypos(j,cr_ang))]
  shaft = [indgen(2),0]
  plots, x(shaft), y(shaft), /normal
  ;
  ;      Create the vector arrow heads
  ;
  headlen = shaftlen * .3
  beta = theta - .5236
  alpha = theta - 1.0472
  dxheadl = headlen * (cos(beta))
  dyheadl = headlen * (sin(beta))
  dxheadr = headlen * (sin(alpha))
  dyheadr = headlen * (cos(alpha))
  xheadl = xpos(j,cr_ang) + dxvel - dxheadl
  yheadl = ypos(j,cr_ang) + dyvel - dyheadl
  xheadr = xpos(j,cr_ang) + dxvel + dxheadr
  yheadr = ypos(j,cr_ang) + dyvel - dyheadr
  xhead = [(xheadl), (xshaft), (xheadr)]
  yhead = [(yheadl), (yshaft), (yheadr)]
  head = [indgen(3)]
  plots, xhead(head), yhead(head), /normal
  ;
  polyfill, xhead(head), yhead(head), /normal
endfor
;
xyouts, 0.195, 0.4, 'cad', /normal
xyouts, 0.07, 0.4, cr_ang, /normal
xyouts, 0.135, 0.44, '10 m/s', /normal
xyouts, 0.75, 0.83, 'LDR', /normal

```

```
xyouts, 0.75, 0.4, 'SMR', /normal
wait,0.01
rotormovie(*,*,0) = tvrd(xpixst,ypixst,512,512)
;
tiff file = string(cr_ang)
;
tiff file = 'LDR' + tiff file + '.tif'
;
tiff file = strcompress(tiff file, /remove_all)
;
tiff_write, tiff file, rotormovie(*,*,0)
;
spawn, 'mv *.tif /usr3/novak/test/'
erase endfor end
```

LIST OF REFERENCES

1. Shih, T.I-P., Yang, S.L., Schock, H.J., "A Two-Dimensional Numerical Study of the Flow Inside the Combustion Chamber of a Motored Rotary Engine," SAE paper 860615, 1986.
2. Grasso, F., Wey, M.J., Abraham, J. and Bracco, F.V., "Three-Dimensional Computations of Flows in a Stratified Charge Rotary Engine," SAE paper 870409, 1987.
3. Shih, T., Schock, H.J., and Ramos, J.I., "Fuel-Air Mixing and Combustion in a Two-Dimensional Wankel Engine," SAE paper 870408, 1987.
4. Shih, T.I., Schock, H.J., Nguyen, H. L., Stegeman, J.D., "Numerical Simulation of the Flowfield in a Motored Two-dimensional Wankel Engine," J. Propulsion, Vol. 3, No. 3, May-June 1987.
5. Steinthorsson, E., Shih, T., Schock, H.J., and Stegemen, J., "Calculations of the Unsteady, Three-Dimensional Flow Field inside a Motored Wankel Engine," SAE paper 880625, 1988.
6. Raju, M.S., Willis, E.A., "Analysis of Rotary Engine Combustion Processes Based on Unsteady, Three-dimensional Computations," AIAA paper 90-0643, 1990.
7. Li, Z., Steinthorsson, E., Shih, T., Nguyen, H., "Modelling and

Simulation of Wankel Engine Flow Fields," SAE paper 900029, 1990.

8. Raju, M., Willis, E., "Three-Dimensional Analysis and Modeling of a Wankel Engine," SAE paper 910701, 1991.
9. Li, Z., Shih, T., Schock, H., Willis, E., "A Numerical Study on the Effects of Apex Seal Leakage on Wankel Engine Flow Fields," SAE paper 910703, 1991.
10. Eberle, M.K., Klomp, E.D., "An Evaluation of the Potential Performance Gain from Leakage Reduction in Rotary Engines," SAE paper 730117, SAE trans., Vol. 82, 1974, pp. 454-460.
11. Roberts, J.A., Norman, T.J., Ekchian J.A., Heywood, J.B., "Computer Models For Evaluating Premixed and Disc Wankel Engine Performance," SAE paper 860613, 1986.
12. Ferguson, C.R., Danieli, G.A., Heywood, J.B., Keck, J.C., "Time Resolved Measurements of Exhaust Composition and Flow Rate in a Wankel Engine," SAE paper 750024, SAE trans. Vol. 84, Sec. 1, pp. 141-154, 1976.
13. Danieli, G., Keck, J., Heywood, J., "Experimental and Theoretical Analysis of Wankel Engine Performance," SAE paper 780416, 1978.
14. Sierens, R., Baert, R., Winterbone, D., Baruah, P., "A Comprehensive Study of Wankel Engine Performance," SAE paper 830332, 1983.
15. Burley, H.A., Meloeny, M.R., Stark, T.L., "Sources of Hydrocarbon

Emissions in Rotary Engines," SAE paper 780419, 1979.

16. Bayer, R.J., DeNagel, S.F., Steiner, J.C., "Rotary Combustion Engine Hydrocarbon Source Studies," SAE paper 780965, SAE trans. Vol. 87, Sec. 4, pp 3619-3636, 1979.
17. Schock, H.J., Rice, W.J., Meng, P.R., "Experimental Analysis of IMEP in a Rotary Combustion Engine," SAE paper 810150, 1981.
18. Yamamoto, K., Kuroda, T., "Toyo Kogyo's Research and Development on Major Rotary Engine Problems," SAE paper 700079, 1970.
19. Kohno, T., Ryozo, I., Morita, M., Mizuno, N., "Analysis of Light-Load Performance in Rotary Engines," SAE paper 790435, 1980.
20. Meng, P. R., Rice, W. J., Schock, H. J., Pringle, D. P., "Preliminary Results on Performance Testing of a Turbocharged Rotary Combustion Engine," SAE paper 820354, 1982.
21. Tashima, S., Taqdokoro, T., Okimoto, H., Niwa, Y., "Development of Sequential Twin Turbo System for Rotary Engine," SAE paper 910624, 1991.
22. Hamady, F.J., Stuecken, T.R., Schock, H.J., "Air Flow Visualization and LDA Measurements in a Motored Rotary Engine Assembly- Part 1: Air Flow visualization," SAE paper 900030.
23. Chouinard, E.N., Hamady, F.J., Schock, H.J., "Air Flow Visualization

and LDA Measurements in a Motored Rotary Engine Assembly-
Part 2: LDA Measurements," SAE paper 900031.

24. Matsuura, K., Terasaki, K., Watanabe, I., "The Relative Behavior of a Rotary Engine Apex Seal to the Walls of a Slot," Bulletin of the JSME, Vol. 19, Nov. 1976, pp. 1367-1375.
25. Matsuura, K., Terasaki, K., Watanabe, I., "The Behavior of a Rotary Engine Apex Seal Against the Trochoidal Surface," Bulletin of the JSME, Vol. 21, Nov. 1978, pp. 1642-1651.
26. Knoll, J., Vilmann, C.R., Schock, H.J., Stumpf, R.P., "A Dynamic Analysis of Rotary Combustion Engine Seals," SAE paper 840035, 1984.
27. Dimpelfeld, P.M., Witze, P.O., "Velocity Measurements in a 5.8 Liter Stratified Charge Rotary Engine," presented at the Fourth International Symposium on Applications of Laser Anemometry to Fluid Mechanics, Lisbon, Portugal, July 11-14, 1988.
28. Rachel, T., Schock, H., Bartand, T., "Analysis of Frictional Power Losses Associated with the Side and Apex Seals of a Wankel Rotary Engine," SAE paper 910626, 1991.
29. Hamady, F.J., DeFilippis, M.S., Stuecken, T.R., Schock, H.J., "Experimental Analysis of Blowby and Flow Field Interaction in a Motored Rotary Engine," SAE paper 910893, 1991.
30. Personal communication with Mark Novak, Michigan State

University Engine Research Laboratory, 1991.

31. Ansdale, R.F., The Wankel RC Engine, A.S. Barnes and Company, Cranbury, NJ, 1969, p. 145.
32. Yamamoto, K., Rotary Engine, Sankaido Co., Ltd., Tokyo, Japan, 1981, p. 15.
33. Chouinard, E.N., "Experimental Investigation of the Flow Field in a Motored Rotary Engine Assembly", Thesis, M.S. 1990, Michigan State University, pp. 28-29.
34. Lindeburg, M.R., Engineer-In-Training Reference Manual, Professional Publications, Inc., Belmont, CA, 1990, p. 11-6.

MICHIGAN STATE UNIV. LIBRARIES



31293008824199